

Competition of small targets in planar domains: from Dirichlet to Robin and Steklov boundary condition

D. S. GREBENKOV, M. J. WARD

Denis S. Grebenkov; CNRS – Université de Montréal CRM – CNRS, 6128 succ Centre-Ville, Montréal QC H3C 3J7, Canada;

Laboratoire de Physique de la Matière Condensée (UMR 7643),

CNRS – Ecole Polytechnique, Institut Polytechnique de Paris, 91120 Palaiseau, France

(corresponding author, email: denis.grebenkov@polytechnique.edu)

Michael J. Ward; Department of Mathematics, University of British Columbia, Vancouver, BC, V6T 1Z2, Canada

(email: ward@math.ubc.ca)

(Received 18 November 2025)

We consider steady-state diffusion in a bounded planar domain with multiple small targets on a smooth boundary. Using the method of matched asymptotic expansions, we investigate the competition of these targets for a diffusing particle and the crucial role of surface reactions on the targets. We start from the classical problem of splitting probabilities for perfectly reactive targets with Dirichlet boundary condition and improve some earlier results. We discuss how this approach can be generalized to partially reactive targets characterized by a Robin boundary condition. In particular, we show how partial reactivity reduces the effective size of the target. In addition, we consider more intricate surface reactions modeled by mixed Steklov-Neumann or Steklov-Neumann-Dirichlet problems. We provide the first derivation of the asymptotic behavior of the eigenvalues and eigenfunctions for these spectral problems in the small-target limit. Finally, we show how our asymptotic approach can be extended to interior targets in the bulk and to exterior problems where diffusion occurs in an unbounded planar domain outside a compact set. Direct applications of these results to diffusion-controlled reactions are discussed.

Keywords: diffusion, matched asymptotics, narrow escape problem, Steklov problem, mixed boundary conditions, diffusion-controlled reactions, first-passage time, Green's functions, Dirichlet-to-Neumann operator.

1 Introduction

Diffusive search for hidden targets is critically important for various physical, chemical and biological systems [20, 58, 60, 62, 67, 73]. In the most basic setting, a point-like particle (e.g., a molecule, an ion, a protein, a virus, a bacterium, etc.) undergoes diffusive motion inside a confining environment and searches for an immobile target (e.g., a catalytic site on a solid surface, a channel on a plasma membrane, a specific site on the DNA, a cell, etc.). If the target is hidden in the bulk, it is often called an interior trap or a sink, whereas a target on the boundary is referred to as a reactive patch or an escape window. In both cases, if the target is small, one usually speaks about the narrow escape problem [47, 48], bearing in mind the picture of an open window, through which the particle can leave the domain and never return. Most former works were dedicated to finding and even optimizing the *mean* first-passage time (FPT) to a single target or to a given arrangement of multiple targets [11, 15, 29, 41, 43, 49, 59, 65, 74, 75]. Other relevant characteristics of the diffusive search such as the whole distribution of the FPT [1, 12, 28, 39, 40] and Laplacian eigenvalues [14, 19, 51], were also studied.

A common limitation of most former works is their emphasis either on a single target, or on multiple targets of the same type. In turn, many biochemical applications involve targets of different types. For instance, signal transduction between neurons relies on diffusive search by calcium ions of a sensor protein on the vesicle with neurotransmitters

inside the presynaptic bouton [44, 47, 63, 68, 70]. While the sensor protein is the primary target, calcium ions can reversibly bind to buffer molecules inside the confining domain or leave it through calcium channels on its boundary. Both buffer molecules and channels play the role of auxiliary targets that compete for calcium ions and thus allow to control the signal transduction. More generally, the successful reaction of a diffusing particle on a “primary” target may fail due to its eventual capture by other targets, or its escape.

When all targets are perfect (i.e., the reaction occurs instantly upon the first arrival), the competition between targets for a diffusing particle is characterized via diffusive fluxes, splitting probabilities and conditional first-passage times [2, 4, 13, 21, 24, 31, 42, 54, 76, 77]. In particular, the asymptotic behavior of these quantities for small interior traps or absorbing patches on the boundary and the dependence on their spatial arrangement have been studied in depth. However, as the targets are not perfectly reactive in most applications [5, 18, 23, 26, 30, 31, 34, 55, 64, 71, 72], their competition also depends on their reactivities. The role of partially reactive traps, as modeled by a Robin condition condition, is not nearly as well understood, especially in the two-dimensional case.

The problem becomes even more challenging for more intricate surface reactions, which cannot be described by the conventional Robin boundary condition on targets. We will refer to such targets as *imperfect*. For instance, the target reactivity can be progressively increased or decreased by encounters with a diffusing particle. Such activation or passivation processes are described within the encounter-based approach [6, 7, 32, 33, 35]. In probabilistic terms, the reaction event occurs when the number of reaction attempts upon each arrival onto the target exceeds some random threshold. The probability distribution of the threshold characterizes the reaction mechanism (see details in [33]). For instance, the particular case of the exponential distribution corresponds to a partially reactive target with a constant reactivity, and its probabilistic description is equivalent to solving the diffusion equation with the Robin boundary condition. In turn, other distributions of the threshold describe more intricate surface reactions and involve integral-type boundary conditions. As shown in [33], such PDE problems can be solved by employing spectral expansions based on the *Steklov problem* (see Sec. 4 and 5 for its formulation and basic properties). In particular, the Steklov eigenfunctions turn out to be particularly suitable for dealing with diffusive motion in the confining domain between successive arrivals onto an imperfect target. The peculiar feature of the Steklov problem that distinguishes it from common spectral problems for the Laplacian, is that the spectral parameter appears in the boundary condition. Various properties of the Steklov problem have been thoroughly investigated (see [17, 27, 45, 50, 56] and references therein). When imperfect targets are located on the inert impenetrable boundary, one needs to combine Steklov and Neumann boundary conditions. Such a mixed Steklov-Neumann problem was already known in hydrodynamics, where it is referred to as the sloshing problem [25, 46, 53, 57]. In the case of a single target, the asymptotic behavior of its eigenvalues and eigenfunctions in the small-target limit was recently studied [37]. However, the scaling arguments and related analysis from [37] are not directly applicable to the case of multiple targets. The asymptotic behavior of the spectrum of the mixed Steklov-Neumann problem is thus unknown, despite the importance of its potential applications. Yet another unstudied setting concerns a single imperfect target with Steklov condition in the presence of multiple escape windows with Dirichlet condition. A mathematical framework for studying such an escape problem relies on the mixed Steklov-Neumann-Dirichlet problem [36]. To our knowledge, the asymptotic behavior of its eigenvalues and eigenfunctions in the small-target limit has not been studied previously.

In this paper, we progressively fill the gap between perfect and imperfect targets. In Sec. 2, we start with the conventional setting of N absorbing sinks and study their splitting probabilities, i.e., the probability of hitting one sink before any other. This relatively simple setting allows us to introduce in a didactic way many notions and tools

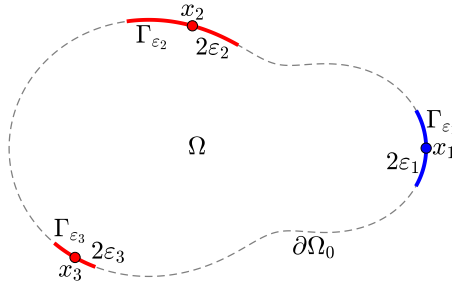


Figure 1. Illustration of a bounded domain $\Omega \subset \mathbb{R}^2$ with a smooth boundary $\partial\Omega$ split into three absorbing patches Γ_{ε_i} of length $2\varepsilon_i$ (in red and blue), and the remaining reflecting part $\partial\Omega_0$ (gray dashed line). For a particle starting from a point $\mathbf{x} \in \Omega$, the splitting probability $S_1(\mathbf{x})$ is the probability of hitting the blue patch Γ_{ε_1} first.

that will be employed throughout the manuscript. Even though this problem was studied in the past (see [4, 13] and references therein), we succeed in improving and generalizing some earlier results. Section 3 presents an extension to partially reactive targets, in which the Dirichlet boundary condition is replaced by a Robin condition. We show how partial reactivity effectively reduces the target size. The major contributions of the paper are presented in Secs. 4 and 5. In Sec. 4, we consider the mixed Steklov-Neumann problem for N imperfect targets. For this novel problem, we obtain the asymptotic behavior of its eigenvalues and eigenfunctions in the small-target limit. In turn, Sec. 5 focuses on the mixed Steklov-Neumann-Dirichlet problem, in which one target is imperfect (with Steklov condition), whereas the other targets are perfect (with Dirichlet condition). We apply matched asymptotic expansion techniques to investigate the asymptotic behavior in the small-target limit. For all considered cases, the accuracy of the derived asymptotic formulas is illustrated on two examples: the case of two patches in an arbitrary domain and the case of N equally-spaced patches on the boundary of a disk. Our analytical results are compared with numerical solutions obtained by a finite-element method in Matlab (its home-made implementation for Steklov problems is described in [10]). In Sec. 6, we discuss two further extensions of the present analysis: the case of interior targets (or traps), and exterior problems for which diffusion occurs outside a compact set. In this way, we cover a broad variety of settings, in which multiple small targets of different types compete for diffusing particles in planar domains. We summarize our main results in Section 7.

2 Splitting probabilities on Dirichlet patches

To introduce the theoretical framework and tools, we begin by revisiting the classical problem of splitting probabilities, which are commonly used to characterize competition between multiple perfectly reactive targets for a diffusing particle. Although this problem has been studied previously (see [4, 13] and references therein), we will improve and generalize some earlier results.

Let $\Omega \subset \mathbb{R}^2$ be a bounded planar domain with a smooth boundary $\partial\Omega$. Let $\{\Gamma_{\varepsilon_1}, \dots, \Gamma_{\varepsilon_N}\}$ be N disjoint subsets of the boundary $\partial\Omega$ that represent multiple patches of lengths $2\varepsilon_1, \dots, 2\varepsilon_N$ that are centered at boundary points $\mathbf{x}_1, \dots, \mathbf{x}_N$ (each patch Γ_{ε_j} is connected). The remaining part of the boundary, denoted as $\partial\Omega_0 = \partial\Omega \setminus (\Gamma_{\varepsilon_1} \cup \dots \cup \Gamma_{\varepsilon_N})$, is reflecting (Fig. 1). We are interested in the small-target limit when all patches are small and comparable (i.e., $\varepsilon_1 \sim o(1)$ and $\varepsilon_j/\varepsilon_1 \sim \mathcal{O}(1)$). We assume that the patches are well-separated in the sense that $|\mathbf{x}_i - \mathbf{x}_j| = \mathcal{O}(1)$ for all $i \neq j$.

In this section, we consider that all patches Γ_{ε_j} are absorbing sinks (i.e., perfectly reactive targets). For a particle

started from a point $\mathbf{x} \in \Omega$, we aim at determining the splitting probability $S_k(\mathbf{x})$ ($k = 1, \dots, N$), i.e., the probability of the arrival onto the Dirichlet patch Γ_{ε_k} *before* hitting any other patch. This probability satisfies the boundary value problem (BVP)

$$\Delta S_k = 0 \quad \text{in } \Omega, \quad (2.1 \text{ } a)$$

$$S_k = \delta_{j,k} \quad \text{on } \Gamma_{\varepsilon_j}, \quad j \in \{1, \dots, N\}, \quad (2.1 \text{ } b)$$

$$\partial_n S_k = 0 \quad \text{on } \partial\Omega_0, \quad (2.1 \text{ } c)$$

where Δ is the Laplacian, ∂_n is the normal derivative oriented outward to the domain Ω , and $\delta_{j,k}$ is the Kronecker symbol. In the analysis below, $k \in \{1, \dots, N\}$ is fixed. In the small-target limit $\varepsilon_j \rightarrow 0$ for each $j \in \{1, \dots, N\}$, we will use the method of matched asymptotic expansions for problems with logarithmic interactions [78] to approximate solutions to (2.1) that are accurate to all powers of $1/\ln(\varepsilon_j)$.

2.1 Inner solutions

The inner solution near each Dirichlet patch Γ_{ε_j} can be found by introducing the local coordinates $\mathbf{y} = \varepsilon_j^{-1} \mathbf{Q}_j(\mathbf{x} - \mathbf{x}_j)$, where \mathbf{Q}_j is an appropriate rotation matrix to restrict $\mathbf{y} = (y_1, y_2)$ to the upper half-plane $\mathbb{H}_2 = \mathbb{R} \times \mathbb{R}_+$ (the matrix \mathbf{Q}_j plays no role since $\mathbf{Q}_j^\dagger \mathbf{Q}_j = \mathbf{I}$ and $|\mathbf{y}| = \varepsilon_j^{-1} |\mathbf{x} - \mathbf{x}_j|$). We look for an inner solution near the patch Γ_{ε_j} in the form

$$S_k(\mathbf{x}_j + \varepsilon_j \mathbf{Q}_j^\dagger \mathbf{y}) = \delta_{j,k} + A_j g_\infty(\mathbf{y}), \quad j \in \{1, \dots, N\}, \quad (2.2)$$

where A_j is an unknown constant, and $g_\infty(\mathbf{y})$ is the Green's function satisfying the canonical BVP given by

$$\Delta g_\infty = 0 \quad \text{in } \mathbb{H}_2, \quad (2.3 \text{ } a)$$

$$\partial_n g_\infty = 0 \quad \text{on } y_2 = 0, |y_1| \geq 1; \quad g_\infty = 0 \quad \text{on } y_2 = 0, |y_1| < 1, \quad (2.3 \text{ } b)$$

$$g_\infty \sim \ln |\mathbf{y}| + \mathcal{O}(1) \quad \text{as } |\mathbf{y}| \rightarrow \infty, \quad (2.3 \text{ } c)$$

(the subscript ∞ highlights infinite reactivity of the perfect patch, see below). The exact solution of this classical problem is given in Appendix A for completeness. The analysis below will require only the knowledge of the asymptotic behavior of $g_\infty(\mathbf{y})$ at infinity. We recall that the constant term in this behavior,

$$g_\infty(\mathbf{y}) \sim \ln |\mathbf{y}| - \ln(d) + o(1) \quad \text{as } |\mathbf{y}| \rightarrow \infty, \quad (2.4)$$

is determined by the logarithmic capacity d of the interval $(-1, 1)$, which is simply $d = 1/2$. Now putting $\mathbf{y} = \varepsilon_j^{-1} \mathbf{Q}_j(\mathbf{x} - \mathbf{x}_j)$, we get that the far-field behavior of the inner solution is

$$S_k \sim \delta_{j,k} + A_j \left[\ln |\mathbf{x} - \mathbf{x}_j| - \ln(\varepsilon_j d) + o(1) \right] \quad \text{as } \mathbf{x} \rightarrow \mathbf{x}_j. \quad (2.5)$$

Setting

$$\nu_j = -\frac{1}{\ln(\varepsilon_j d)}, \quad \text{with} \quad d = \frac{1}{2}, \quad (2.6)$$

we rewrite this far-field behavior, for each $j \in \{1, \dots, N\}$, as

$$S_k \sim \delta_{j,k} + A_j \left[\ln |\mathbf{x} - \mathbf{x}_j| + 1/\nu_j + o(1) \right] \quad \text{as } \mathbf{x} \rightarrow \mathbf{x}_j. \quad (2.7)$$

2.2 Outer solution and matching conditions

Now we consider the outer problem for $S_k(\mathbf{x})$ given by

$$\Delta S_k = 0 \quad \text{in } \Omega, \quad (2.8a)$$

$$S_k \sim \delta_{j,k} + A_j [\ln |\mathbf{x} - \mathbf{x}_j| + 1/\nu_j] \quad \text{as } \mathbf{x} \rightarrow \mathbf{x}_j \in \partial\Omega, \quad j \in \{1, \dots, N\}, \quad (2.8b)$$

$$\partial_n S_k = 0 \quad \text{on } \partial\Omega \setminus \{\mathbf{x}_1, \dots, \mathbf{x}_N\}. \quad (2.8c)$$

To find this solution, we introduce the surface Neumann Green's function $G(\mathbf{x}, \xi)$, which satisfies

$$\Delta G = \frac{1}{|\Omega|} \quad \text{in } \Omega; \quad \partial_n G = 0 \quad \text{on } \partial\Omega \setminus \{\xi\}; \quad \int_{\Omega} G(\mathbf{x}, \xi) d\mathbf{x} = 0, \quad (2.9a)$$

$$G(\mathbf{x}, \xi) \sim -\frac{1}{\pi} \ln |\mathbf{x} - \xi| + R(\xi) + o(1) \quad \text{as } \mathbf{x} \rightarrow \xi \in \partial\Omega, \quad (2.9b)$$

where $|\Omega|$ is the area of Ω , and $R(\xi)$ is the regular part of $G(\mathbf{x}, \xi)$, defined by

$$R(\xi) = \lim_{\mathbf{x} \rightarrow \xi} \left(G(\mathbf{x}, \xi) + \frac{1}{\pi} \ln |\mathbf{x} - \xi| \right). \quad (2.10)$$

Remark 1 For a disk, G and R are known analytically from [51] and [65] (see (2.28) below). For a square domain, they can be represented in terms of rapidly converging infinite series representations (see Sec. 3.3 of [65]). Similar representations can be obtained for rectangles and ellipses from the results for the interior Neumann Green's function in Sec. 4.2 of [52] and in Sec. 5 of [49], respectively, by allowing the interior source point to tend to the domain boundary (see Sec. F.2 for this derivation for an ellipse and Table F1). A numerical method to compute G and R in arbitrary planar domains is described in Sec. 3.3 of [65].

The divergence theorem applied to Eqs. (2.8) yields

$$\sum_{j=1}^N A_j = 0. \quad (2.11)$$

Under this condition, the solution to Eqs. (2.8) can be written as the linear combination

$$S_k(\mathbf{x}) = \chi_k - \sum_{i=1}^N \pi A_i G(\mathbf{x}, \mathbf{x}_i), \quad (2.12)$$

where χ_k is a constant to be found. Matching the inner and outer asymptotic expansions as $\mathbf{x} \rightarrow \mathbf{x}_j$ gives

$$A_j + \nu_j \left[A_j R_j + \sum_{\substack{i=1 \\ i \neq j}}^N G_{j,i} A_i \right] = \chi_k \nu_j - \nu_k \delta_{j,k}, \quad (2.13)$$

for $j \in \{1, \dots, N\}$, where we have defined

$$G_{j,i} = \pi G(\mathbf{x}_j, \mathbf{x}_i) \quad (i \neq j), \quad R_j = \pi R(\mathbf{x}_j). \quad (2.14)$$

Together with the compatibility condition (2.11), we obtain a system of $N + 1$ linear equations that determine the unknown coefficients A_1, \dots, A_N and χ_k .

2.3 Matrix reformulation and general solution

To proceed, we introduce the following vectors and matrices of sizes $N \times 1$ and $N \times N$:

$$\mathbf{e} = \begin{pmatrix} 1 \\ 1 \\ \dots \\ 1 \end{pmatrix}, \quad \boldsymbol{\nu} = \begin{pmatrix} \nu_1 & 0 & \dots & 0 \\ 0 & \nu_2 & \dots & 0 \\ \dots & \dots & \dots & \dots \\ 0 & 0 & \dots & \nu_N \end{pmatrix}, \quad \mathbf{G} = \begin{pmatrix} R_1 & G_{1,2} & \dots & G_{1,N} \\ G_{2,1} & R_2 & \dots & G_{2,N} \\ \dots & \dots & \dots & \dots \\ G_{N,1} & G_{N,2} & \dots & R_N \end{pmatrix} \quad \mathbf{e}_k = \begin{pmatrix} 0 \\ 1 \\ \dots \\ 0 \end{pmatrix}, \quad (2.15)$$

where 1 stands on the k -th row of the vector \mathbf{e}_k .

In terms of this notation, the system (2.13) is written in matrix form as

$$\mathbf{A} + \boldsymbol{\nu} \mathbf{G} \mathbf{A} = \chi_k \boldsymbol{\nu} \mathbf{e} - \boldsymbol{\nu} \mathbf{e}_k. \quad (2.16)$$

Applying \mathbf{e}^\dagger on the left, we isolate χ_k as

$$\chi_k = \frac{\mathbf{e}^\dagger \boldsymbol{\nu} \mathbf{G} \mathbf{A}}{\bar{\nu}} + \frac{\nu_k}{\bar{\nu}}, \quad (2.17)$$

where we used $\mathbf{e}^\dagger \mathbf{A} = 0$ due to Eq. (2.11), and defined

$$\bar{\nu} = \mathbf{e}^\dagger \boldsymbol{\nu} \mathbf{e} = \sum_{j=1}^N \nu_j. \quad (2.18)$$

Eliminating χ_k from Eq. (2.16), we get a matrix equation for \mathbf{A} given by

$$(\mathbf{I} + \boldsymbol{\nu} \mathbf{G}) \mathbf{A} - \boldsymbol{\nu} \mathbf{e} \frac{\mathbf{e}^\dagger \boldsymbol{\nu} \mathbf{G} \mathbf{A}}{\bar{\nu}} = \frac{\nu_k}{\bar{\nu}} \boldsymbol{\nu} \mathbf{e} - \nu_k \mathbf{e}_k. \quad (2.19)$$

By introducing the matrices \mathbf{M}_0 and \mathbf{E} by

$$\mathbf{M}_0 = \mathbf{I} + \left(\mathbf{I} - \frac{\boldsymbol{\nu} \mathbf{E}}{\bar{\nu}} \right) \boldsymbol{\nu} \mathbf{G}, \quad \mathbf{E} = \mathbf{e} \mathbf{e}^\dagger, \quad (2.20)$$

the solution to Eq. (2.19) is

$$\mathbf{A} = \frac{\nu_k}{\bar{\nu}} \mathbf{M}_0^{-1} (\boldsymbol{\nu} \mathbf{e} - \bar{\nu} \mathbf{e}_k), \quad (2.21)$$

where \mathbf{M}_0^{-1} is the inverse of \mathbf{M}_0 . In fact, in the small-target limit, all $\nu_j \ll 1$ so that \mathbf{M}_0 is a small perturbation of the identity matrix \mathbf{I} and is thus invertible. Once the coefficients A_i are found, the constant χ_k follows from Eq. (2.17). As a consequence, the splitting probability $S_k(\mathbf{x})$ is fully determined via the representation (2.12). This is the main result of this section. The shape of the confining domain Ω and the arrangement of Dirichlet patches are captured by the matrix \mathbf{G} , whereas the sizes of patches are accounted for via the matrix $\boldsymbol{\nu}$. When the surface Neumann Green's function is known analytically, a numerical computation of the coefficients A_i and χ_k is fast, at least if the number of targets is not too large. We emphasize that the solution \mathbf{A} in (2.21) to the linear system (2.19) has accounted for all logarithmic correction terms in the asymptotic expansion of the splitting probability. This technique for effectively summing what otherwise would be an infinite logarithmic expansion in powers of ν_k was developed in [78], and has been used in other contexts (see [19], [54], [65]).

We further emphasize that Eq. (2.12) is only applicable in the outer region, i.e., when $|\mathbf{x} - \mathbf{x}_j| \gg \mathcal{O}(\varepsilon_j)$ for all $j \in \{1, \dots, N\}$. In turn, if the starting point \mathbf{x} is too close to \mathbf{x}_j , this asymptotic formula may give wrong values (e.g., negative or exceeding 1). In practice, the outer solution can be capped by 0 and 1 to avoid such invalid values, i.e., one can use $\max\{0, \min\{1, S_k(\mathbf{x})\}\}$ instead of $S_k(\mathbf{x})$. We remark that if an accurate approximation of the splitting probability is needed near the patch, one has to use the corresponding inner solution.

We also note that the constant χ_k can be interpreted as the volume-averaged splitting probability. In fact, if the

starting point \mathbf{x} is not fixed but uniformly distributed in Ω , the average over the starting point yields

$$\bar{S}_k = \frac{1}{|\Omega|} \int_{\Omega} S_k(\mathbf{x}) d\mathbf{x} = \chi_k, \quad (2.22)$$

where we used $\int_{\Omega} G(\mathbf{x}, \mathbf{x}_i) d\mathbf{x} = 0$.

2.4 Example of two patches

In the case of two targets ($N = 2$), the matrix \mathbf{M}_0 from Eq. (2.20) reads

$$\mathbf{M}_0 = \mathbf{I} + \gamma \begin{pmatrix} R_1 - G_{1,2} & G_{1,2} - R_2 \\ G_{1,2} - R_1 & R_2 - G_{1,2} \end{pmatrix}, \quad (2.23)$$

where $\gamma = \nu_1 \nu_2 / (\nu_1 + \nu_2)$. The inverse of this matrix is

$$\mathbf{M}_0^{-1} = \frac{1}{1 + \gamma(R_1 + R_2 - 2G_{1,2})} \left(\mathbf{I} + \gamma \begin{pmatrix} R_2 - G_{1,2} & R_2 - G_{1,2} \\ R_1 - G_{1,2} & R_1 - G_{1,2} \end{pmatrix} \right). \quad (2.24)$$

Substituting this expression into Eq. (2.21), we find for $k = 1$ that

$$-A_1 = A_2 = \left(\frac{1}{\nu_1} + \frac{1}{\nu_2} + [R_1 + R_2 - 2G_{1,2}] \right)^{-1}. \quad (2.25)$$

Then, by using Eq. (2.17) we determine χ_1 as

$$\chi_1 = \frac{\nu_1 - A_2 \nu_1 (R_1 - G_{1,2}) + A_2 \nu_2 (R_2 - G_{1,2})}{\nu_1 + \nu_2}, \quad (2.26)$$

which can be further simplified as

$$\chi_1 = \frac{1/\nu_2 + (R_2 - G_{1,2})}{1/\nu_1 + 1/\nu_2 + (R_1 + R_2 - 2G_{1,2})}. \quad (2.27)$$

For instance, if Ω is the unit disk, the surface Neumann Green's function is well known [65]:

$$G(\mathbf{x}, \boldsymbol{\xi}) = -\frac{1}{\pi} \ln |\mathbf{x} - \boldsymbol{\xi}| + \frac{|\mathbf{x}|^2}{4\pi} - \frac{1}{8\pi}, \quad R(\boldsymbol{\xi}) = \frac{1}{8\pi}. \quad (2.28)$$

Substitution of these expressions into Eqs. (2.25, 2.27) yields

$$-A_1 = A_2 = \left(-\ln(\varepsilon_1 \varepsilon_2) + 2 \ln(2) + 2 \ln |\mathbf{x}_1 - \mathbf{x}_2| \right)^{-1}, \quad (2.29a)$$

$$\chi_1 = \frac{-\ln(\varepsilon_2/2) + \ln |\mathbf{x}_1 - \mathbf{x}_2|}{-\ln(\varepsilon_1 \varepsilon_2/4) + 2 \ln |\mathbf{x}_1 - \mathbf{x}_2|}, \quad (2.29b)$$

and we conclude that

$$S_1(\mathbf{x}) = \chi_1 + A_2 \ln \left(\frac{|\mathbf{x} - \mathbf{x}_2|}{|\mathbf{x} - \mathbf{x}_1|} \right). \quad (2.30)$$

We can easily check that $S_1(\mathbf{x})$ approaches 0 [resp., 1] as $\varepsilon_1 \rightarrow 0$ [resp., $\varepsilon_2 \rightarrow 0$], as expected.

In the special case of two identical targets, $\nu_1 = \nu_2 = \nu$, one has $\chi_1 = 1/2$ and $A_2 = 1/(2/\nu + 2 \ln |\mathbf{x}_1 - \mathbf{x}_2|)$ so that

$$S_1(\mathbf{x}) = \frac{1}{2} \left[1 + \frac{\nu}{1 + \nu \ln |\mathbf{x}_1 - \mathbf{x}_2|} \ln \left(\frac{|\mathbf{x} - \mathbf{x}_2|}{|\mathbf{x} - \mathbf{x}_1|} \right) \right]. \quad (2.31)$$

We remark that if we were to expand the denominator of the second term into a Taylor series in powers of $\nu \ll 1$ up to $\mathcal{O}(\nu^2)$, we would recover the truncated approximation given in Eq. (98) from [13]. However, as $\nu = -1/\ln(\varepsilon/2)$ is not necessarily small enough, our new result Eq. (2.31) that incorporates all logarithmic terms is preferable than using the previous truncated approximation from [13].

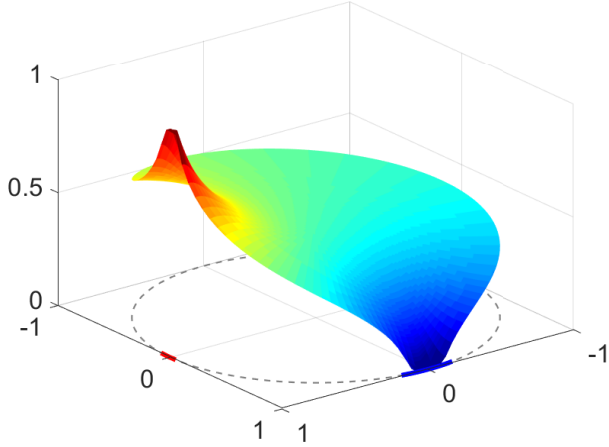


Figure 2. Splitting probability $S_1(\mathbf{x})$, given by Eq. (2.30), for the unit disk with two Dirichlet patches of length $2\varepsilon_1 = 0.2$ (red) and $2\varepsilon_2 = 0.4$ (blue). Note that $S_1(\mathbf{x})$ was capped by 0 and 1, i.e., we plotted $\max\{0, \min\{1, S_1(\mathbf{x})\}\}$.

Figure 2 illustrates the splitting probability $S_1(\mathbf{x})$ from Eq. (2.30). As explained earlier, we plot the capped version of this quantity, $\max\{0, \min\{1, S_1(\mathbf{x})\}\}$, to avoid invalid values near two patches. Expectedly, $S_1(\mathbf{x})$ increases as \mathbf{x} gets closer to the first patch (red arc) and decreases as \mathbf{x} gets closer to the second patch (blue arc). However, as the outer solution (2.30) is not applicable in the vicinity of these patches, we can observe some discrepancy, e.g., $S_1(\mathbf{x})$ does not vanish on the second patch, as it should. To amend this discrepancy, we can use the inner solution when $|\mathbf{x} - \mathbf{x}_j| \lesssim \varepsilon_j$.

2.5 Example of equally-spaced identical patches on the boundary of the unit disk

If there are N identical targets, one has $\nu_j = \nu$ so that $\boldsymbol{\nu} = \nu\mathbf{I}$, $\bar{\nu} = N\nu$, and thus $\mathbf{M}_0 = \mathbf{I} + \nu(\mathbf{I} - \mathbf{E}/N)\mathbf{G}$ from Eq. (2.20). Moreover, if the patches are equally-spaced on the boundary of the unit circle, the matrix \mathbf{G} defined in Eq. (2.15) is circulant and symmetric. As a consequence, its eigenvectors can be written as

$$\mathbf{q}_j = \frac{1}{\sqrt{N}}(\omega^{-j}, \omega^{-2j}, \dots, \omega^{-Nj})^\dagger, \quad j \in \{1, \dots, N\}, \quad (2.32)$$

where $\omega = e^{2\pi i/N}$, and the transposition \dagger now denotes the Hermitian conjugate. Upon taking the real and imaginary parts of \mathbf{q}_j , the resulting real-valued eigenvectors form an orthonormal basis in \mathbb{R}^N since \mathbf{G} is symmetric. Let us denote by κ_j the associated eigenvalues of \mathbf{G} :

$$\kappa_j = R_1 + \sum_{m=1}^{N-1} \omega^{mj} G_{1,1+m}, \quad j \in \{1, \dots, N\}. \quad (2.33)$$

For any $j \in \{1, \dots, N-1\}$, we get

$$\mathbf{M}_0 \mathbf{q}_j = (\mathbf{I} + \nu[\mathbf{I} - \mathbf{E}/N]) \kappa_j \mathbf{q}_j = (1 + \nu\kappa_j) \mathbf{q}_j, \quad (2.34)$$

because $\mathbf{E}\mathbf{q}_j = \mathbf{e}\mathbf{e}^\dagger \mathbf{q}_j = 0$ for any $1 \leq j \leq N-1$ due to orthogonality of \mathbf{q}_j to $\mathbf{q}_N = \mathbf{e}/\sqrt{N}$. As a consequence, each \mathbf{q}_j with $j \in \{1, \dots, N-1\}$ is also the eigenvector of \mathbf{M}_0 , associated to the eigenvalue $1 + \nu\kappa_j$. In addition, we have

$$\mathbf{M}_0 \mathbf{q}_N = (\mathbf{I} + \nu[\mathbf{I} - \mathbf{E}/N]) \kappa_N \mathbf{q}_N = \mathbf{q}_N, \quad (2.35)$$

since $\mathbf{Eq}_N/N = \mathbf{q}_N$. Therefore, \mathbf{q}_N is the eigenvector of \mathbf{M}_0 associated with the eigenvalue 1. We use this spectral information to invert the matrix \mathbf{M}_0 as

$$\mathbf{M}_0^{-1} = \mathbf{q}_N \mathbf{q}_N^\dagger + \sum_{j=1}^{N-1} \mathbf{q}_j (1 + \nu \kappa_j)^{-1} \mathbf{q}_j^\dagger. \quad (2.36)$$

Substituting this spectral representation into Eq. (2.21), we get

$$\mathbf{A} = -\nu \sum_{j=1}^{N-1} \mathbf{q}_j (1 + \nu \kappa_j)^{-1} \mathbf{q}_j^\dagger \mathbf{e}_k, \quad (2.37)$$

where we used the orthogonality of the eigenvectors \mathbf{q}_j . Substitution of this expression into Eq. (2.17) yields $\chi_k = 1/N$. This is consistent with the interpretation of χ_k as the volume-averaged splitting probability: when all patches are identical and equally-spaced on the boundary of the unit disk, they are equivalent from the uniformly distributed starting point, so that $\bar{S}_k = 1/N$ from Eq. (2.22).

To complete this example, we will simplify Eq. (2.33) by using the explicit form (2.28) of the surface Neumann Green's function for the unit disk. Since the centers of the patches \mathbf{x}_j are equally-spaced on the domain boundary, we have $\mathbf{x}_j = e^{2\pi i(j-1)/N} = \omega^{j-1}$ for $j \in \{1, \dots, N\}$. In this way, substituting Eq. (2.28) into Eq. (2.33), we get

$$\kappa_j = \frac{1}{8} \sum_{m=0}^{N-1} \omega^{jm} - \sum_{m=1}^{N-1} \omega^{mj} \ln |1 - \omega^m|, \quad j \in \{1, \dots, N\}, \quad (2.38)$$

where we interpret points as complex numbers and $|z|$ as the modulus of z . For $j = N$, for which $\omega^{Nm} = 1$, we get

$$\kappa_N = \frac{N}{8} - \ln \left| \prod_{m=1}^{N-1} (1 - \omega^m) \right| = \frac{N}{8} - \ln N, \quad (2.39)$$

where the product in Eq. (2.39) was evaluated by using the roots of unity together with L'Hopital's rule to get $\lim_{z \rightarrow 1} (z^N - 1)/(z - 1) = N = \prod_{m=1}^{N-1} (1 - \omega^m)$. For $j < N$, the first term in Eq. (2.38) vanishes and we obtain

$$\kappa_j = - \sum_{m=1}^{N-1} \omega^{mj} \ln |1 - \omega^m|, \quad j \in \{1, \dots, N-1\}, \quad (2.40)$$

which reduces after some simplifications to

$$\kappa_j = \ln 2 - \sum_{m=1}^{N-1} \cos \left(\frac{2\pi jm}{N} \right) \ln \left[\sin \left(\frac{\pi m}{N} \right) \right], \quad (2.41)$$

for $j \in \{1, \dots, N-1\}$. The asymptotic behavior of κ_j for large N is derived in Appendix B.

3 Splitting probability on Robin patches

In most applications, targets are not perfectly reactive [5, 18, 23, 26, 30, 31, 34, 55, 64, 71, 72]. Starting from Collins and Kimball [18], partial reactivity is usually implemented by replacing a Dirichlet boundary condition by a Robin condition. In the case of splitting probabilities, a straightforward generalization of the previous setting consists in replacing Dirichlet boundary condition (2.1 b) by the Robin boundary condition:

$$\partial_n S_k + q_j S_k = q_j \delta_{j,k} \quad \text{on } \Gamma_{\varepsilon_j}, \quad j \in \{1, \dots, N\}, \quad (3.1)$$

where the constant $0 < q_j < \infty$ characterizes the reactivity of the j -th patch Γ_{ε_j} . Here we excluded the limit $q_j = 0$ that would correspond to an inert patch that could be treated as a part of the reflecting boundary $\partial\Omega_0$. The Dirichlet condition is recovered in the limit $q_j \rightarrow +\infty$.

The change of the boundary condition on the patch is a local effect that does not impact the outer solution. In turn, the inner solution near each patch Γ_{ε_j} in Eq. (2.2) should now be replaced by

$$S_k(\mathbf{x}_j + \varepsilon_j \mathbf{Q}_j^\dagger \mathbf{y}) = \delta_{j,k} + A_j g_{\varepsilon_j q_j}(\mathbf{y}), \quad j \in \{1, \dots, N\}, \quad (3.2)$$

where $g_\mu(\mathbf{y})$ is the Robin Green's function, which satisfies

$$\Delta g_\mu = 0 \quad \text{in } \mathbb{H}_2, \quad (3.3a)$$

$$\partial_n g_\mu = 0 \quad \text{on } y_2 = 0, |y_1| \geq 1; \quad \partial_n g_\mu + \mu g_\mu = 0 \quad \text{on } y_2 = 0, |y_1| < 1, \quad (3.3b)$$

$$g_\mu \sim \ln |\mathbf{y}| + \mathcal{O}(1) \quad \text{as } |\mathbf{y}| \rightarrow \infty. \quad (3.3c)$$

In Appendix C, we derive a spectral expansion for this Green's function:

$$g_\mu(\mathbf{y}) = g_\infty(\mathbf{y}) + \pi \sum_{k=0}^{\infty} \frac{\Psi_{2k}(\infty)}{\mu_{2k} + \mu} \Psi_{2k}(\mathbf{y}), \quad (3.4)$$

for any $\mu \notin \bigcup_{k=0}^{\infty} \{-\mu_{2k}\}$. Here μ_k and $\Psi_k(\mathbf{y})$ are the eigenvalues and eigenfunctions of the auxiliary Steklov-Neumann problem in the upper half-plane:

$$\Delta \Psi_k = 0 \quad \text{in } \mathbb{H}_2, \quad (3.5a)$$

$$\partial_n \Psi_k = \mu_k \Psi_k \quad \text{on } y_2 = 0, |y_1| < 1; \quad \partial_n \Psi_k = 0 \quad \text{on } y_2 = 0, |y_1| \geq 1, \quad (3.5b)$$

$$\Psi_k = \mathcal{O}(1) \quad \text{as } |\mathbf{y}| \rightarrow \infty. \quad (3.5c)$$

An efficient numerical procedure for computing these eigenmodes is summarized in Appendix D. Once tabulated, these eigenfunctions play a role of “special functions”, like orthogonal polynomials.

As a consequence, Eq. (3.4) determines the constant term $\mathcal{C}(\mu)$ in the asymptotic behavior of $g_\mu(\mathbf{y})$ at infinity, defined by

$$g_\mu(\mathbf{y}) \sim \ln |\mathbf{y}| + \mathcal{C}(\mu) + o(1) \quad \text{as } |\mathbf{y}| \rightarrow \infty. \quad (3.6)$$

In the limit $|\mathbf{y}| \rightarrow \infty$, we get

$$\mathcal{C}(\mu) = \ln(2) + \frac{\pi}{2\mu} + \pi \sum_{k=1}^{\infty} \frac{[\Psi_{2k}(\infty)]^2}{\mu_{2k} + \mu}, \quad (3.7)$$

for any $\mu \notin \bigcup_{k=0}^{\infty} \{-\mu_{2k}\}$, where we used $\mu_0 = 0$ and $\Psi_0(\infty) = 1/\sqrt{2}$ (see Appendix C for more details). The first ten coefficients contributing to $\mathcal{C}(\mu)$ are listed in Table C 1, while Fig. 3 illustrates the behavior of the function $\mathcal{C}(\mu)$.

A Taylor expansion of Eq. (3.7) near $\mu = 0$ yields

$$\mathcal{C}(\mu) = \frac{\pi}{2\mu} + \sum_{n=0}^{\infty} (-\mu)^n C_{n+1}, \quad (3.8)$$

where the coefficients C_n can be expressed in terms of μ_{2k} and $\Psi_{2k}(\infty)$ (see Appendix C). Moreover, we calculated in Appendix E the exact values of the first two coefficients as

$$C_1 = \frac{3}{2} - \ln(2) \approx 0.8069, \quad C_2 = \frac{21 - 2\pi^2}{18\pi} \approx 0.0223. \quad (3.9)$$

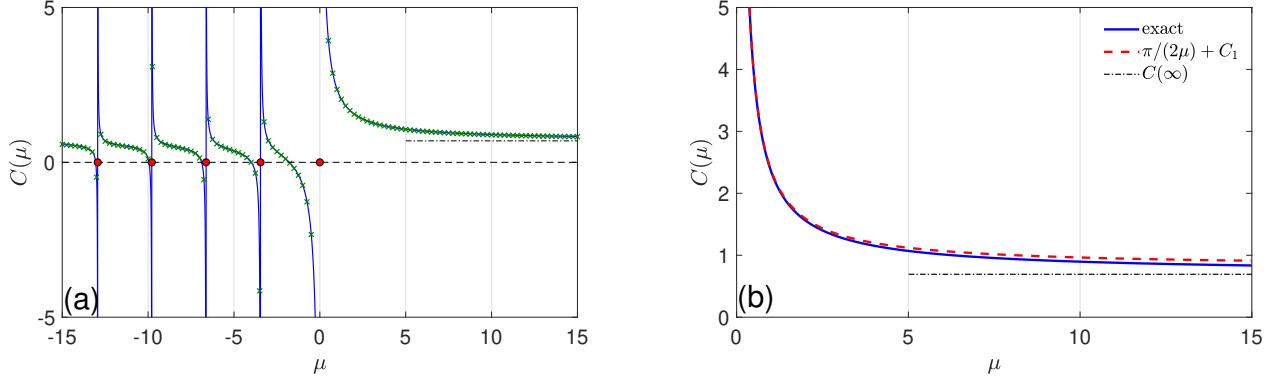


Figure 3. (a) Function $C(\mu)$ from Eq. (3.7), in which the infinite series is truncated either to 50 terms (solid line) or to 10 terms (crosses), to highlight the accuracy of both truncations. Filled circles indicate the values $-\mu_{2k}$, at which $C(\mu)$ diverges. Dash-dotted line outlines the asymptotic limit $\ln(2)$ of $C(\mu)$ as $\mu \rightarrow \infty$. (b) Comparison of $C(\mu)$ and its approximation (3.10), which is accurate over a broad range of μ .

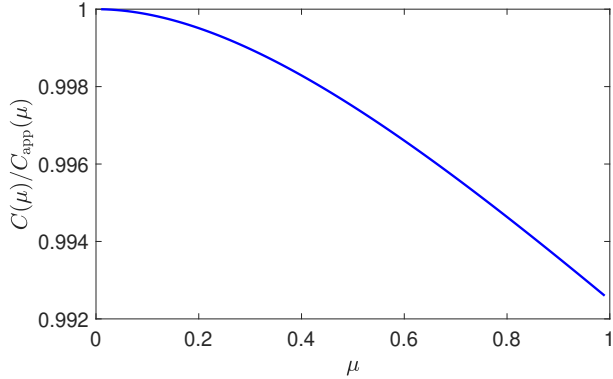


Figure 4. The ratio of $C(\mu)$ with its approximation (3.10) is very close to unity on the range $0 < \mu < 1$.

Since the second and higher-order coefficients turn out to be small, the following small- μ approximation,

$$C(\mu) \approx C_{\text{app}}(\mu) \equiv \frac{\pi}{2\mu} + C_1 \quad \text{for } \mu \ll 1, \quad (3.10)$$

is remarkably accurate as seen in both Fig. 3(b) and Fig. 4. This approximation is one of the key results needed for sections 4 and 5 below.

The relation (3.6) implies

$$S_k \sim \delta_{j,k} + A_j \left[\ln |\mathbf{x} - \mathbf{x}_j| + 1/\nu_j + o(1) \right] \quad \text{as } \mathbf{x} \rightarrow \mathbf{x}_j, \quad (3.11)$$

where we now redefine ν_j as

$$\nu_j = \frac{1}{-\ln(\varepsilon_j) + \mathcal{C}(\varepsilon_j q_j)}. \quad (3.12)$$

It follows that the far-field behavior of the inner solution is identical to that in Eq. (2.7) for Dirichlet patches, whereas the partial reactivity is fully taken into account through the new definition (3.12) of ν_j . As a consequence, we retrieve the same representation (2.12) for the splitting probability $S_k(\mathbf{x})$, with the coefficients A_i and χ_k given by Eqs. (2.17, 2.21). This equivalence shows that partially reactive targets with $q_j > 0$ can still be treated as the perfect ones but

with the reduced effective length, defined by

$$\varepsilon_j^{\text{eff}} = \varepsilon_j \exp(\ln(2) - \mathcal{C}(\varepsilon_j q_j)). \quad (3.13)$$

Together with the spectral expansion (3.7), this is the main result of this section.

From Eq. (3.7), the function $\mathcal{C}(\mu)$ decreases monotonically from $+\infty$ to $\ln(2)$ on the range $\mu > 0$ (see Fig. 3). As a consequence, ν_j in Eq. (3.12) decreases monotonically from $-1/\ln(\varepsilon_j/2)$ (this is the former definition of ν_j for the Dirichlet patch) to 0, whereas $\varepsilon_j^{\text{eff}}$ decreases from ε_j to 0 as the reactivity q_j drops from infinity to 0. This shows that a target with a smaller reactivity has less chance to capture the diffusing particle. When $q_j \sim \mathcal{O}(1)$, one has $\varepsilon_j q_j \ll 1$, so that the approximation (3.10) is applicable. This yields, that $\nu_j \approx 2\varepsilon_j q_j/\pi \ll 1$ and so to leading order

$$\varepsilon_j^{\text{eff}} \approx \varepsilon_j e^{-\pi/(2q_j \varepsilon_j)} \quad (\varepsilon_j q_j \ll 1). \quad (3.14)$$

For weakly reactive targets (i.e., if $q_j \varepsilon_j \ll 1$ for all $j = 1, \dots, N$), we get $\nu_j \approx 2\varepsilon_j q_j/\pi \ll 1$. According to Eq. (2.21), all the coefficients A_i are small (of the order of ε) so that the first term in Eq. (2.17) can be neglected, yielding

$$\chi_k \approx \frac{\nu_k}{\nu_1 + \dots + \nu_N}, \quad (3.15)$$

and thus

$$\overline{S}_k \approx \frac{\varepsilon_k q_k}{\varepsilon_1 q_1 + \dots + \varepsilon_N q_N}, \quad (3.16)$$

independently of the location of the patches. We emphasize that the approximation (3.15) is generally not accurate for perfect targets: even if ε_j are very small, the gauge function $\nu_j = -1/\ln(\varepsilon_j/2)$ may not be small enough to neglect higher-order terms in powers of ν_j .

For the case of two partially reactive patches on the boundary of the unit disk, substitution of the effective lengths $\varepsilon_j^{\text{eff}}$ from Eq. (3.13) into Eqs. (2.29) yields

$$A_2 = \left(-\ln(\varepsilon_1 \varepsilon_2) + \mathcal{C}(q_1 \varepsilon_1) + \mathcal{C}(q_2 \varepsilon_2) + 2 \ln |\mathbf{x}_1 - \mathbf{x}_2| \right)^{-1}, \quad (3.17a)$$

$$\chi_1 = \frac{-\ln(\varepsilon_2) + \mathcal{C}(q_2 \varepsilon_2) + \ln |\mathbf{x}_1 - \mathbf{x}_2|}{-\ln(\varepsilon_1 \varepsilon_2) + \mathcal{C}(q_1 \varepsilon_1) + \mathcal{C}(q_2 \varepsilon_2) + 2 \ln |\mathbf{x}_1 - \mathbf{x}_2|}. \quad (3.17b)$$

Figure 5 shows the behavior of χ_1 for two patches of equal length. In this figure, the high accuracy of our asymptotic solution (3.17b) is confirmed by comparison with a numerical solution of the BVP (2.1b) with Robin boundary condition (3.1) by a finite-element method.

3.1 The mean first-reaction time

Although our asymptotic analysis has focused on calculating splitting probabilities it can be easily modified to calculate the mean first-reaction time (MFRT).

The dimensionless MFRT $u(\mathbf{x})$ satisfies a Poisson equation with mixed Neumann-Robin boundary conditions:

$$\Delta u = -1, \quad \mathbf{x} \in \Omega, \quad (3.18a)$$

$$\partial_n u + q_i u = 0, \quad \mathbf{x} \in \Gamma_{\varepsilon_i}, \quad i \in \{1, \dots, N\}, \quad (3.18b)$$

$$\partial_n u = 0, \quad \mathbf{x} \in \partial\Omega_0 = \partial\Omega \setminus (\Gamma_{\varepsilon_1} \cup \dots \cup \Gamma_{\varepsilon_N}). \quad (3.18c)$$

As previously, each reactive boundary patch Γ_{ε_i} has length $2\varepsilon_i$, reactivity parameter q_i , and is centered at $\mathbf{x}_i \in \partial\Omega$.

The matched asymptotic analysis of Eq. (3.18) in the small-target limit $\varepsilon_i \ll 1$ is very similar to that for analyzing

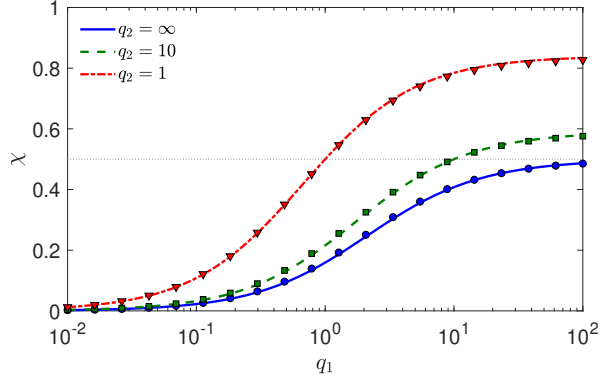


Figure 5. Volume-averaged splitting probability $\bar{S}_1 = \chi_1$ for the unit disk, calculated from (3.17b), with two patches of equal length $2\varepsilon = 0.2$ located at boundary points $(\pm 1, 0)$. Three curves correspond to three values of the reactivity parameter q_2 of the second patch. Symbols present the numerical solution of the BVP (2.1b) with Robin boundary condition (3.1) by a finite-element method in Matlab PDEtool, with the maximal meshsize 0.02.

the splitting probability. The inner solution near the j -th patch in terms of an unknown coefficient A_j is

$$V_j(\mathbf{y}) = u(\mathbf{x}_j + \varepsilon_j \mathbf{Q}_j^\dagger \mathbf{y}) = A_j g_{\mu_j}(\mathbf{y}), \quad j \in \{1, \dots, N\}, \quad (3.19)$$

where $\mu_j \equiv \varepsilon_j q_j$ and $g_{\mu_j}(\mathbf{y})$ is the Robin Green's satisfying Eq. (3.3) with far-field behavior Eq. (3.6). Upon matching the far-field behavior of $V_j(\mathbf{y})$ to the outer solution, we find that to within all logarithmic terms the outer solution satisfies

$$\Delta u = -1 \quad \text{in } \Omega, \quad (3.20a)$$

$$u \sim A_j [\ln |\mathbf{x} - \mathbf{x}_j| + 1/\nu_j] \quad \text{as } \mathbf{x} \rightarrow \mathbf{x}_j \in \partial\Omega, \quad j \in \{1, \dots, N\}, \quad (3.20b)$$

$$\partial_n u = 0 \quad \text{on } \partial\Omega \setminus \{\mathbf{x}_1, \dots, \mathbf{x}_N\}, \quad (3.20c)$$

where ν_j is defined by (3.12). The solvability condition for (3.20) is that $\sum_{j=1}^N A_j = |\Omega|/\pi$. We then represent u in terms of the surface Neumann Green's function and the volume average $\bar{u}_0 = |\Omega|^{-1} \int_{\Omega} u(\mathbf{x}) d\mathbf{x}$ as

$$u(\mathbf{x}) = \bar{u}_0 - \pi \sum_{i=1}^N A_i G(\mathbf{x}, \mathbf{x}_i). \quad (3.21)$$

Imposing the singularity behavior in Eq. (3.20b), we obtain an $(N+1)$ -dimensional linear algebraic system for \bar{u}_0 and A_1, \dots, A_N given by

$$A_j + \nu_j \left[A_j R_j + \sum_{\substack{i=1 \\ i \neq j}}^N G_{j,i} A_i \right] = \bar{u}_0 \nu_j, \quad j \in \{1, \dots, N\}; \quad \sum_{j=1}^N A_j = \frac{|\Omega|}{\pi}, \quad (3.22)$$

where $G_{j,i}$ and R_i were defined in (2.14). In matrix form Eq. (3.22) is written for $\mathbf{A} \equiv (A_1, \dots, A_N)^\dagger$ as

$$\mathbf{A} + \boldsymbol{\nu} \mathbf{G} \mathbf{A} = \bar{u}_0 \boldsymbol{\nu} \mathbf{e}, \quad \mathbf{e}^T \mathbf{A} = \frac{|\Omega|}{\pi}, \quad (3.23)$$

where \mathbf{e} , $\boldsymbol{\nu}$ and the Green's matrix \mathbf{G} were defined in Eq. (2.15). By eliminating \bar{u}_0 in Eq. (3.23), we conclude that

$$\bar{u}_0 = \frac{|\Omega|}{\pi \bar{\nu}} + \frac{\mathbf{e}^\dagger \boldsymbol{\nu} \mathbf{G} \mathbf{A}}{\bar{\nu}}, \quad (3.24)$$

where $\bar{\nu} \equiv \sum_{j=1}^N \nu_j$, while \mathbf{A} is the solution to

$$\mathbf{M}_0 \mathbf{A} = \frac{|\Omega|}{\pi \bar{\nu}} \boldsymbol{\nu}, \quad (3.25)$$

with \mathbf{M}_0 and \mathbf{E} being defined in Eq. (2.20).

By using Eq. (3.12) for ν_j , which involves the local reactivity parameter q_j on the patch, one can invert \mathbf{M}_0 in Eq. (3.25) to get the coefficients A_j . As a consequence, Eq. (3.24) gives access to the volume-averaged MFRT \bar{u}_0 , whereas Eq. (3.21) determines the MFRT $u(\mathbf{x})$ for any well-separated spatial configuration of partially reactive patches. This result generalizes that in [65], where perfect reactivities ($q_j = \infty$) were assumed.

4 Steklov-Neumann problem

As discussed in Sec. 1, the Robin boundary condition describes targets with a constant reactivity. In turn, more sophisticated surface reactions can be incorporated by using the encounter-based approach [32, 33, 35], which relies on the mixed Steklov-Neumann problem. In this section, we apply the tools described above to derive the asymptotic properties of this spectral problem in the small-target limit.

As before, we consider a bounded planar domain Ω with a smooth boundary $\partial\Omega$, which has N small well-separated patches Γ_{ε_j} , and $\partial\Omega_0 = \partial\Omega \setminus (\Gamma_{\varepsilon_1} \cup \dots \cup \Gamma_{\varepsilon_N})$. We study the mixed Steklov-Neumann spectral problem:

$$\Delta V = 0 \quad \text{in } \Omega, \quad (4.1 \text{ a})$$

$$\partial_n V = \sigma V \quad \text{on } \Gamma_{\varepsilon_1} \cup \dots \cup \Gamma_{\varepsilon_N}, \quad (4.1 \text{ b})$$

$$\partial_n V = 0 \quad \text{on } \partial\Omega_0. \quad (4.1 \text{ c})$$

This spectral problem is known to have a discrete positive spectrum [56], i.e., infinitely many eigenpairs $\{\sigma_k, V_k\}$ that are enumerated by $k = 0, 1, \dots$ to form an increasing sequence of eigenvalues: $0 = \sigma_0 < \sigma_1 \leq \sigma_2 \leq \dots \nearrow \infty$. Note that the Steklov boundary condition (4.1 b) with a nonnegative σ differs from the previous Robin condition by the opposite sign. We aim at determining the asymptotic behavior of the eigenvalues σ_k and the associated eigenfunctions V_k in the small-target limit.

In the case of a single Steklov patch ($N = 1$), the small- ε_1 asymptotic behavior of the eigenvalues and eigenfunctions was analyzed in [37]. In fact, a simple scaling argument suggests that $\sigma_j \approx \mu_j/\varepsilon_1$ ($j = 1, 2, \dots$) to leading order, where μ_j are the eigenvalues of the mixed Steklov-Neumann problem (3.5) for the interval in the upper half-plane (see also Appendix C).

If there are two well-separated Steklov patches, it is tempting to apply the same scaling argument in the vicinity of each patch. In this way, we can expect that the spectrum of the problem (4.1) with $N = 2$ is composed of two sequences of eigenvalues: $\{\mu_j/\varepsilon_1\}$ from the first patch of length $2\varepsilon_1$, and $\{\mu_j/\varepsilon_2\}$ from the second patch of length $2\varepsilon_2$. In other words, the two patches might be expected to not interact with each other in the small-target limit as $\varepsilon_j \rightarrow 0$. This intuitive argument turns out to be correct for all the eigenvalues, except for the first nontrivial eigenvalue σ_1 . Indeed, if two patches could be treated as independent, the eigenvalue σ_1 would have to be zero, as σ_0 . However, the zero eigenvalue can only correspond to a constant eigenfunction, so that if σ_1 was zero, one would have $V_1 = \text{const} = V_0$, which is impossible. We conclude that even if the patches are extremely small, the eigenvalue σ_1 must be strictly positive, and its asymptotic behavior must result from long-range interactions between two patches.

In this section, we adapt the analysis from Sec. 3 to the case of N Steklov patches and determine the asymptotic behavior of the first $N - 1$ eigenvalues σ_j , for $j \in \{1, \dots, N - 1\}$, in this setting.

4.1 Matched asymptotic analysis

As before, we look at the inner solution near each Steklov patch Γ_{ε_j} . Upon comparing the Robin and Steklov conditions (3.1, 4.1 b), we notice two differences: (i) q_j is replaced by $-\sigma$, and (ii) there is no inhomogeneous term $q_j \delta_{j,k}$ in the right-hand side. Apart from these two points, the boundary value problems for $S_k(\mathbf{x})$ and $V(\mathbf{x})$ are identical. As a consequence, we can immediately rewrite the asymptotic behavior (3.11) for each $j \in \{1, \dots, N\}$ as

$$V \sim A_j \left[\ln |\mathbf{x} - \mathbf{x}_j| + 1/\nu_j + \mathcal{C}(-\sigma\varepsilon_j) + o(1) \right] \quad \text{as } \mathbf{x} \rightarrow \mathbf{x}_j, \quad (4.2)$$

where we now redefine ν_j as

$$\nu_j = -1/\ln(\varepsilon_j), \quad (4.3)$$

and where A_j is an unknown coefficient. Note that the constant term $\mathcal{C}(-\sigma\varepsilon_j)$ is not incorporated into the new definition of ν_j , as we did earlier in the Robin case.

As before, the outer solution is represented as

$$V = \chi - \pi \sum_{i=1}^N A_i G(\mathbf{x}, \mathbf{x}_i), \quad (4.4)$$

with an unknown constant χ . The divergence theorem still ensures the compatibility condition (2.11). Upon enforcing the singularity behavior (4.2) for the solution in Eq. (4.4), we get

$$\chi - (\mathbf{G}\mathbf{A})_j = A_j(1/\nu_j + \mathcal{C}(-\sigma\varepsilon_j)), \quad j \in \{1, \dots, N\}, \quad (4.5)$$

where we used the matrix notations introduced in Eq. (2.15) of Sec. 2.3. Multiplying this equation by ν_j and introducing the diagonal matrix \mathbf{C} formed by $\{\mathcal{C}(-\sigma\varepsilon_1), \dots, \mathcal{C}(-\sigma\varepsilon_N)\}$, we rewrite Eq. (4.5) as

$$(\mathbf{I} + \boldsymbol{\nu}\mathbf{G} + \boldsymbol{\nu}\mathbf{C})\mathbf{A} = \chi\boldsymbol{\nu}\mathbf{e}. \quad (4.6)$$

Left-multiplying this equation by \mathbf{e}^\dagger , and using $\mathbf{e}^\dagger\mathbf{A} = 0$, we isolate χ as

$$\chi = \frac{1}{\bar{\nu}}(\mathbf{e}^\dagger\boldsymbol{\nu}\mathbf{G} + \mathbf{e}^\dagger\boldsymbol{\nu}\mathbf{C})\mathbf{A}, \quad (4.7)$$

where $\bar{\nu}$ was defined by Eq. (2.18). Substituting this expression back into Eq. (4.6), we obtain that

$$\left(\mathbf{I} + \left(\mathbf{I} - \frac{\boldsymbol{\nu}\mathbf{E}}{\bar{\nu}} \right) \boldsymbol{\nu}(\mathbf{G} + \mathbf{C}) \right) \mathbf{A} = \mathbf{0}. \quad (4.8)$$

The necessary and sufficient condition for the existence of a nontrivial solution to this matrix equation is

$$\det \left(\mathbf{I} + \left(\mathbf{I} - \frac{\boldsymbol{\nu}\mathbf{E}}{\bar{\nu}} \right) \boldsymbol{\nu}(\mathbf{G} + \mathbf{C}) \right) = \mathbf{0}. \quad (4.9)$$

The matrices $\boldsymbol{\nu}$ and \mathbf{G} are determined by the sizes and arrangement of the Steklov patches, while the matrix \mathbf{C} is formed by $\{\mathcal{C}(-\sigma\varepsilon_1), \dots, \mathcal{C}(-\sigma\varepsilon_N)\}$, with the function $\mathcal{C}(\mu)$ given by Eq. (3.7). As a consequence, Eq. (4.9) determines the unknown parameter σ . Moreover, the functional form (3.7) implies that there are infinitely many *negative* solutions, denoted as $-\sigma_j$, which are actually small-target approximations of the Steklov eigenvalues.

Let us first provide qualitative insights on these solutions. If the matrix \mathbf{C} was fixed in the small-target limit, the condition $\nu_j \ll 1$ would imply the smallness of the second matrix term in Eq. (4.9) as compared to the identity

matrix \mathbf{I} , thus ensuring the positivity of the determinant. To compensate the smallness of the matrix $\boldsymbol{\nu}$, the matrix \mathbf{C} must therefore be large in the small-target limit. This is possible when at least one $\sigma\varepsilon_i$ is close to $-\mu_{2k}$ for some k . In other words, one can expect that a solution $-\sigma_j$ of Eq. (4.9) is close to μ_{2k}/ε_i for some i and k . This intuitive picture suggests that an eigenvalue σ_j of the mixed Steklov-Neumann problem with N patches can be approximated by that on a single patch (say, Γ_{ε_i}), as if there were no other patches and the associated eigenfunction was localized on Γ_{ε_i} . The situation is, however, more subtle in the vicinity of $\mu_0 = 0$. In the analysis below, we focus on the asymptotic behavior of the first N eigenvalues σ_j .

4.2 First N eigenvalues

Let us assume that $-\mu = \sigma\varepsilon_j \ll 1$ for all $j = 1, \dots, N$, so that we can apply the approximate relation (3.10) for the function $\mathcal{C}(\mu)$. Introducing the diagonal matrix $\boldsymbol{\eta}$ formed by $\{\pi/(2\varepsilon_1), \dots, \pi/(2\varepsilon_N)\}$, we get $\mathbf{C} \approx -\boldsymbol{\eta}/\sigma + C_1\mathbf{I}$. Its substitution into Eq. (4.9) yields

$$\det\left(\mathbf{I} + \left(\mathbf{I} - \frac{\boldsymbol{\nu}\mathbf{E}}{\bar{\nu}}\right)\boldsymbol{\nu}[\mathbf{G} - \boldsymbol{\eta}/\sigma + C_1\mathbf{I}]\right) = \mathbf{0}. \quad (4.10)$$

Upon defining \mathbf{M}_1 and \mathbf{B}_1 by

$$\mathbf{M}_1 = \mathbf{I} + \left(\mathbf{I} - \frac{\boldsymbol{\nu}\mathbf{E}}{\bar{\nu}}\right)\boldsymbol{\nu}(\mathbf{G} + C_1\mathbf{I}), \quad \mathbf{B}_1 = \left(\mathbf{I} - \frac{\boldsymbol{\nu}\mathbf{E}}{\bar{\nu}}\right)\boldsymbol{\nu}\boldsymbol{\eta}, \quad (4.11)$$

we can rewrite Eq. (4.10) in a more compact form as

$$\det(\sigma\mathbf{M}_1 - \mathbf{B}_1) = 0. \quad (4.12)$$

In the small-target limit, one has $\nu_j \ll 1$ so that \mathbf{M}_1 is invertible since it is a small perturbation of the identity matrix. As a consequence, we get that

$$\det(\sigma\mathbf{I} - \mathbf{M}_1^{-1}\mathbf{B}_1) = 0. \quad (4.13)$$

We now prove that the eigenvalues $\hat{\sigma}_j$ for $j = 0, \dots, N-1$ of the matrix $\mathbf{M}_1^{-1}\mathbf{B}_1$ are real. To do so, we first write \mathbf{M}_1 in Eq. (4.11) as

$$\mathbf{M}_1 = \mathbf{I} - \hat{\mathbf{B}}_1\hat{\mathbf{G}}, \quad (4.14)$$

where we define the symmetric matrices $\hat{\mathbf{B}}_1$ and $\hat{\mathbf{G}}$ by

$$\hat{\mathbf{B}}_1 = \mathbf{B}_1\boldsymbol{\eta}^{-1} = \left(\mathbf{I} - \frac{\boldsymbol{\nu}\mathbf{E}}{\bar{\nu}}\right)\boldsymbol{\nu}, \quad \hat{\mathbf{G}} = -\mathbf{G} - C_1\mathbf{I}. \quad (4.15)$$

By using the Neumann series to calculate \mathbf{M}_1^{-1} , which converges since $\nu_j \ll 1$, we obtain that

$$\mathbf{M}_1^{-1}\hat{\mathbf{B}}_1 = \hat{\mathbf{B}}_1 + \hat{\mathbf{B}}_1\left(\sum_{n=1}^{\infty} \mathbf{K}_n\right)\hat{\mathbf{B}}_1, \quad \mathbf{K}_n = \left(\hat{\mathbf{G}}\hat{\mathbf{B}}_1\right)^{n-1}\hat{\mathbf{G}}. \quad (4.16)$$

Since \mathbf{K}_n is symmetric for each $n = 1, 2, \dots$, it follows that $\mathbf{M}_1^{-1}\hat{\mathbf{B}}_1$ is symmetric. Finally, we denote $\mathbf{D} = \mathbf{M}_1^{-1}\mathbf{B}_1 = \mathbf{M}_1^{-1}\hat{\mathbf{B}}_1\boldsymbol{\eta}$ and introduce $\hat{\mathbf{D}} = \boldsymbol{\eta}^{\frac{1}{2}}\mathbf{D}\boldsymbol{\eta}^{-\frac{1}{2}} = \boldsymbol{\eta}^{\frac{1}{2}}\mathbf{M}_1^{-1}\hat{\mathbf{B}}_1\boldsymbol{\eta}^{\frac{1}{2}}$, which is symmetric, so that its eigenvalues are real. Since $\boldsymbol{\eta}$ is positive definite, $\hat{\mathbf{D}}$ is related to \mathbf{D} by a similarity transformation so that the latter must also have real eigenvalues $\hat{\sigma}_j$ for $j = 0, \dots, N-1$.

Moreover, we note that $\hat{\sigma}_0 = 0$. This follows since $\mathbf{B}_1^\dagger \mathbf{e} = 0$, so that \mathbf{e} is an eigenvector of \mathbf{B}_1^\dagger and thus of $[\mathbf{M}_1^\dagger]^{-1}\mathbf{B}_1^\dagger$. The associated eigenvalue 0 is thus an eigenvalue of $\mathbf{B}_1\mathbf{M}_1^{-1}$ as well as of $\mathbf{M}_1^{-1}\mathbf{B}_1$.

In summary, the eigenvalues of the matrix $\mathbf{M}_1^{-1}\mathbf{B}_1$ provide the leading terms in the asymptotic behavior of the first N eigenvalues σ_j of the Steklov-Neumann problem:

$$\sigma_j \approx \hat{\sigma}_j, \quad j \in \{1, \dots, N-1\}. \quad (4.17)$$

This is the main result of this section. We observe that $\sigma_0 = \hat{\sigma}_0 = 0$, as expected.

4.3 Associated eigenfunctions

In addition, we construct the associated eigenfunctions of the first N eigenvalues. For this purpose, let us rewrite Eq. (4.8) as

$$(\sigma\mathbf{I} - \mathbf{M}_1^{-1}\mathbf{B}_1)\mathbf{A} = \mathbf{0}. \quad (4.18)$$

While each eigenvalue $\hat{\sigma}_j$ of the matrix $\mathbf{M}_1^{-1}\mathbf{B}_1$ approximates the j -th eigenvalue of the mixed Steklov-Neumann problem, the corresponding eigenvector of this matrix is the vector of coefficients A_i determining the associated eigenfunction V_j via Eq. (4.4), up to a multiplicative factor; we recall that χ is given by Eq. (4.7).

The missing multiplicative factor can be fixed by imposing an appropriate normalization of eigenfunctions. For the Steklov problem, the natural normalization is

$$\int_{\Gamma} V^2 ds = 1, \quad (4.19)$$

where $\Gamma = \Gamma_{\varepsilon_1} \cup \dots \cup \Gamma_{\varepsilon_N}$. For the trivial eigenvalue $\sigma_0 = 0$, one has a constant eigenfunction V_0 , whose normalization yields: $V_0^2 = 1/|\Gamma|$. In the following, we assume that $\sigma > 0$.

To proceed, we recall that the inner solution near the i -th patch reads in local coordinates is

$$V(\mathbf{x}_i + \varepsilon_i \mathbf{Q}_i^\dagger \mathbf{y}) \approx A_i g_{-\sigma \varepsilon_i}(\mathbf{y}). \quad (4.20)$$

Using the representation (3.4) of the Green's function $g_\mu(\mathbf{y})$, the restriction of V onto Γ_i becomes

$$V|_{\Gamma_i}(y_1) = V(\mathbf{x}_i + \varepsilon_i \mathbf{Q}_i^\dagger(y_1, 0)^\dagger) \approx \pi A_i \sum_{k=0}^{\infty} \frac{\Psi_{2k}(\infty) \Psi_{2k}(y_1, 0)}{\mu_{2k} - \sigma \varepsilon_i}. \quad (4.21)$$

This equation helps to deduce the required condition on the coefficients A_i :

$$1 = \sum_{i=1}^N \int_{\Gamma_i} V^2 ds = \sum_{i=1}^N \varepsilon_i \pi^2 A_i^2 \sum_{k=0}^{\infty} \frac{[\Psi_{2k}(\infty)]^2}{(\mu_{2k} - \sigma \varepsilon_i)^2},$$

where we used the orthogonality of the eigenfunctions Ψ_k (see Appendix C). The last sum can be re-written as the derivative of $\mathcal{C}(\mu)$, denoted as $\mathcal{C}'(\mu)$:

$$1 = -\pi \sum_{i=1}^N \varepsilon_i A_i^2 \mathcal{C}'(-\sigma \varepsilon_i). \quad (4.22)$$

When $0 < \sigma \varepsilon_i \ll 1$, the Taylor expansion (3.8) implies $\mathcal{C}'(\mu) \approx -\pi/(2\mu^2)$ and thus

$$\frac{2\sigma^2}{\pi^2} \approx \sum_{i=1}^N \frac{A_i^2}{\varepsilon_i}. \quad (4.23)$$

To complete this section, let us briefly discuss the positivity of Steklov eigenfunctions on patches Γ_{ε_j} . For a single patch, all Steklov eigenfunctions V_j must change sign on the patch due to their orthogonality to $V_0 = 1/\sqrt{|\Gamma|}$. When there are N Steklov patches, the orthogonality still holds so that any eigenfunction V_j with $j > 0$ must change sign

on the union of patches $\Gamma = \Gamma_{\varepsilon_1} \cup \dots \cup \Gamma_{\varepsilon_N}$. However, it is generally unknown whether V_j changes the sign or not on each patch Γ_i . Looking at Eq. (4.21), one can expect that if $\sigma\varepsilon_i$ is small enough, the eigenfunction V does not change sign on the patch Γ_i (i.e., it is either positive, or negative on it). Indeed, the term $1/(-2\sigma\varepsilon_i)$ of the sum in Eq. (4.21) that corresponds to $k = 0$, is expected to provide the dominant contribution as compared to the remaining terms. This property follows from the conjectured inequality (C9). In other words, if the patches are small enough, the first N eigenfunctions do not change their signs on each patch. This conjecture is confirmed by several numerical examples (not shown).

4.4 Example of two patches

When $N = 2$, we calculate that

$$(\mathbf{I} - \boldsymbol{\nu}\mathbf{E}/\bar{\nu})\boldsymbol{\nu} = \gamma \begin{pmatrix} 1 & -1 \\ -1 & 1 \end{pmatrix}, \quad (4.24)$$

where we label $\gamma = \nu_1\nu_2/(\nu_1 + \nu_2)$. Then, from Eq. (4.11), we get

$$\mathbf{M}_1 = \mathbf{I} + \gamma \begin{pmatrix} (R_1 - G_{1,2}) + C_1 & (G_{1,2} - R_2) - C_1 \\ (G_{1,2} - R_1) - C_1 & (R_2 - G_{1,2}) + C_1 \end{pmatrix}, \quad \mathbf{B}_1 = \frac{\pi}{2}\gamma \begin{pmatrix} 1/\varepsilon_1 & -1/\varepsilon_2 \\ -1/\varepsilon_1 & 1/\varepsilon_2 \end{pmatrix}.$$

Since \mathbf{e} is a left-eigenvector of \mathbf{M}_1 with eigenvalue one, the second eigenvalue of \mathbf{M}_1 is simply $\text{trace}(\mathbf{M}_1) - 1$. As a consequence, we find

$$\det(\mathbf{M}_1) = \text{trace}(\mathbf{M}_1) - 1 = 1 + \gamma[(R_1 + R_2 - 2G_{1,2}) + 2C_1], \quad (4.25)$$

and

$$\mathbf{M}_1^{-1} = \frac{1}{\det(\mathbf{M}_1)} \left[\mathbf{I} + \gamma C_1 \mathbf{E} + \gamma \begin{pmatrix} R_2 - G_{1,2} & R_2 - G_{1,2} \\ R_1 - G_{1,2} & R_1 - G_{1,2} \end{pmatrix} \right], \quad (4.26)$$

from which we calculate

$$\mathbf{M}_1^{-1}\mathbf{B}_1 = \frac{\pi\gamma/2}{\det(\mathbf{M}_1)} \begin{pmatrix} 1/\varepsilon_1 & -1/\varepsilon_2 \\ -1/\varepsilon_1 & 1/\varepsilon_2 \end{pmatrix}. \quad (4.27)$$

The two eigenvalues of this matrix are $\hat{\sigma}_0 = 0$ and

$$\hat{\sigma}_1 = \frac{\pi\gamma(1/\varepsilon_1 + 1/\varepsilon_2)}{2\det(\mathbf{M}_1)}, \quad (4.28)$$

so that upon solving for $\hat{\sigma}_1^{-1}$, we get

$$\frac{1}{\hat{\sigma}_1} = \frac{2\varepsilon_1\varepsilon_2}{\pi(\varepsilon_1 + \varepsilon_2)} \left[\frac{1}{\gamma} + (R_1 + R_2 - 2G_{1,2}) + 2C_1 \right]. \quad (4.29)$$

To simplify this expression, we use

$$\gamma = \frac{1}{1/\nu_1 + 1/\nu_2} = \frac{1}{-\ln(\varepsilon_1\varepsilon_2)}. \quad (4.30)$$

This yields the following asymptotic behavior for the Steklov eigenvalue:

$$\frac{1}{\sigma_1} \approx \frac{2\varepsilon_1\varepsilon_2}{\pi(\varepsilon_1 + \varepsilon_2)} \left[-\ln(\varepsilon_1\varepsilon_2) + 2C_1 + (R_1 + R_2 - 2G_{1,2}) \right]. \quad (4.31)$$

For instance, if Ω is the unit disk, Eq. (2.28) yields

$$\frac{1}{\sigma_1} \approx \frac{2\varepsilon_1\varepsilon_2}{\pi(\varepsilon_1 + \varepsilon_2)} \left(-\ln(\varepsilon_1\varepsilon_2) + 2C_1 + 2\ln|\mathbf{x}_1 - \mathbf{x}_2| \right). \quad (4.32)$$

Moreover, the corresponding eigenfunction V_1 can be easily found by noting that $A_1 = -A_2$ from Eq. (2.11),

whereas Eq. (4.23) implies

$$A_1 = -A_2 \approx \frac{\sqrt{2}\sigma_1}{\pi\sqrt{1/\varepsilon_1 + 1/\varepsilon_2}}. \quad (4.33)$$

These coefficients determine $(V_1)|_{\Gamma_i}$ via Eq. (4.21).

4.5 Example of identical equally-spaced patches on the boundary of the unit disk

When all patches are of the same size, $\varepsilon_j = \varepsilon$, we have $\boldsymbol{\nu} = \nu\mathbf{I}$ and $\boldsymbol{\eta} = \mathbf{I}\pi/(2\varepsilon)$, so that

$$\mathbf{M}_1 = \mathbf{I} + \nu\left(\mathbf{I} - \frac{\mathbf{E}}{N}\right)(\mathbf{G} + C_1\mathbf{I}), \quad \mathbf{B}_1 = \frac{\pi\nu}{2\varepsilon}\left(\mathbf{I} - \frac{\mathbf{E}}{N}\right). \quad (4.34)$$

If the patches are equally-spaced on the boundary of the unit disk, \mathbf{G} is circulant and symmetric, and its eigenvectors and eigenvalues were given in Eqs. (2.32, 2.33). As shown earlier in Sec. 2.5, one has $(\mathbf{I} - \mathbf{E}/N)\mathbf{q}_j = \mathbf{q}_j$ for any $j = 1, 2, \dots, N-1$, and $(\mathbf{I} - \mathbf{E}/N)\mathbf{q}_N = 0$. As a consequence, $\mathbf{M}_1\mathbf{q}_N = \mathbf{q}_N$ and $\mathbf{M}_1\mathbf{q}_j = (1 + \nu(\kappa_j + C_1))\mathbf{q}_j$, where κ_j are given explicitly by Eq. (2.40). Upon calculating $\mathbf{M}_1^{-1}\mathbf{q}_j$, we readily find that

$$\mathbf{B}_1\mathbf{M}_1^{-1}\mathbf{q}_N = 0, \quad \mathbf{B}_1\mathbf{M}_1^{-1}\mathbf{q}_j = \frac{\pi\nu}{2\varepsilon}(1 + \nu(\kappa_j + C_1))^{-1}\mathbf{q}_j.$$

Since the eigenvalues of the matrices $\mathbf{B}_1\mathbf{M}_1^{-1}$ and $\mathbf{M}_1^{-1}\mathbf{B}_1$ are identical, we have from Eq. (4.13) that $\hat{\sigma}_0 = 0$ and

$$\hat{\sigma}_j = \frac{\pi\nu}{2\varepsilon[1 + \nu(\kappa_j + C_1)]}, \quad j \in \{1, \dots, N-1\}. \quad (4.35)$$

Substituting $C_1 = 3/2 - \ln 2$ from Eq. (3.9) and $\nu = -1/\ln\varepsilon$ into Eq. (4.35), we obtain the following small- ε asymptotic result for the first $N-1$ eigenvalues of the mixed Steklov-Neumann problem:

$$\frac{1}{\varepsilon\sigma_j} \approx \frac{2}{\pi}\left(-\ln(\varepsilon) + \frac{3}{2} - \ln(2) + \kappa_j\right), \quad (4.36)$$

for $j = 1, 2, \dots, N-1$. When the number of patches is large, i.e. $N \gg 1$, while still enforcing the well-separated patch assumption $\varepsilon N \ll \pi$, we can use the asymptotic relation (B 12) for κ_j , valid for $j \ll N$, to conclude that

$$\frac{1}{\varepsilon\sigma_j} \approx \frac{2}{\pi}\left(\frac{N}{2j} - \ln\left(\frac{N\varepsilon}{\pi}\right) - \frac{1}{3}\right). \quad (4.37)$$

If $N\varepsilon$ is not too small, the logarithmic and constant terms can be neglected to yield to a first approximation

$$\sigma_j \approx \frac{\pi j}{N\varepsilon} \quad \text{for } j \ll N, \quad (4.38)$$

when $N \gg 1$. It is instructive to compare this approximation to the case of a single Steklov patch of half-length $\varepsilon_1 = N\varepsilon$, for which $\sigma_j \approx \mu_j/\varepsilon_1 \approx (\pi j/2)/(N\varepsilon)$, where we used the asymptotic relation (C 11). As a consequence, the configuration with a single patch of half-length $N\varepsilon$ yields approximately twice smaller eigenvalues. This suggests that the fragmentation of a patch will increase the eigenvalues.

5 Steklov-Neumann-Dirichlet problem

In this section, we consider the last setting of a single Steklov patch Γ_{ε_1} and $N-1$ Dirichlet patches Γ_{ε_j} ($j = 2, \dots, N$). This is a typical situation when the diffusing particle needs to react on Γ_{ε_1} before escaping the domain Ω through multiple opening windows $\Gamma_{\varepsilon_2}, \dots, \Gamma_{\varepsilon_N}$. A formal solution of such an escape problem was provided in [36] on the

basis of the mixed Steklov-Neumann-Dirichlet spectral problem, formulated as

$$\Delta V = 0 \quad \text{in } \Omega, \quad (5.1 \text{ } a)$$

$$\partial_n V = \sigma V \quad \text{on } \Gamma_{\varepsilon_1}; \quad V = 0 \quad \text{on } \Gamma_{\varepsilon_2} \cup \dots \cup \Gamma_{\varepsilon_N}, \quad (5.1 \text{ } b)$$

$$\partial_n V = 0 \quad \text{on } \partial\Omega_0. \quad (5.1 \text{ } c)$$

As previously, this spectral problem is known to have a discrete positive spectrum [56], i.e., infinitely many eigenpairs $\{\sigma_k, V_k\}$ that are enumerated by $k = 0, 1, \dots$ to form an increasing sequence of eigenvalues: $0 < \sigma_0 \leq \sigma_1 \leq \dots \nearrow \infty$. The presence of Dirichlet patches implies that the principal eigenvalue σ_0 is strictly positive. We aim at determining the asymptotic behavior of the eigenvalues and eigenfunctions of this spectral problem in the small-target limit $\varepsilon_j \rightarrow 0$.

In the analysis below, we treat separately two cases depending on the integral of the Steklov eigenfunction on the Steklov patch Γ_{ε_1} . In particular, if

$$\int_{\Gamma_{\varepsilon_1}} \partial_n V \, ds = \sigma \int_{\Gamma_{\varepsilon_1}} V \, ds \neq 0, \quad (5.2)$$

then, from the divergence theorem, the Steklov patch produces a logarithmic contribution to the far field. We will mainly focus on this generic case. However, if the integral in Eq. (5.2) is zero (e.g., if $V|_{\Gamma_{\varepsilon_1}}$ is antisymmetric, see below), there is no logarithmic contribution, and such an eigenfunction vanishes in the far field. This situation is actually simpler because the decay of V away from the Steklov patch is compatible with Dirichlet patches. In other words, we can restrict the analysis to the inner solution near the Steklov patch as if there were no Dirichlet patches. We will illustrate this situation in Sec. 5.4.

5.1 Matched asymptotic analysis

Expectedly, we can combine formerly derived inner solutions for Dirichlet and Steklov patches, whereas the outer solution is still written as the linear combination (4.4). As a consequence, we must enforce the singularity behavior

$$V \sim A_j \left[\ln |\mathbf{x} - \mathbf{x}_j| + 1/\nu_j + \delta_{j,1} \mathcal{C}(-\sigma \varepsilon_1) + o(1) \right], \quad (5.3)$$

as $\mathbf{x} \rightarrow \mathbf{x}_j$ for all patches $j \in \{1, \dots, N\}$. Here we have used the former definition $\nu_j = -1/\ln(\varepsilon_j/2)$ for Dirichlet patches and $\nu_1 = -1/\ln(\varepsilon_1)$ for the Steklov patch. By ensuring that V in Eq. (4.4) satisfies Eq. (5.3) we obtain that

$$A_j + \nu_j \left[A_j R_j + \sum_{\substack{i=1 \\ i \neq j}}^N G_{j,i} A_i \right] = \chi \nu_j - \nu_1 A_1 \mathcal{C}(-\sigma \varepsilon_1) \delta_{j,1}. \quad (5.4)$$

Together with Eq. (2.11), they form a system of $N+1$ linear equations for the unknowns A_i and χ . Using the former matrix notation in Eqs. (2.15), Eq. (5.4) becomes

$$(\mathbf{I} + \boldsymbol{\nu} \mathbf{G}) \mathbf{A} = \chi \boldsymbol{\nu} \mathbf{e} - \nu_1 \mathcal{C}(-\sigma \varepsilon_1) \mathbf{e}_1 \mathbf{e}_1^\dagger \mathbf{A}, \quad (5.5)$$

with $\mathbf{e}^\dagger \mathbf{A} = 0$. Upon left-multiplying by \mathbf{e}^\dagger , we get

$$\chi = \frac{1}{\bar{\nu}} \left[\mathbf{e}^\dagger \boldsymbol{\nu} \mathbf{G} \mathbf{A} + \mathcal{C}(-\sigma \varepsilon_1) \nu_1 \mathbf{e}^\dagger \mathbf{E}_1 \mathbf{A} \right], \quad (5.6)$$

where $\bar{\nu}$ was defined in Eq. (2.18), and we introduced the matrix $\mathbf{E}_1 = \mathbf{e}_1 \mathbf{e}_1^\dagger$ for a shorter notation. Eliminating χ from Eq. (5.5), we obtain that

$$\left(\mathbf{I} + \nu \left(\mathbf{I} - \frac{\mathbf{E}\nu}{\bar{\nu}} \right) \mathbf{G} \right) \mathbf{A} + \mathcal{C}(-\sigma\varepsilon_1)\nu_1 \left(\mathbf{I} - \frac{\nu\mathbf{E}}{\bar{\nu}} \right) \mathbf{E}_1 \mathbf{A} = \mathbf{0}, \quad (5.7)$$

where we recall that $\mathbf{E} = \mathbf{e}\mathbf{e}^\dagger$. Upon introducing \mathbf{B} by

$$\mathbf{B} = \left(\mathbf{I} - \frac{\nu\mathbf{E}}{\bar{\nu}} \right) \mathbf{E}_1, \quad (5.8)$$

and using the matrix \mathbf{M}_0 from Eq. (2.20), we rewrite the matrix system in Eq. (5.7) as

$$(\mathbf{M}_0 + \mathcal{C}(-\sigma\varepsilon_1)\nu_1 \mathbf{B}) \mathbf{A} = \mathbf{0}. \quad (5.9)$$

The condition, under which this matrix equation admits a nontrivial solution is

$$\det(\mathbf{M}_0 + \mathcal{C}(-\sigma\varepsilon_1)\nu_1 \mathbf{B}) = 0, \quad (5.10)$$

which is a scalar problem that determines σ .

To rewrite this problem in a more explicit form, we first observe that $\text{rank}(\mathbf{B}) = 1$ since $\mathbf{E}_1 \mathbf{q} = 0$ for any vector $\mathbf{q} \in \mathbb{R}^N$ such that $\mathbf{e}_1^\dagger \mathbf{q} = 0$. Since $\mathbf{e}_1^\dagger \mathbf{e}_1 = 1$, we can rewrite \mathbf{B} in a more convenient rank-one form as

$$\mathbf{B} = \left(\mathbf{e}_1 - \frac{\nu\mathbf{e}}{\bar{\nu}} \right) \mathbf{e}_1^\dagger = \mathbf{a}\mathbf{b}^\dagger, \quad \text{where } \mathbf{a} = \mathbf{e}_1 - \frac{\nu\mathbf{e}}{\bar{\nu}}, \quad \mathbf{b} = \mathcal{C}(-\sigma\varepsilon_1)\nu_1 \mathbf{e}_1. \quad (5.11)$$

To proceed, we need the matrix determinant lemma [22].

Lemma: *Let $\mathbf{M} = \mathbf{M}_0 + \mathbf{a}\mathbf{b}^\dagger$ be a perturbation of an invertible matrix $\mathbf{M}_0 \in \mathbb{R}^{N,N}$ by a rank-one matrix $\mathbf{a}\mathbf{b}^\dagger$. Then*

$$\det(\mathbf{M}_0 + \mathbf{a}\mathbf{b}^\dagger) = (1 + \mathbf{b}^\dagger \mathbf{M}_0^{-1} \mathbf{a}) \det(\mathbf{M}_0). \quad (5.12)$$

It follows that $\det(\mathbf{M}) = 0$ if and only if $\mathbf{b}^\dagger \mathbf{M}_0^{-1} \mathbf{a} = -1$.

In the small-target limit, all $\nu_j \ll 1$ so that the matrix \mathbf{M}_0 is invertible since it is a small perturbation of the identity matrix in Eq. (2.20). Applying the lemma above to our setting, we determine the condition on σ as

$$\mathcal{C}(-\sigma\varepsilon_1) = C, \quad (5.13)$$

where

$$C = -\frac{1}{\nu_1} \left(\mathbf{e}_1^\dagger \mathbf{M}_0^{-1} \left[\mathbf{e}_1 - \frac{\nu\mathbf{e}}{\bar{\nu}} \right] \right)^{-1}, \quad (5.14)$$

with the vectors and matrices \mathbf{e} , \mathbf{e}_1 , ν , and \mathbf{M}_0 being defined in Eqs. (2.15, 2.20). This is the main result of this section that will allow us to determine the asymptotic behavior of the Steklov eigenvalues and their dependence on the configuration and sizes of all patches that are captured via the constant C in Eq. (5.14). We further emphasize that the homogeneous matrix equation (5.9) cannot uniquely determine the coefficients A_i . In fact, an eigenfunction V can be found up to a multiplicative factor that has to be fixed by normalization (see below).

As stated above, the matrix \mathbf{M}_0 is a small perturbation of the identity matrix in the small-target limit, so that $\mathbf{M}_0^{-1} \sim \mathbf{I}$ to leading order, which implies that $\mathbf{e}_1^\dagger \mathbf{M}_0^{-1} [\mathbf{e}_1 - \nu\mathbf{e}/\bar{\nu}] \sim 1 - \nu_1/\bar{\nu} > 0$. Since $0 < \nu_1 \ll 1$, we conclude that the constant C in Eq. (5.14) is negative and large:

$$C < 0, \quad |C| \gg 1. \quad (5.15)$$

5.2 Asymptotic behavior of eigenvalues and eigenfunctions

Denoting $\mu = -\sigma\varepsilon_1$, we recast Eq. (5.13) as

$$\mathcal{C}(\mu) = C. \quad (5.16)$$

The spectral expansion (3.7) of the function $\mathcal{C}(\mu)$ allows one to solve this equation numerically for any fixed negative value C given by Eq. (5.14). Since the derivative $\mathcal{C}'(\mu) = d\mathcal{C}(\mu)/d\mu$ is negative, $\mathcal{C}(\mu)$ is a continuous and monotonically decreasing function on each interval $(-\mu_{2j+2}, -\mu_{2j})$, with $j = 0, 1, \dots$. Moreover, it ranges from $+\infty$ to $-\infty$ on each interval. As a consequence, for any fixed value C , there exist infinitely many *negative* solutions of Eq. (5.16), denoted as $-\hat{\mu}_{2j}$, such that

$$\mu_{2j} \leq \hat{\mu}_{2j} \leq \mu_{2j+2} \quad \text{for } j = 0, 1, \dots. \quad (5.17)$$

This property facilitates the numerical solution, as a single zero has to be searched on each interval. Moreover, as the coefficients $[\Psi_{2k}(\infty)]^2$ are small (see Table C 1) and decrease with k , whereas C is negative and large, one has $\hat{\mu}_{2j} \approx \mu_{2j}$ for $j > 0$. This is consistent with the intuitive picture that large Steklov eigenvalues become insensitive to Dirichlet patches in the small-target limit, and one retrieves the asymptotic behavior for a single Steklov patch [37].

The solutions $\hat{\mu}_{2j} \approx \mu_{2j}$ determine the leading-order term in the asymptotic behavior of the eigenvalues σ_{2j} :

$$\sigma_{2j} \approx \frac{\mu_{2j}}{\varepsilon_1} \quad \text{for } j = 1, 2, \dots. \quad (5.18)$$

In contrast, the smallest eigenvalue σ_0 involves the solution $\hat{\mu}_0$, which may actually be small in the small-target limit. We discuss this case separately in Sec. 5.3.

We also mention that the analysis above provides the leading-order approximation to the associated Steklov eigenfunction, restricted to Γ_{ε_1} . We recall that the inner solution near the Steklov patch is $V_{2j} \sim A_1 g_{-\sigma_{2j}\varepsilon_1}(\mathbf{y})$, with the Green's function $g_\mu(\mathbf{y})$ given by Eq. (3.4). As a consequence, its restriction onto the patch reads

$$V_{2j} \Big|_{\Gamma_{\varepsilon_1}} \approx a_{2j} \sum_{k=0}^{\infty} \frac{\Psi_{2k}(\infty)}{\mu_{2k} - \varepsilon_1 \sigma_{2j}} \Psi_{2k}(\mathbf{y}), \quad (5.19)$$

where the proportionality coefficient a_{2j} is fixed by the conventional normalization of the Steklov eigenfunction:

$$1 = \int_{\Gamma_{\varepsilon_1}} V_{2j}^2 ds \approx \varepsilon_1 a_{2j}^2 \sum_{k=0}^{\infty} \frac{[\Psi_{2k}(\infty)]^2}{(\mu_{2k} - \varepsilon_1 \sigma_{2j})^2}, \quad (5.20)$$

where the orthogonality of Ψ_{2k} was used. Since $\varepsilon_1 \sigma_{2j} \approx \mu_{2j}$, the eigenfunction Ψ_{2j} provides the dominant contribution, and one gets for each $j \in \{1, 2, \dots\}$ that

$$V_{2j}(\mathbf{x}_1 + \varepsilon_1 \mathbf{Q}_1^\dagger(\mathbf{y}_1, 0)^\dagger) \approx \frac{1}{\sqrt{\varepsilon_1}} \Psi_{2j}(\mathbf{y}_1, 0) \quad (5.21)$$

on the Steklov patch (i.e., for $|\mathbf{y}_1| \leq 1$).

We emphasize that the analysis above allowed us to access only half of eigenvalues with even indices $2j$ that correspond to symmetric eigenmodes. In turn, the eigenvalues with odd indices correspond to antisymmetric eigenmodes, for which the integral over the Steklov patch is zero. As discussed at the beginning of Sec. 5, such eigenfunctions vanish away from the Steklov patch so that their asymptotic behavior can be determined directly from the local solution. As a consequence, we get a leading-order approximation

$$\sigma_{2j+1} \approx \frac{\mu_{2j+1}}{\varepsilon_1} \quad \text{for } j = 0, 1, \dots, \quad (5.22)$$

and on the Steklov patch we have

$$V_{2j+1}(\mathbf{x}_1 + \varepsilon_1 \mathbf{Q}_1^\dagger(y_1, 0)^\dagger) \approx \frac{1}{\sqrt{\varepsilon_1}} \Psi_{2j+1}(y_1, 0). \quad (5.23)$$

In summary, our analysis justifies theoretically the intuitively appealing scaling argument that the eigenvalues σ_j and eigenfunctions $(V_j)|_{\Gamma_{\varepsilon_1}}$ (on the Steklov patch) can be approximated by the eigenvalues μ_j and eigenfunctions Ψ_j of the auxiliary problem (3.5), as if there were no Dirichlet patches. Regardless of the symmetry of eigenfunctions (and parity of its index), we can combine the former leading-order approximations as

$$\sigma_j \approx \frac{\mu_j}{\varepsilon_1} \quad \text{for } j = 1, 2, \dots, \quad (5.24 \text{ a})$$

$$V_j(\mathbf{x}_1 + \varepsilon_1 \mathbf{Q}_1^\dagger(y_1, 0)^\dagger) \approx \frac{1}{\sqrt{\varepsilon_1}} \Psi_j(y_1, 0). \quad (5.24 \text{ b})$$

In contrast, the presence of Dirichlet patches must affect the principal eigenvalue σ_0 and the associated eigenfunction V_0 , as explained below.

5.3 The principal eigenvalue

Since $\mu_0 = 0$, the smallest solution of Eq. (5.16), $\hat{\mu}_0$, is close to 0. Indeed, as the constant C is large and negative, one needs to have $|\mu| \ll 1$ to ensure that $\mathcal{C}(\mu)$ is also large and negative. Under the condition $|\mu| \ll 1$, we can use the approximation (3.10), which can be easily inverted to get the explicit result

$$\frac{1}{\mu} \approx \frac{2}{\pi} [\mathcal{C}(\mu) - C_1] = \frac{2}{\pi} [C - C_1]. \quad (5.25)$$

As a consequence, substitution of Eq. (5.14) here yields the asymptotic behavior of the principal eigenvalue σ_0 :

$$\frac{1}{\varepsilon_1 \sigma_0} \approx -\frac{2}{\pi} \left[\ln(\varepsilon_1) \left(\mathbf{e}_1^\dagger \mathbf{M}_0^{-1} \left[\mathbf{e}_1 - \frac{\nu \mathbf{e}}{\bar{\nu}} \right] \right)^{-1} - C_1 \right]. \quad (5.26)$$

In sharp contrast to Eq. (5.18) for σ_j with $j \geq 1$, the principal eigenvalue σ_0 exhibits a slower divergence $\mathcal{O}(1/(\varepsilon_1 \ln(\varepsilon_1)))$. This is one of the main results of this section. The associated eigenfunction V_0 is given by Eq. (5.19) with the normalization condition (5.20). We stress that Eq. (5.19) cannot be reduced to the approximation (5.21) in this case.

5.4 Example of two patches

When there are two patches ($N = 2$), Eqs. (5.14, 5.26) can be readily solved. Substituting \mathbf{M}_0^{-1} from Eq. (2.24) and

$$\mathbf{e}_1 - \frac{\nu \mathbf{e}}{\bar{\nu}} = \frac{\nu_2}{\nu_1 + \nu_2} (1, -1)^\dagger \quad (5.27)$$

into Eq. (5.14), we get after simplifications that

$$C = \ln(\varepsilon_1 \varepsilon_2 / 2) - (R_1 + R_2 - 2G_{1,2}). \quad (5.28)$$

Using Eq. (5.25) with $C_1 = 3/2 - \ln 2$ from Eq. (3.9), the asymptotic behavior of the principal eigenvalue is

$$\frac{1}{\varepsilon_1 \sigma_0} \approx \frac{2}{\pi} \left(-\ln(\varepsilon_1 \varepsilon_2) + \frac{3}{2} + (R_1 + R_2 - 2G_{1,2}) \right). \quad (5.29)$$

For instance, when Ω is the unit disk, one can substitute Eq. (2.28) into Eq. (5.29) to get

$$\frac{1}{\varepsilon_1 \sigma_0} \approx \frac{2}{\pi} \left(-\ln(\varepsilon_1 \varepsilon_2) + \frac{3}{2} + 2 \ln |\mathbf{x}_1 - \mathbf{x}_2| \right). \quad (5.30)$$

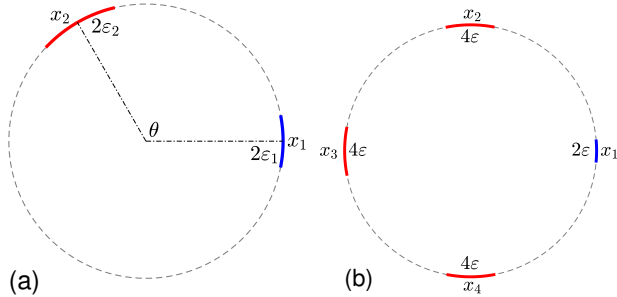


Figure 6. Illustration for the unit disk with Steklov and Dirichlet patches. (a) One Steklov patch of length $2\epsilon_1 = 0.4$ at $\mathbf{x}_1 = (1, 0)$ (blue) and one Dirichlet patch of length $2\epsilon_2 = 0.6$ (red), whose center \mathbf{x}_2 is at angle $\theta = 2\pi/3$. (b) One Steklov patch of length $2\epsilon_1 = 2\epsilon = 0.2$ at $\mathbf{x}_1 = (1, 0)$ (blue) and three Dirichlet patches of length $2\epsilon_j = 0.4$ (red), whose centers \mathbf{x}_j are equally-spaced on the boundary of the unit disk.

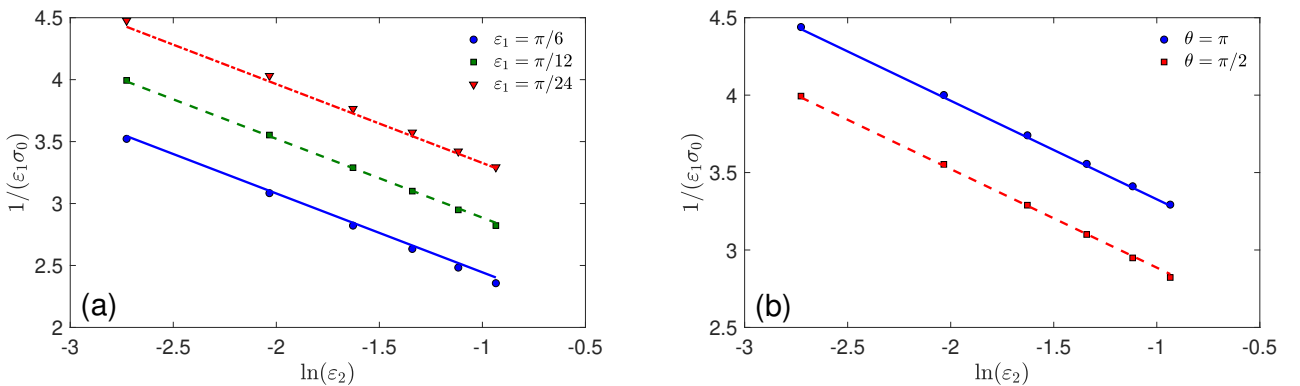


Figure 7. Dependence of $1/(\epsilon_1 \sigma_0)$ on $\ln(\epsilon_2)$ for the unit disk with a Steklov patch of length $2\epsilon_1$ (located at $\mathbf{x}_1 = (1, 0)$), and one Dirichlet patch of length $2\epsilon_2$, located at \mathbf{x}_2 . Symbols present the numerical solution by a FEM with the maximal meshsize $h_{\max} = 0.005$ and lines show Eq. (5.30). (a) $\mathbf{x}_2 = (0, 1)$ and three values of ϵ_1 : $\epsilon_1 = \pi/6$ (circles), $\epsilon_1 = \pi/12$ (squares), and $\epsilon_1 = \pi/24$ (triangles). (b) $\epsilon_1 = \pi/12$ and two locations of the Dirichlet patch: $\mathbf{x}_2 = (-1, 0)$ (circles, $\theta = \pi$), and $\mathbf{x}_2 = (0, 1)$ (squares, angle $\theta = \pi/2$).

Figure 7 illustrates the remarkable accuracy of this asymptotic relation.

Figure 8 shows the behavior of the Steklov eigenfunctions V_j restricted onto the Steklov patch. For the principal eigenmode with $j = 0$, this restriction is positive, as expected. The asymptotic formula (5.19) yields an accurate approximation. Let us now look at other eigenmodes with $j = 1, 2, 3$, for which $\sigma_j \approx \mu_j/\epsilon_1$. We see that the restriction of V_j and its approximation (5.24) are in excellent agreement, for both symmetric and antisymmetric eigenfunctions, even though both considered patches are not small.

5.5 Example of equally-spaced patches on the unit disk

We now consider another setting where the general formulas (5.13) and (5.14) can be simplified. We suppose that all Dirichlet patches with $j = 2, \dots, N$ are of the same length, so that $\epsilon_j = \epsilon$ for $j \in \{2, \dots, N\}$, whereas for the Steklov patch we have $\epsilon_1 = \ell_1 \epsilon/2$, for some $\ell_1 > 0$. To treat this case, we can impose in our general formula (5.14) for C that

$$\nu = \nu_1 = \dots = \nu_N = -1/\ln(\epsilon/2), \quad \boldsymbol{\nu} = \boldsymbol{\nu}\mathbf{I}, \quad (5.31)$$

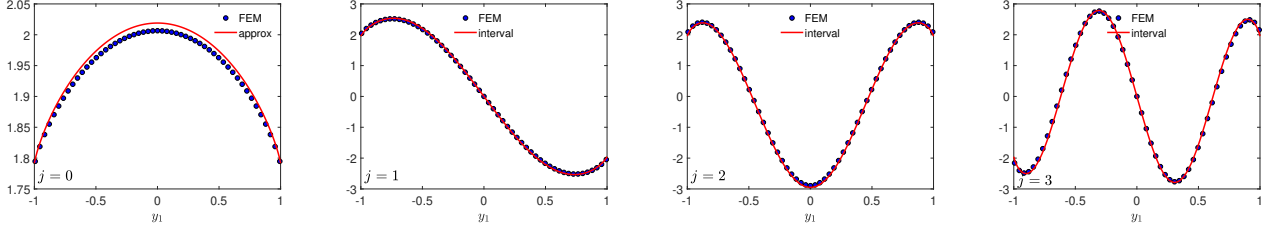


Figure 8. The eigenfunctions V_j restricted on the Steklov patch Γ_{ε_1} , for the unit disk with a Steklov patch of length $2\varepsilon_1 = \pi/12 \approx 0.26$ (located at $\mathbf{x}_1 = (1, 0)$), and one Dirichlet patch of length $2\varepsilon_2 = \pi/6 \approx 0.52$, located at $\mathbf{x}_2 = (-1, 0)$. Filled circles present the numerical solution by a FEM with the maximal meshsize $h_{\max} = 0.005$, while solid lines show Eq. (5.19) for $j = 0$ and Eq. (5.24) for $j > 0$. Four panels present the cases $j = 0, 1, 2, 3$.

provided that we shift $\mathcal{C}(-\sigma\varepsilon_1)$ appropriately in the relation (5.13). To determine this shift, we write the singularity condition (5.3) as $\mathbf{x} \rightarrow \mathbf{x}_1$ associated with the Steklov patch $j = 1$ as

$$\begin{aligned} V &\sim A_1 \left[\ln |\mathbf{x} - \mathbf{x}_1| - \ln \varepsilon_1 + \mathcal{C}(-\sigma\varepsilon_1) + o(1) \right] \\ &\sim A_1 \left[\ln |\mathbf{x} - \mathbf{x}_1| + 1/\nu + \tilde{\mathcal{C}}(-\sigma\varepsilon_1) + o(1) \right], \end{aligned}$$

where we have defined $\tilde{\mathcal{C}}(-\sigma\varepsilon_1)$ by

$$\tilde{\mathcal{C}}(-\sigma\varepsilon_1) = \mathcal{C}(-\sigma\varepsilon_1) - \ln \left(\frac{2\varepsilon_1}{\varepsilon} \right). \quad (5.32)$$

As a result, by repeating the steps of Sec. 5.1, we need only replace Eq. (5.13) by

$$\mathcal{C}(-\sigma\varepsilon_1) - \ln \left(\frac{2\varepsilon_1}{\varepsilon} \right) = C, \quad (5.33)$$

where C is given by Eq. (5.14) with $\nu = \nu\mathbf{I}$, $\bar{\nu} = N\nu$, and $\nu = -1/\ln(\varepsilon/2)$, which yields

$$C = \frac{1}{\nu} \left(\frac{\mathbf{e}_1^\dagger \mathbf{M}_0^{-1} \mathbf{e}}{N} - \mathbf{e}_1^\dagger \mathbf{M}_0^{-1} \mathbf{e}_1 \right)^{-1}. \quad (5.34)$$

If all \mathbf{x}_j are equally-spaced on the boundary of the unit disk (such as shown in Fig. 6(b)), then the matrix \mathbf{G} is circulant and symmetric, so that its eigenvectors and eigenvalues are known exactly (see Sec. 2.5). Moreover, the matrix \mathbf{M}_0 admits a spectral representation and thus can be inverted explicitly. Using Eq. (2.36), we get

$$\mathbf{e}_1^\dagger \mathbf{M}_0^{-1} \mathbf{e} = 1, \quad \mathbf{e}_1^\dagger \mathbf{M}_0^{-1} \mathbf{e}_1 = (\mathbf{e}_1^\dagger \mathbf{q}_N)(\mathbf{q}_N^\dagger \mathbf{e}_1) + \sum_{j=1}^{N-1} \frac{(\mathbf{e}_1^\dagger \mathbf{q}_j)(\mathbf{q}_j^\dagger \mathbf{e}_1)}{1 + \nu\kappa_j}, \quad (5.35)$$

where \mathbf{q}_j and κ_j were defined by Eqs. (2.32, 2.40). However, since $(\mathbf{e}_1^\dagger \mathbf{q}_j) = \omega^j/\sqrt{N}$ and $(\mathbf{q}_j^\dagger \mathbf{e}_1) = \omega^{-j}/\sqrt{N}$, we get

$$\mathbf{e}_1^\dagger \mathbf{M}_0^{-1} \mathbf{e}_1 = \frac{1}{N} \left[1 + \sum_{j=1}^{N-1} (1 + \nu\kappa_j)^{-1} \right]. \quad (5.36)$$

Substituting this expression together with Eq. (5.35) into Eq. (5.34), we find

$$C = -\frac{N}{\nu} \left(\sum_{j=1}^{N-1} \frac{1}{1 + \nu\kappa_j} \right)^{-1}. \quad (5.37)$$

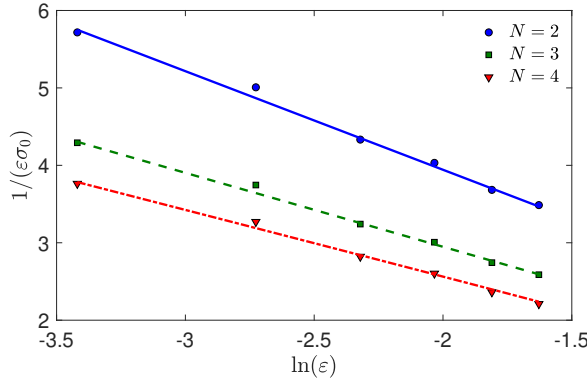


Figure 9. Dependence of $1/(\varepsilon\sigma_0)$ on ε for the unit disk with one Steklov patch of length 2ε (located at $\mathbf{x}_0 = (1, 0)$), and $N - 1$ Dirichlet patches of length 4ε , equally-spaced on the boundary of the unit disk. Symbols present the numerical solution by a FEM with the maximal meshsize $h_{\max} = 0.005$ and lines show Eq. (5.38).

As a result, Eqs. (5.25, 5.33) with $C_1 = 3/2 - \ln 2$ imply

$$\begin{aligned} \frac{1}{\varepsilon_1\sigma_0} &\approx -\frac{2}{\pi} [\mathcal{C}(-\sigma\varepsilon_1) - C_1] = -\frac{2}{\pi} [C + \ln\left(\frac{2\varepsilon_1}{\varepsilon}\right) - C_1] \\ &\approx \frac{2}{\pi} \left[\frac{N}{\sum_{j=1}^{N-1} (\ln(2/\varepsilon) + \kappa_j)^{-1}} + C_1 - \ln\left(\frac{2\varepsilon_1}{\varepsilon}\right) \right]. \end{aligned} \quad (5.38)$$

Figure 9 illustrates the behavior of $1/(\varepsilon_1\sigma_0)$ as a function of $\ln(\varepsilon)$ for the unit disk with one Steklov patch of length 2ε , and several Dirichlet patches of length 4ε , which are equally-spaced on the boundary of the unit disk. We observe an excellent agreement between the asymptotic formula (5.38) and numerical results.

Although the eigenvalues κ_j are known explicitly via Eq. (2.40), it is instructive to inspect their asymptotic behavior for large N (see Appendix B). We aim at approximating the sum in the denominator of Eq. (5.38):

$$S = \frac{1}{N} \sum_{j=1}^{N-1} \frac{1}{\ln(2/\varepsilon) + \kappa_j}. \quad (5.39)$$

The degeneracy $\kappa_{N-j} = \kappa_j$ allows us to limit this sum to $j \leq N/2$ when N is even. By using the asymptotic result in Eq. (B 13) for κ_j when $N \gg 1$, we find that

$$\ln(2/\varepsilon) + \kappa_j \approx \frac{1}{2\xi} + \zeta + a \frac{\pi^2 \xi^2}{9}, \quad (5.40)$$

where we have defined $\xi = j/N$,

$$\zeta = -\ln\left(\frac{N\varepsilon}{b}\right), \quad \text{and} \quad b = 4\pi e^{-11/6} \approx 2.009. \quad (5.41)$$

Here the coefficient $a = 1.25$ was empirically introduced to improve the accuracy of the approximation of κ_j (see Appendix B for details). In terms of ζ , and substituting $j/N = \xi$, we view S as a Riemannian approximation of the integral defined by

$$S \approx S(\zeta) = 4 \int_0^{1/2} \frac{\xi d\xi}{1 + 2\xi(\zeta + a\pi^2\xi^2/9)}. \quad (5.42)$$

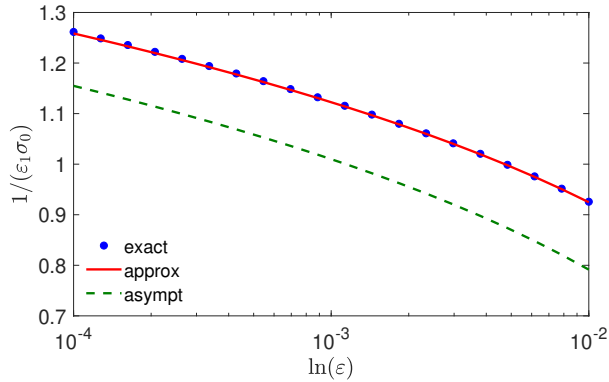


Figure 10. Dependence of $1/(\varepsilon_1 \sigma_0)$ on ε for the unit disk with the Steklov patch of length $2\varepsilon_1 = 0.2$ and 63 Dirichlet patches (each of length 2ε) that are equally-spaced on the boundary of the unit disk. Filled circles correspond to κ_j obtained via the discrete sum (5.38), the solid line indicates its large- N approximation (5.43), and the dashed line is the low-order approximation (5.44).

As a result, Eq. (5.38) is approximated for $N \gg 1$ by

$$\frac{1}{\varepsilon_1 \sigma_0} \approx \frac{2}{\pi} \left[\frac{1}{S(\zeta)} + C_1 - \ln \left(\frac{2\varepsilon_1}{\varepsilon} \right) \right], \quad (5.43)$$

where ζ is defined in Eq. (5.41). In this way, we have reduced the problem of estimating $1/(\varepsilon_1 \sigma_0)$ to a simple numerical quadrature of the function $S(\zeta)$ in Eq. (5.42). To obtain a more explicit, but less accurate, approximation, we neglect the $a\pi^2\xi^2/9$ term in Eq. (5.42), which corresponds to using the result (B 12) for κ_j , and then evaluate the resulting integral to get $S = (\zeta - \ln(1 + \zeta)) / \zeta^2$. In this way, Eq. (5.38) can be approximated more explicitly as

$$\frac{1}{\varepsilon_1 \sigma_0} \approx \frac{2}{\pi} \left[\frac{\zeta^2}{\zeta - \ln(1 + \zeta)} + C_1 - \ln \left(\frac{2\varepsilon_1}{\varepsilon} \right) \right]. \quad (5.44)$$

For 63 Dirichlet patches (i.e. $N = 64$) and with $\varepsilon_1 = 0.1$, Fig. 10 compares the asymptotic results obtained by using the discrete sum (5.38) with its large- N approximation (5.43) and with the simpler, more explicit, result (5.44). We observe that Eq. (5.43) provides an excellent approximation, while Eq. (5.44) has a small systematic underestimate.

6 Further extensions

In the previous four sections, we progressively increased the complexity of the problem: (i) N perfectly reactive (Dirichlet) patches; (ii) N partially reactive (Robin) patches; (iii) N imperfect (Steklov) patches; and (iv) one imperfect patch with $N - 1$ Dirichlet patches. We showed that the asymptotic analysis required to study these settings is similar, although the resulting formulas became progressively more intricate. In the same vein, we can treat any combination of perfectly reactive, partially reactive and imperfect patches.

In this section, we briefly discuss two other extensions that are relevant for applications: the case of interior targets (Sec. 6.1) and the exterior problem (Sec. 6.2).

6.1 Interior targets

Throughout this paper, we focused on reactive patches on the boundary of a bounded domain. In many applications, however, absorbing sinks, traps and/or reactive targets can be hidden *inside* a bounded domain Ω_0 , surrounded by

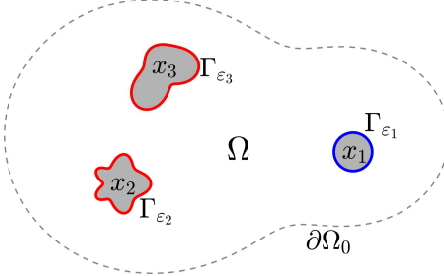


Figure 11. Illustration of a bounded domain $\Omega \subset \mathbb{R}^2$ with a smooth reflecting boundary $\partial\Omega_0$ (gray dashed line) and three interior targets Ω_{ε_j} (filled in gray), centered at \mathbf{x}_j , with reactive boundaries Γ_{ε_j} (in red and blue). For a particle started from a point $\mathbf{x} \in \Omega$, the splitting probability $S_1(\mathbf{x})$ is the probability of hitting the boundary Γ_{ε_1} first.

a reflecting boundary $\partial\Omega_0$. Let us consider the problem with N interior targets, where each target is a compact set $\Omega_{\varepsilon_j} \subset \Omega_0$ of size ε_j , centered at a point \mathbf{x}_j (Fig. 11). Since the targets are impenetrable for a diffusing particle, we still consider surface reactions on their boundaries, denoted as $\Gamma_{\varepsilon_j} = \partial\Omega_{\varepsilon_j}$. As before, the targets are small ($\varepsilon_j \sim o(1)$), comparable in size, and well-separated from each other: $|\mathbf{x}_j - \mathbf{x}_k| \sim \mathcal{O}(1)$ for $j \neq k$, and from the domain boundary $\partial\Omega_0$: $|\mathbf{x}_j - \mathbf{x}| \sim \mathcal{O}(1)$ for any $\mathbf{x} \in \partial\Omega_0$. This setting represents diffusion in a perforated domain $\Omega = \Omega_0 \setminus (\Omega_{\varepsilon_1} \cup \dots \cup \Omega_{\varepsilon_N})$ with the boundary $\partial\Omega = \partial\Omega_0 \cup \Gamma_{\varepsilon_1} \cup \dots \cup \Gamma_{\varepsilon_N}$. These notations allow us to make an equivalence with the earlier setting introduced at the beginning of Sec. 2. In particular, we can retain the same formulations of the four considered problems. As expected, their solutions can be constructed analogously, but with some modifications in the ‘‘building blocks’’. In this section, we briefly describe these modifications and illustrate a few results.

Perfectly reactive targets: Dirichlet boundary condition

If the j -th target is perfectly reactive (with Dirichlet condition), the inner solution around this target is proportional to the exterior Dirichlet Green’s function

$$\Delta g_\infty = 0 \quad \text{in } \mathbb{R}^2 \setminus \Omega_j ; \quad g_\infty = 0 \quad \text{on } \partial\Omega_j ; \quad g_\infty \sim \ln |\mathbf{y}| + \mathcal{O}(1) \quad \text{as } |\mathbf{y}| \rightarrow \infty , \quad (6.1)$$

where $\Omega_j = \varepsilon_j^{-1} \Omega_{\varepsilon_j}$ is the rescaled target Ω_{ε_j} . In contrast to the earlier studied case of a Dirichlet patch, the Green’s function $g_\infty(\mathbf{y})$ depends on the shape of the target Ω_j and thus is not universal. In particular, its asymptotic behavior is $g_\infty(\mathbf{y}) \sim \ln |\mathbf{y}| - \ln(d_j) + o(1)$ as $|\mathbf{y}| \rightarrow \infty$, where d_j is the logarithmic capacity of Ω_j . For instance, if Ω_j is the unit disk, its logarithmic capacity is 1. Numerical values for d_j for various shapes of Ω_j are given in Table 1 of [54].

In addition, the outer solution involves the Neumann Green’s function $G_b(\mathbf{x}, \xi)$ (also known as pseudo-Green’s function) that satisfies

$$\Delta G_b = \frac{1}{|\Omega_0|} - \delta(\mathbf{x} - \xi) \quad \text{in } \Omega_0 ; \quad \partial_n G_b = 0 \quad \text{on } \partial\Omega_0 ; \quad \int_{\Omega_0} G_b(\mathbf{x}, \xi) d\mathbf{x} = 0 , \quad (6.2a)$$

$$G_b(\mathbf{x}, \xi) \sim -\frac{1}{2\pi} \ln |\mathbf{x} - \xi| + R_b(\xi) + o(1) \quad \text{as } \mathbf{x} \rightarrow \xi \in \Omega_0 , \quad (6.2b)$$

where we added the subscript b to distinguish it from the surface Neumann Green’s function $G(\mathbf{x}, \xi)$. The main difference between this Green’s function and the surface Neumann Green’s function defined by Eqs. (2.9) is that the singularity at ξ is located in the bulk and not on the boundary (accordingly, there is the factor $1/(2\pi)$ in Eq. (6.2b)

instead of $1/\pi$). For instance, when Ω_0 is the unit disk, the Neumann Green's function is well-known [51]:

$$G_b(\mathbf{x}, \boldsymbol{\xi}) = -\frac{1}{2\pi} \ln |\mathbf{x} - \boldsymbol{\xi}| - \frac{1}{4\pi} \ln (|\mathbf{x}|^2 |\boldsymbol{\xi}|^2 + 1 - 2\mathbf{x} \cdot \boldsymbol{\xi}) + \frac{|\mathbf{x}|^2 + |\boldsymbol{\xi}|^2}{4\pi} - \frac{3}{8\pi}, \quad (6.3a)$$

$$R_b(\boldsymbol{\xi}) = -\frac{1}{2\pi} \ln (1 - |\boldsymbol{\xi}|^2) + \frac{|\boldsymbol{\xi}|^2}{2\pi} - \frac{3}{8\pi}. \quad (6.3b)$$

We remark that rapidly converging infinite series representations for G_b and R_b are also known explicitly for ellipses (see Eqs. (4.6, 4.7) from [49]) and for rectangles (see Eq. (4.13) of Section 4.2 of [52], as well as [61]).

With these minor changes in the “building blocks”, we can repeat the steps in Secs. 2.2 and 2.3 to obtain that the splitting probability $S_k(\mathbf{x})$ is

$$S_k(\mathbf{x}) = \chi_k - \sum_{i=1}^N 2\pi A_i G_b(\mathbf{x}, \mathbf{x}_i), \quad (6.4)$$

where the coefficients χ_k and A_i are still determined via Eqs. (2.17, 2.21), but now with $\nu_j = -1/\ln(\varepsilon_j d_j)$. Note also that the matrix \mathbf{G} from Eq. (2.15) is now based on the Neumann Green's function $G_b(\mathbf{x}, \boldsymbol{\xi})$ from Eqs. (6.2) and its regular part $R_b(\boldsymbol{\xi})$. In addition, the factor π in the definition (2.14) of the elements of the matrix \mathbf{G} should be replaced by 2π . The example of two targets can be worked out explicitly. Moreover, equally-spaced targets located on a circular ring that is concentric within a unit disk can also be treated explicitly.

Partially reactive targets: Robin boundary condition

If the j -th target is *partially reactive*, we should replace the Dirichlet boundary condition by a Robin condition with the reactivity parameter q_j . In the same vein, the former Robin Green's function $g_\mu(\mathbf{y})$ now satisfies

$$\Delta g_\mu = 0 \quad \text{in } \mathbb{R}^2 \setminus \Omega_j; \quad \partial_n g_\mu + \mu g_\mu = 0 \quad \text{on } \partial \Omega_j; \quad g_\mu \sim \ln |\mathbf{y}| + \mathcal{C}_j(\varepsilon_j q_j) + o(1) \quad \text{as } |\mathbf{y}| \rightarrow \infty, \quad (6.5)$$

with $\mu = \varepsilon_j q_j$. In particular, the constant term $\mathcal{C}_j(\mu)$ of its asymptotic behavior at infinity is not universal and depends on the shape of Ω_j . We can still employ the eigenmodes of the exterior Steklov problem in $\mathbb{R}^2 \setminus \Omega_j$ to construct $g_\mu(\mathbf{y})$ and to determine the spectral expansion for $\mathcal{C}_j(\mu)$:

$$\mathcal{C}_j(\mu) = -\ln(d_j) + \frac{2\pi}{\mu |\partial \Omega_j|} + 2\pi \sum_{k=1}^{\infty} \frac{[\Psi_k^j(\infty)]^2}{\mu_k^j + \mu}, \quad (6.6)$$

where μ_k^j and Ψ_k^j are the eigenvalues and eigenfunctions of the auxiliary exterior Steklov problem,

$$\Delta \Psi_k^j = 0 \quad \text{in } \mathbb{R}^2 \setminus \Omega_j; \quad \partial_n \Psi_k^j = \mu_k^j \Psi_k^j \quad \text{on } \partial \Omega_j; \quad \Psi_k^j \sim \mathcal{O}(1) \quad \text{as } |\mathbf{y}| \rightarrow \infty. \quad (6.7)$$

We also used the normalization $\Psi_0^j = 1/\sqrt{|\partial \Omega_j|}$ of the principal eigenfunction associated to $\mu_0^j = 0$. As earlier, a partially reactive target can be treated a perfect one, but with the reduced size:

$$\varepsilon_j^{\text{eff}} = \varepsilon_j \exp(-\ln(d_j) - \mathcal{C}_j(\varepsilon_j q_j)), \quad (6.8)$$

(see further discussion and examples in Sec. 3).

For the target Ω_j of an arbitrary shape, the computation of the Steklov eigenmodes μ_k^j and Ψ_k^j requires numerical techniques (e.g., a finite-element method, see [10, 38] and references therein). However, if the rescaled target Ω_j is the unit disk, the eigenmodes are known explicitly and they all vanish at infinity, except Ψ_0^j . As the logarithmic capacity of the unit disk is equal to 1, we get a particularly simple *exact* expression:

$$\mathcal{C}_{\text{disk}}(\mu) = \frac{1}{\mu}. \quad (6.9)$$

This is not surprising given that the exterior Green's function for the unit disk is simply $g_\mu(\mathbf{y}) = 1/\mu + \ln|\mathbf{y}|$.

Imperfect targets

In a similar way, we can easily reproduce the derivations of Secs. 4 and 5 for the mixed Steklov-Neumann and Steklov-Neumann-Dirichlet problems. For an imperfect target Ω_{ε_j} of arbitrary shape, the main difficulty is the lack of knowledge of the function $\mathcal{C}_j(\mu)$, which is formally accessible via the spectral expansion (6.6) but its “ingredients” require numerical computations. Moreover, as the coefficients of the Taylor expansion of $\mathcal{C}_j(\mu)$ are unknown, we cannot rely on the approximation (3.10). As a consequence, many numerical steps would be involved, and the analytical, almost explicit form of the asymptotic results would in general be lost. An interesting extension of this work consists of a systematic study of the function $\mathcal{C}_j(\mu)$ for targets of various shapes.

A drastic simplification appears when the imperfect targets are disks due the explicit form (6.9) of the function $\mathcal{C}(\mu)$. In this case, the analysis of Secs. 4 and 5 can be reproduced and will actually be even simpler. For instance, for the mixed Steklov-Neumann-Dirichlet problem with a single disk-shaped target Ω_{ε_1} and one perfectly reactive target Ω_{ε_2} (of arbitrary shape), one can rewrite Eq. (5.28) as

$$C = \ln(d_2 \varepsilon_1 \varepsilon_2) - 2\pi [R_b(\mathbf{x}_1) + R_b(\mathbf{x}_2) - 2G_b(\mathbf{x}_1, \mathbf{x}_2)], \quad (6.10)$$

from which the principal eigenvalue reads

$$\frac{1}{\varepsilon_1 \sigma_0} \approx -\ln(d_2 \varepsilon_1 \varepsilon_2) + 2\pi [R_b(\mathbf{x}_1) + R_b(\mathbf{x}_2) - 2G_b(\mathbf{x}_1, \mathbf{x}_2)]. \quad (6.11)$$

Figure 12 illustrates the accuracy of the asymptotic relation (6.11) for the unit disk with two interior circular targets. We observe a close agreement between a numerical solution and the asymptotic formula. One can notice a small deviation between two lines that slightly increases as the target radius ε_2 decreases. This minor discrepancy seems to be a numerical artefact due to the available meshsize 0.005, which becomes comparable to the target at small ε_2 . To check this point, we computed the eigenvalue of the mixed Steklov-Dirichlet problem for a circular annulus with radii ε_2 and $R = 1$, with Steklov condition on the outer circle and Dirichlet condition on the inner circle. As the exact solution of this problem is known, $\sigma_0 = 1/(R \ln(R/\varepsilon_2))$, we could compare it with the numerical results, and found the same minor discrepancy.

In summary, we conclude that interior targets can be handled in essentially the same way as boundary patches, even though the asymptotic analysis becomes sensitive to the shapes of the targets. Moreover, one can combine interior targets with boundary patches that opens a way to access a broad variety of various geometric settings.

6.2 Exterior problems

Another extension of the present approach is related to exterior problems in $\Omega = \mathbb{R}^2 \setminus \Omega_0$, where Ω_0 is a simply-connected compact domain. While the inner solutions remain unchanged, the outer solution is now constructed using the exterior surface Neumann Green's function, labeled by G_e , which satisfies

$$\Delta G_e = 0 \quad \text{in } \mathbb{R}^2 \setminus \Omega_0, \quad (6.12a)$$

$$G_e(\mathbf{x}, \boldsymbol{\xi}) \sim -\frac{1}{\pi} \ln |\mathbf{x} - \boldsymbol{\xi}| + R_e(\boldsymbol{\xi}) + o(1) \quad \text{as } \mathbf{x} \rightarrow \boldsymbol{\xi} \in \partial\Omega_0; \quad \partial_n G_e = 0 \quad \text{on } \partial\Omega_0 \setminus \{\boldsymbol{\xi}\}, \quad (6.12b)$$

$$G_e(\mathbf{x}, \boldsymbol{\xi}) \sim -\frac{1}{2\pi} \ln |\mathbf{x}| + o(1) \quad \text{as } |\mathbf{x}| \rightarrow \infty, \quad (6.12c)$$

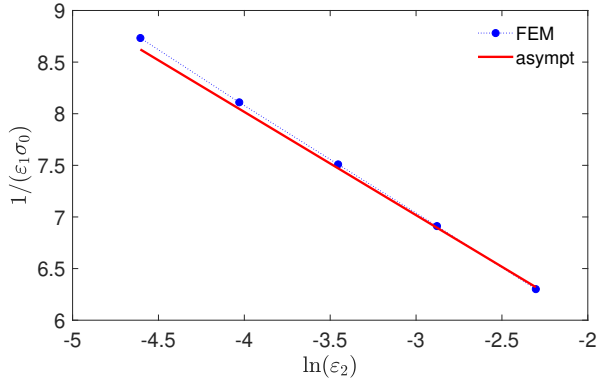


Figure 12. The asymptotic behavior of the principal eigenvalue of the mixed Steklov-Neumann-Dirichlet problem, plotted as $1/(\varepsilon_1 \sigma_0)$ versus ε_2 , for the unit disk with two interior circular targets of radii $\varepsilon_1 = 0.05$ and ε_2 (variable from 0.01 to 0.1), located at $\mathbf{x}_1 = (-0.5, 0)$ and $\mathbf{x}_2 = (0.5, 0)$. Filled circles present the numerical solution by a FEM with the maximal meshsize of 0.005, solid line indicates Eq. (6.11).

where $R_e(\xi)$ is the regular part of $G_e(\mathbf{x}, \xi)$ at ξ . The condition that $G_e(\mathbf{x}, \xi) + (2\pi)^{-1} \ln |\mathbf{x}| \rightarrow 0$ as $|\mathbf{x}| \rightarrow \infty$ determines G_e uniquely.

In the case when Ω_0 is the unit disk and $|\xi| = 1$, we claim that

$$G_e(\mathbf{x}, \xi) = -\frac{1}{\pi} \ln |\mathbf{x} - \xi| + \frac{1}{2\pi} \ln |\mathbf{x}|, \quad R_e(\xi) = 0. \quad (6.13)$$

Clearly Eq. (6.13) satisfies the behavior (6.12 c) as $|\mathbf{x}| \rightarrow \infty$ as well as Eq. (6.12 b) as $\mathbf{x} \rightarrow \xi$, where we identify that $R_e(\xi) = 0$ (see more details in Appendix F.1).

For instance, if there are two patches on the unit circle, the solution of any of four earlier considered problems involves

$$R_e(\mathbf{x}_1) + R_e(\mathbf{x}_2) - 2G_e(\mathbf{x}_1, \mathbf{x}_2) = \frac{2}{\pi} \ln |\mathbf{x}_1 - \mathbf{x}_2|, \quad (6.14)$$

which is identical for both interior and exterior domains. This property is consistent with the fact that the eigenvalues of interior and exterior mixed Steklov problems for the unit disk are identical. In contrast, the associated eigenfunctions behave differently.

7 Discussion

In this paper, we have established a general mathematical framework for studying the competition of small targets for a diffusing particle in planar domains. Using the method of matched asymptotic expansions, as tailored for problems with localized defects [79] and with logarithmic gauge functions [78], we solved four different problems of increasing complexity in the boundary conditions: (i) splitting probabilities for perfectly reactive patches with Dirichlet condition; (ii) their extension to partially reactive patches with Robin condition; (iii) mixed Steklov-Neumann problem describing imperfect patches; and (iv) mixed Steklov-Neumann-Dirichlet problem describing the escape of a particle through Dirichlet patches in the presence of an imperfect patch. Although the first problem was thoroughly studied in the past, we have improved some former results. To our knowledge, the asymptotic behavior for the three other problems in the small-target limit has not been reported previously. Moreover, we discussed two further extensions of our results to the case of interior targets and to exterior problems. The established asymptotic formalism in our 2-D

setting can be applied to a broad variety of natural and industrial phenomena such as diffusion-controlled reactions in chemistry and biology.

It would be worthwhile to extend our analytical framework to determine high-order asymptotic expansions to treat analogous 3-D problems with many either partially reactive or imperfect (Steklov) patches on the domain boundary. For a locally circular partially reactive patch on the boundary of a 3-D domain, a leading-order asymptotic theory was derived in [9] to determine the mean first-passage time for small, intermediate, and large patch reactivities. In [43], the large reactivity limit was analyzed in detail. However, it is an open problem to derive high-order asymptotic expansions allowing for multiple partially reactive or imperfect patches, as the local geometry of the domain boundary will play a key role in the analysis.

Acknowledgements

The authors thank professors I. Polterovich and M. Levitin for fruitful discussions, and A. Chaigneau for his implementation of the FEM code. D.S.G. acknowledges the Simons Foundation for supporting his sabbatical sojourn in 2024 at the CRM, University of Montréal, Canada, and the Alexander von Humboldt Foundation for support within a Bessel Prize award. M.J.W. was supported by the NSERC Discovery grant program.

Competing interests declaration

Competing interests: The author(s) declare none

Appendix A Green's function for the Dirichlet patch in the half-plane

The Green's function satisfying Eq. (2.3) can be found exactly. Even though this solution is classical [69] we reproduce it here for completeness. For this purpose, we use the elliptic coordinates for an ellipse with semi-axes $a > b$:

$$y_1 = a_E \cosh \alpha \cos \theta, \quad y_2 = a_E \sinh \alpha \sin \theta, \quad (\text{A } 1)$$

where $a_E = \sqrt{a^2 - b^2}$, $\alpha \geq 0$ and $-\pi < \theta \leq \pi$. It is worth noting that all points on the horizontal interval $(-a_E, a_E) \times \{0\}$ correspond to $\alpha = \theta = 0$ and are thus indistinguishable.

In our setting, we fix $a = 1$ and $b = 0$. We search for $g_\infty(\mathbf{y})$ in the form

$$g_\infty(\mathbf{y}) = \ln |\mathbf{y}| - \ln(d) - \sum_{n=1}^{\infty} c_n \cos(n\theta) e^{-n\alpha}, \quad (\text{A } 2)$$

with unknown coefficients c_n . This is a general form of a harmonic function, which behaves as $\ln |\mathbf{y}| - \ln(d)$ at infinity and satisfies the condition $\partial_n g_\infty = 0$ on $|y_1| > 1$, $y_2 = 0$. The coefficients c_n are determined by the condition $g_\infty = 0$ on $|y_1| \leq 1$, $y_2 = 0$, which yields

$$0 = \ln |\cos \theta| - \ln(d) - \sum_{n=1}^{\infty} c_n \cos(n\theta), \quad (0 \leq \theta \leq \pi) \quad (\text{A } 3)$$

(here we restrict the analysis to the upper half-plane, with $\theta \geq 0$). Using the expansion

$$\ln(2|z - z_0|) = - \sum_{n=1}^{\infty} \frac{2}{n} T_n(z) T_n(z_0), \quad (\text{A } 4)$$

where $T_n(\cos z) = \cos(nz)$ are the Chebyshev polynomials and $z_0 = 0$, we immediately see that the boundary

condition (A 3) implies

$$\ln(d) = -\ln(2), \quad c_n = \frac{2}{n}. \quad (\text{A } 5)$$

The solution then reads

$$g_\infty(\mathbf{y}) = \ln|\mathbf{y}| + \ln(2) - \sum_{n=1}^{\infty} \frac{2}{n} \cos(n\theta) e^{-n\alpha}. \quad (\text{A } 6)$$

By summing this series in terms of the logarithm we get

$$g_\infty(\mathbf{y}) = \ln|\mathbf{y}| + \ln(2) - \ln(1 - 2\cos\theta e^{-\alpha} + e^{-2\alpha}). \quad (\text{A } 7)$$

Note that the elliptic coordinates α and θ can be easily expressed in terms of $\mathbf{y} = (y_1, y_2)$ by setting

$$r_\pm = \sqrt{(y_1 \pm a_E)^2 + y_2^2} = a_E(\cosh\alpha \pm \cos\theta), \quad (\text{A } 8)$$

from which

$$\cosh\alpha = \frac{r_+ + r_-}{2a_E}, \quad \cos\theta = \frac{r_+ - r_-}{2a_E}. \quad (\text{A } 9)$$

Using Eq. (A 6), we calculate that

$$-\partial_n g_\infty|_{(-1,1)} = \left(\frac{1}{h_\alpha} \partial_\alpha g_\infty \right)_{\alpha=0} = \frac{1}{|\sin\theta|} = \frac{1}{\sqrt{1 - y_1^2}}, \quad (\text{A } 10)$$

where we used $h_\alpha = a_E \sqrt{\cosh^2\alpha - \cos^2\theta} = |\sin\theta|$ at $\alpha = 0$ for the scale factor. In particular, the integral of this expression over the interval $(-1, 1)$ is equal to π , as expected from the divergence theorem.

Appendix B Limit of many small targets

In this Appendix, we study the large- N behavior of the eigenvalues κ_j , given in Eq. (2.41), of the matrix \mathbf{G} for N identical equally-spaced patches on the boundary of the unit disk. Since the κ_j are the eigenvalues of the symmetric and circulant matrix \mathbf{G} , we have $\kappa_j = \kappa_{N-j}$ for $j = 1, \dots, N/2$ when N is even. As such, we need only estimate κ_j for $j = 1, \dots, N/2$ when $N \gg 1$ is even.

To do so, we use the Euler-Maclaurin expansion for a C^∞ function $f(\theta)$ on $1 \leq \theta \leq N-1$, which is given by

$$\sum_{m=1}^{N-1} f(m) = \int_1^{N-1} f(\theta) d\theta + \frac{1}{2} [f(N-1) + f(1)] + \frac{1}{12} [f'(N-1) - f'(1)] + \dots, \quad (\text{B } 1)$$

where from Eq. (2.41) we define $f(\theta)$ by

$$f(\theta) = \cos(2ja\theta) \ln[\sin(a\theta)], \quad a = \frac{\pi}{N}. \quad (\text{B } 2)$$

From Eq. (2.41) we identify

$$\kappa_j = \ln 2 - \sum_{m=1}^{N-1} f(m), \quad j \in \{1, \dots, N/2\}. \quad (\text{B } 3)$$

We first estimate the integral in Eq. (B 1), labeled by $I = \int_1^{N-1} f(\theta) d\theta$. Upon substituting $x = a\theta$, we get

$$I = \frac{N}{\pi} \int_0^\pi \cos(2jx) \ln(\sin x) dx - \frac{2N}{\pi} \int_0^{\pi/N} \cos(2jx) \ln(\sin x) dx. \quad (\text{B } 4)$$

The first integral on the right-side of Eq. (B 4) can be evaluated explicitly as $-\pi/(2j)$, whereas in the second integral

we use $\sin(x) \approx x$ on the range $0 < x < \pi/N$, which is valid for $N \gg 1$. In this way, for $N \gg 1$ we obtain

$$I \sim -\frac{N}{2j} - \frac{2N}{\pi} \int_0^{\pi/N} \cos(2jx) \ln x \, dx. \quad (\text{B } 5)$$

Upon integrating by parts in Eq. (B 5), we find that

$$I \sim -\frac{N}{2j} - \frac{N}{\pi j} \sin\left(\frac{2\pi j}{N}\right) \ln\left(\frac{\pi}{N}\right) + \frac{N}{\pi j} \text{Si}\left(\frac{2\pi j}{N}\right), \quad (\text{B } 6)$$

where $\text{Si}(x) = \int_0^x \xi^{-1} \sin \xi \, d\xi$ is the sine integral function. Moreover, we readily calculate for $N \gg 1$ that

$$f(1) = f(N-1) \sim \cos\left(\frac{2\pi j}{N}\right) \ln\left(\frac{\pi}{N}\right), \quad (\text{B } 7a)$$

$$f'(1) = -f'(N-1) \sim -\frac{2\pi j}{N} \sin\left(\frac{2\pi j}{N}\right) \ln\left(\frac{\pi}{N}\right) + \cos\left(\frac{2\pi j}{N}\right). \quad (\text{B } 7b)$$

Upon substituting Eqs. (B 6, B 7) into Eq. (B 1), and recalling Eq. (B 3), we conclude for $N \gg 1$ and for $j = 1, \dots, N/2$ that

$$\kappa_j \sim \frac{N}{2j} + \ln\left(\frac{\pi}{N}\right) \mathcal{B}\left(\frac{j}{N}\right) + \ln 2 + \frac{1}{6} \cos\left(\frac{2\pi j}{N}\right) - \frac{N}{\pi j} \text{Si}\left(\frac{2\pi j}{N}\right), \quad (\text{B } 8)$$

where $\mathcal{B}(\xi)$, with $\xi = j/N$, is defined by

$$\mathcal{B}(\xi) = \frac{1}{\pi \xi} \sin(2\pi \xi) - \cos(2\pi \xi) - \frac{\pi \xi}{3} \sin(2\pi \xi). \quad (\text{B } 9)$$

We calculate from a Maclaurin series that $\mathcal{B}(\xi) = 1 + (2\pi \xi)^4/360 + \mathcal{O}(\xi^6)$, and so we will approximate $\mathcal{B}(\xi) \approx 1$ on $0 < \xi < 1/2$. We then write Eq. (B 8) as

$$\kappa_j \sim \frac{N}{2j} + \ln\left(\frac{2\pi e^{-11/6}}{N}\right) + \mathcal{D}\left(\frac{j}{N}\right), \quad (\text{B } 10a)$$

where $\mathcal{D}(\xi)$, with $\mathcal{D}(0) = 0$, is defined by

$$\mathcal{D}(\xi) = \frac{11}{6} + \frac{1}{6} \cos(2\pi \xi) - \frac{1}{\pi \xi} \text{Si}(2\pi \xi). \quad (\text{B } 10b)$$

By using $\cos z \sim 1 - z^2/2$ and $\text{Si}(z) \sim z - z^3/18$, the Maclaurin series for $\mathcal{D}(\xi)$ is $\mathcal{D}(\xi) = \pi^2 \xi^2/9 + \mathcal{O}(\xi^4)$. From this lowest-order approximation, Eq. (B 10) becomes

$$\kappa_j \sim \frac{N}{2j} + \ln\left(\frac{2\pi e^{-11/6}}{N}\right) + \frac{\pi^2 j^2}{9N^2}, \quad (\text{B } 11)$$

which should be rather accurate if $j \ll N/2$. Neglecting the correction term in Eq. (B 11) gives a simpler, but less accurate, approximation

$$\kappa_j \sim \frac{N}{2j} + \ln\left(\frac{2\pi e^{-11/6}}{N}\right). \quad (\text{B } 12)$$

Table B 1 illustrates the accuracy of the three approximate relations (B 8, B 11, B 12) for two cases: $N = 16$ and $N = 64$. Even for a moderate number of patches ($N = 16$), these three relations approximate κ_1 very accurately. As the index j increases, the accuracy of both relations expectedly reduces but remains good. The accuracy is even higher when $N = 64$.

In turn, Fig. B 1 illustrates the accuracy of the approximations (B 11) and (B 12) on a broader range $1/5 < j/N < 1/2$, for $N = 64$. While both approximations are accurate at small j/N , one can still observe deviations for j/N around $1/2$. These deviations have (at least) two origins: (i) neglection of higher-order terms $\mathcal{O}(\xi^4)$, and (ii) omission of the higher-order derivatives in the Euler-Maclaurin expansion (B 1). A careful examination of the next-order term

	j	1	2	3	4	5	6	7	8
$N = 16$	Eq. (2.41)	5.2321	1.2465	-0.0623	-0.6931	-1.0443	-1.2465	-1.3529	-1.3863
	Eq. (B8)	5.2362	1.2489	-0.0634	-0.6986	-1.0514	-1.2442	-1.3179	-1.2804
	Eq. (B11)	5.2320	1.2491	-0.0628	-0.6995	-1.0610	-1.2805	-1.4153	-1.2740
	Eq. (B12)	5.2362	1.2320	-0.1014	-0.7680	-1.1680	-1.4347	-1.4939	-1.7680
$N = 64$	Eq. (2.41)	27.8414	11.8423	6.5104	3.8458	2.2485	1.1851	0.4271	-0.1398
	Eq. (B8)	27.8459	11.8467	6.5147	3.8498	2.2521	1.1881	0.4293	-0.1388
	Eq. (B11)	27.846	11.8470	6.5147	3.8499	2.2524	1.1886	0.43021	-0.1372
	Eq. (B12)	27.8457	11.8457	6.5123	3.8457	2.2457	1.1790	0.4171	-0.1543

Table B 1. Comparison between the exact values of κ_j from Eq. (2.41), their approximation (B8), and its simpler asymptotic forms (B11) and (B12).

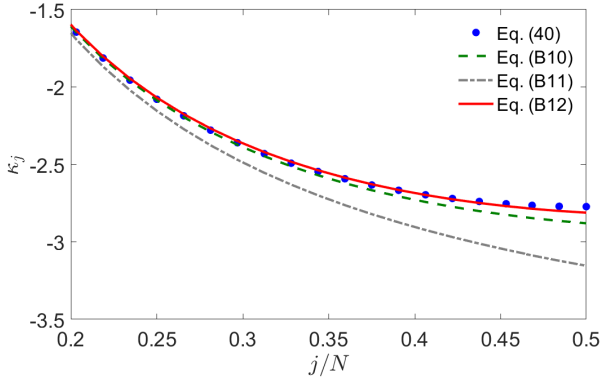


Figure B 1. Exact values of κ_j versus j/N on $0.2 < j/N < 0.5$ for $N = 64$ from Eq. (2.41), shown by filled circles, and their approximations (B11, B12, B13) shown by lines.

in this expansion, $-\frac{1}{720}(f'''(N-1) - f'''(1))$, reveals that it yields the contribution $\frac{1}{90}\pi^2 j^2/N^2$ to κ_j that increases by 10% the last term in Eq. (B11). Skipping a systematic analysis of these higher-order contributions, we adjust the coefficient in front of this term to get an empirical approximation:

$$\kappa_j \sim \frac{N}{2j} + \ln\left(\frac{2\pi e^{-11/6}}{N}\right) + 1.25 \frac{\pi^2 j^2}{9N^2}. \quad (\text{B13})$$

In this way, we achieve a decent approximation over the whole range of j/N , as illustrated by the solid line in Fig. B 1.

Appendix C Green's function for the Robin patch in the half-plane

In this Appendix, we obtain the exact form of the Robin Green's function satisfying Eq. (3.3) in the upper half-plane. We will determine $g_\mu(\mathbf{y})$ in the form

$$g_\mu(\mathbf{y}) = g_\infty(\mathbf{y}) + \sum_{k=0}^{\infty} c_k \Psi_k(\mathbf{y}), \quad (\text{C1})$$

where $g_\infty(\mathbf{y})$ is the Dirichlet Green's function satisfying (2.3) with Dirichlet condition on the interval $(-1, 1)$, c_k are unknown coefficients, and $\Psi_k(\mathbf{y})$ are the eigenfunctions of the auxiliary Steklov-Neumann problem (3.5) in the upper-half plane \mathbb{H}_2 , with μ_k being the associated eigenvalues. We recall that this spectral problem has infinitely

many solutions, enumerated by the index $k = 0, 1, 2, \dots$, with the nonnegative eigenvalues increasing up to infinity, $0 = \mu_0 \leq \mu_1 \leq \mu_2 \leq \dots \nearrow +\infty$, while the restrictions of Steklov eigenfunctions $\Psi_k(\mathbf{y})$ onto the interval $(-1, 1)$ of the horizontal axis form a complete orthonormal basis of $L^2(-1, 1)$:

$$\int_{-1}^1 \Psi_j(y_1, 0) \Psi_k(y_1, 0) dy_1 = \delta_{j,k}. \quad (\text{C2})$$

Note that this condition fixes the normalization of the Steklov eigenfunctions Ψ_k . A rigorous formulation of the exterior Steklov problem in the plane is discussed in [8] (see also [16]), whereas a numerical construction of the eigenfunctions in elliptic coordinates, described in [37], is summarized in Appendix D.

We substitute Eq. (C1) into Eq. (3.3 b) to get

$$(\partial_n g_\infty)|_{y_2=0} + \sum_{k=0}^{\infty} c_k(\mu_k + \mu) \Psi_k(y_1, 0) = 0, \quad |y_1| < 1,$$

where we used $g_\infty|_{(-1,1)} = 0$. Multiplying this equation by Ψ_j , integrating over the interval $(-1, 1)$ on the horizontal axis, and using the orthonormality (C2), we identify the coefficients c_k and thus the Green's function as

$$g_\mu(\mathbf{y}) = g_\infty(\mathbf{y}) + \sum_{k=0}^{\infty} \frac{b_k}{\mu + \mu_k} \Psi_k(\mathbf{y}), \quad (\text{C3})$$

where

$$b_k = \int_{-1}^1 \Psi_k(y_1, 0) (-\partial_n g_\infty) dy_1. \quad (\text{C4})$$

Note that explicit formulas for $g_\infty(\mathbf{y})$ and $\partial_n g_\infty$ are given by Eqs. (A7, A10). However, we can actually get the coefficients b_k without computing the integral in Eq. (C4). For this purpose, Eq. (3.5 a) is multiplied by $g_\infty(\mathbf{y})$, Eq. (2.3 a) is multiplied by $\Psi_k(\mathbf{y})$, they are subtracted from each other, and integrated over the upper half-plane, to get using Green's second identity that

$$0 = \int_{\mathbb{H}_2} (g_\infty \Delta \Psi_k - \Psi_k \Delta g_\infty) d\mathbf{y} = -\pi \Psi_k(\infty) - \int_{-1}^1 \Psi_k(y_1, 0) (\partial_n g_\infty) dy_1,$$

from which we identify that

$$b_k = \pi \Psi_k(\infty). \quad (\text{C5})$$

Moreover, the symmetry of the problem (3.5) with respect to the vertical axis implies that the eigenfunctions Ψ_k should be either symmetric or antisymmetric:

$$\Psi_{2k}(-y_1, y_2) = \Psi_{2k}(y_1, y_2), \quad (\text{C6 a})$$

$$\Psi_{2k+1}(-y_1, y_2) = -\Psi_{2k+1}(y_1, y_2), \quad (\text{C6 b})$$

(even and odd indices are used to distinguish them). Since the function $(\partial_n g_\infty)$ is symmetric, the integrals in Eq. (C4) are zero for odd indices, implying

$$b_{2k+1} = 0. \quad (\text{C7})$$

We conclude that

$$g_\mu(\mathbf{y}) = g_\infty(\mathbf{y}) + \pi \sum_{k=0}^{\infty} \frac{\Psi_{2k}(\infty)}{\mu + \mu_{2k}} \Psi_{2k}(\mathbf{y}). \quad (\text{C8})$$

As $g_\mu(\mathbf{y})$ is the Robin Green's function of the Laplace equation, it is necessarily positive for any \mathbf{y} and $\mu > 0$ [3, Chapter V.1]. Moreover, we observed numerically the following property: there exists $\hat{\mu} < 0$ such that, for any $\hat{\mu} < \mu < 0$, the restriction of $g_\mu(\mathbf{y})$ onto the interval $(-1, 1)$ is negative:

$$g_\mu(y_1, 0) < 0 \quad \text{for any } -1 \leq y_1 \leq 1. \quad (\text{C9})$$

We obtained numerically that $\hat{\mu} \approx -2.006$, which is very close to and possibly identical with $-\mu_1$. Qualitatively, when μ is negative but small, the first term of the sum, $\pi/(2\mu)$, provides the dominant (negative) contribution to $g_\mu(y_1, 0)$, as compared to the remaining terms whose sum is expected to be bounded by a constant. However, we are not aware of the proof of this statement.

According to the spectral expansion (C8), the constant term $\mathcal{C}(\mu)$ of the Robin Green's function $g_\mu(\mathbf{y})$ at infinity, as defined in Eq. (3.6), is

$$\mathcal{C}(\mu) = \ln(2) + \frac{\pi}{2\mu} + \pi \sum_{k=1}^{\infty} \frac{[\Psi_{2k}(\infty)]^2}{\mu_{2k} + \mu}, \quad (\text{C10})$$

where we used Eq. (2.4) with $d = 1/2$ and wrote explicitly the term with $k = 0$, for which $\mu_0 = 0$ and $\Psi_0 = 1/\sqrt{2}$ that yielded $\pi/(2\mu)$. The numerical eigenvalues μ_{2k} and the coefficients $[\Psi_{2k}(\infty)]^2$ for the first ten terms are reported in Table C1. The asymptotic behavior of the eigenvalues is well known (see [37, 66] and references therein):

$$\mu_k \sim \frac{\pi}{2} k \quad (k \gg 1). \quad (\text{C11})$$

In turn, the oscillating eigenfunction $\Psi_{2k}(y_1)$ can be roughly approximated as $\cos(\pi k y_1)$ at large k (see Appendix D). As a consequence, we get

$$\Psi_{2k}(\infty) = \frac{1}{\pi} \int_{-1}^1 \frac{\Psi_{2k}(y_1)}{\sqrt{1 - y_1^2}} dy_1 \approx \frac{1}{\pi} \int_{-1}^1 \frac{\cos(k\pi y_1)}{\sqrt{1 - y_1^2}} dy_1 = J_0(\pi k) \simeq \frac{(-1)^k}{\pi \sqrt{k}}, \quad (k \gg 1). \quad (\text{C12})$$

The decay of $[\Psi_{2k}(\infty)]^2/\mu_{2k} \propto 1/k^2$ is rapid enough to ensure that the reported ten coefficients are sufficient for an accurate approximation of $\mathcal{C}(\mu)$, at least for small μ .

To get the small- μ approximation, we expand the last term of Eq. (C10) into a Taylor series in powers of μ as

$$\mathcal{C}(\mu) = \frac{\pi}{2\mu} + \sum_{n=0}^{\infty} (-\mu)^n C_{n+1}, \quad (\text{C13})$$

with

$$C_n = \delta_{n,1} \ln 2 + \pi \sum_{k=1}^{\infty} \frac{[\Psi_{2k}(\infty)]^2}{[\mu_{2k}]^n}, \quad (n = 1, 2, \dots). \quad (\text{C14})$$

Substituting the first ten contributing terms from Table C1, we get $C_1 \approx 0.7976$ and $C_2 \approx 0.0222$. In Appendix E, we provide an exact computation of these coefficients that yields

$$C_1 = 3/2 - \ln 2 \approx 0.8069, \quad C_2 = \frac{21 - 2\pi^2}{18\pi} \approx 0.0223. \quad (\text{C15})$$

One sees that the numerically computed values are very close to the exact ones. Most importantly, the coefficient C_2 , as well as higher-order coefficients, are small and can thus be neglected when $\mu \ll 1$.

	k	1	2	3	4	5	
μ_{2k-1}	2.0061	5.1253	8.2600	11.3982	14.5378		
	3.4533	6.6286	9.7839	12.9330	16.0794		
	3.1416	6.2832	9.4248	12.5664	15.7080		
	$[\Psi_{2k}(\infty)]^2$	0.0664	0.0391	0.0279	0.0218	0.0178	
	$1/(\pi^2 k)$	0.1013	0.0507	0.0338	0.0253	0.0203	
	k	6	7	8	9	10	
μ_{2k-1}	17.6780	20.8187	23.9596	27.1006	30.2418		
	19.2242	22.3682	25.5116	28.6547	31.7974		
	18.8496	21.9911	25.1327	28.2743	31.4159		
	$[\Psi_{2k}(\infty)]^2$	0.0151	0.0131	0.0116	0.0104	0.0094	
	$1/(\pi^2 k)$	0.0169	0.0145	0.0127	0.0113	0.0101	

Table C1. List of eigenvalues μ_{2k} and coefficients $[\Psi_{2k}(\infty)]^2$ of the first 10 contributing terms in the spectral expansion (C10) for $\mathcal{C}(\mu)$ (in addition, one has $\mu_0 = 0$ and $\Psi_0(\infty) = 1/\sqrt{2}$). The reported values were obtained numerically by using a matrix representation of the Steklov problem in elliptic coordinates (see Appendix D). The matrix was truncated to the size 100×100 and then diagonalized numerically. The shown values did not change when the truncation order was increased to 500×500 . For comparison, the large- k asymptotic approximations of μ_{2k} and $[\Psi_{2k}(\infty)]^2$ from Eqs. (C11, C12) are also present. For completeness, we also present the first ten eigenvalues μ_{2k-1} that correspond to antisymmetric eigenfunctions Ψ_{2k-1} that vanish at infinity.

Appendix D Steklov eigenmodes

In this Appendix, we recall a numerical computation of the Steklov eigenfunctions Ψ_k satisfying Eqs. (3.5). The details of this computation are provided in Appendix D of Ref. [37]. Since $\Psi_0 = 1/\sqrt{2}$ is known, we focus on the other eigenfunctions with $k = 1, 2, \dots$.

In elliptic coordinates (α, θ) , one has

$$y_1 = \cosh \alpha \cos \theta, \quad y_2 = \sinh \alpha \sin \theta, \quad (\text{D } 1)$$

with $0 \leq \alpha < +\infty$ and $0 \leq \theta \leq \pi$. Note that Eqs. (A8, A9) with $a_E = 1$ allow one to express α and θ in terms of y_1 and y_2 .

The Steklov eigenfunctions can be written as

$$\Psi_k(\alpha, \theta) = \sum_{n=0}^{\infty} c_{k,n} \cos(n\theta) e^{-n\alpha}, \quad (\text{D } 2)$$

with unknown coefficients $c_{k,n}$. Imposing the Steklov condition yields the infinite system of linear equations:

$$\sum_{n=1}^{\infty} c_{k,n} \mathbf{M}_{n,m} = \frac{1}{\mu_k} c_{k,m} \quad \text{for } m = 1, 2, \dots, \quad (\text{D } 3)$$

where

$$\mathbf{M}_{n,m} = \frac{1}{m} \left[\mathbf{A}_{n,m} - \frac{\mathbf{A}_{n,0} \mathbf{A}_{0,m}}{\mathbf{A}_{0,0}} \right], \quad (\text{D } 4)$$

and

$$\mathbf{A}_{n,m} = \frac{1 + (-1)^{m+n}}{\pi} \left(\frac{1}{1 - (m-n)^2} + \frac{1}{1 - (m+n)^2} \right).$$

This matrix equation determines the coefficients $c_{k,n}$ up to a multiplicative factor that has to be fixed by the

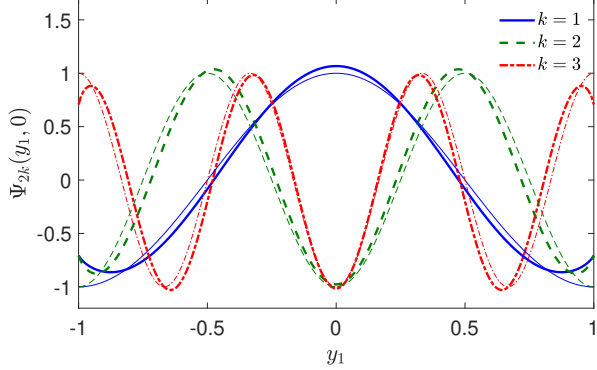


Figure D1. The Steklov eigenfunctions $\Psi_{2k}(y_1, 0)$, restricted onto the interval $(-1, 1)$, are shown by thick lines. These eigenfunctions are obtained by truncating the series in Eq. (D2) to $n \leq 100$, with the coefficients $c_{k,n}$ found by diagonalizing the truncated matrix \mathbf{M} from Eq. (D4). For comparison, functions $\cos(\pi k y_1)$ are plotted by thin lines.

normalization (C2) of Steklov eigenfunctions. Using the following relation derived in [37] for $k = 1, 2, \dots$

$$1 = \int_{-1}^1 |\Psi_k(y_1, 0)|^2 dy_1 = \frac{\pi}{2\mu_k} \sum_{m=1}^{\infty} m |c_{k,m}|^2, \quad (\text{D } 5)$$

one can ensure the required normalization to the coefficients $c_{k,m}$. Once the coefficients $c_{k,n}$ with $n = 1, 2, \dots$ are found, one also gets

$$c_{k,0} = -\frac{1}{\mathbf{A}_{0,0}} \sum_{n=1}^{\infty} c_{k,n} \mathbf{A}_{n,0}. \quad (\text{D } 6)$$

Note that $c_{k,0}$ is actually the value of Ψ_k at infinity.

In practice, one can truncate the infinite-dimensional matrix \mathbf{M} to a finite size $M \times M$ and then diagonalize it numerically. Its eigenvalues and eigenvectors approximate $1/\mu_k$ and $c_{k,n}$, respectively. We checked numerically that these approximations converge very rapidly as M increases. We used this technique to obtain the numerical values reported in Table C1. Figure D1 shows several eigenfunctions $\Psi_{2k}(y_1, 0)$ and their approximations by $\cos(\pi k y_1)$.

Appendix E Asymptotic behavior of $\mathcal{C}(\mu)$

In this Appendix, we derive the exact values of the coefficients C_1 and C_2 of the Taylor expansion (3.8) of $\mathcal{C}(\mu) - \pi/(2\mu)$ as $\mu \rightarrow 0$.

From the divergence theorem, there is no solution to Eq. (3.3) for $\mu = 0$. As such, for $\mu \ll 1$, the solution should bifurcate from infinity, so that $\mathcal{C}(\mu)$ is expected to be large in this limit. For this reason, we expand the solution for $0 < \mu \ll 1$ as

$$g_{\mu}(\mathbf{y}) = -\frac{C_0}{\mu} + v_1(\mathbf{y}) - \mu v_2(\mathbf{y}) + \mu^2 v_3(\mathbf{y}) + \dots \quad (\text{E } 1)$$

Inserting this expansion into Eq. (3.3), we obtain three BVPs:

$$\Delta v_1 = 0 \quad \text{in } \mathbb{H}_2, \quad (\text{E } 2 \text{ a})$$

$$\partial_n v_1 = C_0 \quad \text{on } y_2 = 0, |y_1| < 1; \quad \partial_n v_1 = 0 \quad \text{on } y_2 = 0, |y_1| \geq 1, \quad (\text{E } 2 \text{ b})$$

$$v_1 \sim \ln |\mathbf{y}| + \mathcal{O}(1) \quad \text{as } |\mathbf{y}| \rightarrow \infty, \quad (\text{E } 2 \text{ c})$$

for $v_1(\mathbf{y})$,

$$\Delta v_2 = 0 \quad \text{in } \mathbb{H}_2, \quad (\text{E 3 } a)$$

$$\partial_n v_2 = v_1 \quad \text{on } y_2 = 0, \quad |y_1| < 1; \quad \partial_n v_2 = 0 \quad \text{on } y_2 = 0, \quad |y_1| \geq 1, \quad (\text{E 3 } b)$$

$$v_2 \sim \mathcal{O}(1) \quad \text{as } |\mathbf{y}| \rightarrow \infty, \quad (\text{E 3 } c)$$

for $v_2(\mathbf{y})$, and

$$\Delta v_3 = 0 \quad \text{in } \mathbb{H}_2, \quad (\text{E 4 } a)$$

$$\partial_n v_3 = v_2 \quad \text{on } y_2 = 0, \quad |y_1| < 1; \quad \partial_n v_3 = 0 \quad \text{on } y_2 = 0, \quad |y_1| \geq 1, \quad (\text{E 4 } b)$$

$$v_3 \sim \mathcal{O}(1) \quad \text{as } |\mathbf{y}| \rightarrow \infty, \quad (\text{E 4 } c)$$

for $v_3(\mathbf{y})$. Note that the solutions v_1 , v_2 and v_3 are known only up to additive constants. These constants are needed for ensuring that Eqs. (E 2, E 3, E 4) have solutions. In particular, by the divergence theorem, there exists a solution to (E 2) provided that

$$0 = \int_{-1}^1 \partial_n v_1|_{y_2=0} dy_1 + \lim_{R \rightarrow \infty} \int_{B_R \cap \mathbb{H}_2} \partial_n v_1 ds = 2C_0 + \pi, \quad (\text{E 5})$$

where B_R is a large disk of radius R . This yields

$$C_0 = -\frac{\pi}{2}. \quad (\text{E 6})$$

To get the next-order terms, we will use the following lemma, which follows by using the method of images.

Lemma: For a given function $f(\xi)$ such that $\left| \int_{-\infty}^{\infty} f(\xi) d\xi \right| < \infty$, the solution $w(\mathbf{y})$ to the boundary value problem

$$\Delta w = 0 \quad \text{in } \mathbb{H}_2, \quad \partial_n w = f(y_1) \quad \text{on } y_2 = 0, \quad (\text{E 7})$$

is

$$w(\mathbf{y}) = -\frac{1}{2\pi} \int_{-\infty}^{\infty} \ln[(\xi - y_1)^2 + y_2^2] f(\xi) d\xi. \quad (\text{E 8})$$

In particular, one has

$$w(\mathbf{y}) \sim \left(-\frac{1}{\pi} \int_{-\infty}^{\infty} f(\xi) d\xi \right) \ln |\mathbf{y}| + o(1) \quad \text{as } |\mathbf{y}| \rightarrow \infty. \quad (\text{E 9})$$

To apply this lemma, we decompose the solution v_1 as $v_1(\mathbf{y}) = u_1(\mathbf{y}) + C_1$, where $u_1(\mathbf{y})$ is a solution for which $u_1(\mathbf{y}) \sim \ln |\mathbf{y}| + o(1)$ as $|\mathbf{y}| \rightarrow \infty$. In this way, using Eq. (E 6) and setting

$$f(\xi) = -(\pi/2)\Theta(1 - |\xi|), \quad (\text{E 10})$$

where $\Theta(z)$ is the Heaviside step function ($\Theta(z) = 1$ for $z > 0$ and 0 otherwise), we get

$$u_1(\mathbf{y}) = \frac{1}{4} \int_{-1}^1 \ln[(\xi - y_1)^2 + y_2^2] d\xi, \quad (\text{E 11})$$

which satisfies the required condition $u_1(\mathbf{y}) \sim \ln |\mathbf{y}| + o(1)$ as $|\mathbf{y}| \rightarrow \infty$.

Now we turn to the next-order term v_2 satisfying Eq. (E 3), in which $v_1|_{y_2=0} = C_1 + u_1|_{y_2=0}$. The divergence

theorem yields that the necessary and sufficient condition for v_2 to be bounded (i.e., $v_2 \sim \mathcal{O}(1)$ as $|\mathbf{y}| \rightarrow \infty$) is

$$\int_{-1}^1 v_1(y_1, 0) dy_1 = 0, \quad (\text{E12})$$

from which

$$C_1 = -\frac{1}{2} \int_{-1}^1 u_1(y_1, 0) dy_1, \quad (\text{E13})$$

where from an integration of Eq. (E11) with $y_2 = 0$ we get

$$u_1(y_1, 0) = \frac{1}{2} \left[-2 + y_1 \ln \left(\frac{1+y_1}{1-y_1} \right) + \ln(1-y_1^2) \right]. \quad (\text{E14})$$

Substituting this expression into Eq. (E13), we get

$$C_1 = \frac{3}{2} - \ln 2. \quad (\text{E15})$$

Similarly, we write $v_2 = u_2 + C_2$ such that $u_2(\mathbf{y}) \sim o(1)$ as $|\mathbf{y}| \rightarrow \infty$. Using again the above lemma with $f(\xi) = u_1(\xi, 0) + C_1$, we conclude that

$$u_2(\mathbf{y}) = -\frac{1}{2\pi} \int_{-1}^1 \ln[(\xi - y_1)^2 + y_2^2] (u_1(\xi, 0) + C_1) d\xi. \quad (\text{E16})$$

In particular, we find

$$u_2(y_1, 0) = -\frac{1}{\pi} \int_{-1}^1 \ln |\xi - y_1| (u_1(\xi, 0) + C_1) d\xi = -\frac{2C_1}{\pi} u_1(y_1, 0) - \frac{1}{\pi} \int_{-1}^1 \ln |\xi - y_1| u_1(\xi, 0) d\xi,$$

where we used Eq. (E11) with $y_2 = 0$ for the first term. Rewriting Eq. (E14) as

$$u_1(y_1, 0) = -1 + \frac{1}{2} w(y_1) \quad (\text{E17})$$

with

$$w(y_1) = y_1 \ln \left(\frac{1+y_1}{1-y_1} \right) + \ln(1-y_1^2), \quad (\text{E18})$$

we get

$$u_2(y_1, 0) = \frac{2(1-C_1)}{\pi} u_1(y_1, 0) - \frac{1}{2\pi} \int_{-1}^1 \ln |\xi - y_1| w(\xi) d\xi. \quad (\text{E19})$$

The divergence theorem applied to Eq. (E4) yields

$$\int_{-1}^1 v_2(y_1, 0) dy_1 = 0, \quad (\text{E20})$$

from which

$$C_2 = -\frac{1}{2} \int_{-1}^1 u_2(y_1, 0) dy_1 = \frac{-(1-C_1)}{\pi} \underbrace{\int_{-1}^1 u_1(y_1, 0) dy_1}_{=-2C_1} + \frac{1}{4\pi} \int_{-1}^1 \left\{ \int_{-1}^1 \ln |\xi - y_1| w(\xi) d\xi \right\} dy_1.$$

	Interior problem		Exterior problem	
	surface	bulk	surface	bulk
Definition	(2.9)	(6.2)	(6.12)	(F1)
Disk	(2.28)	(6.3)	(6.13), see Sec. F.1	(F3)
Ellipse	(F11, F13)	(F9)	(F23, F24)	(F21, F22)
Rectangle accessible		Eq. (4.13) from [52], and [61]	unavailable	unavailable

Table F 1. Summary of available formulas for various Neumann Green's functions. Note that the surface Neumann Green's function for rectangles can be derived from the results in [52, 61]. In turn, its extension to the exterior problem is not available.

Exchanging the order of integrals in the second term and using (E11) with $y_2 = 0$, we get

$$\begin{aligned} C_2 &= \frac{2(1-C_1)C_1}{\pi} + \frac{1}{2\pi} \int_{-1}^1 w(\xi)u_1(\xi, 0) d\xi = \frac{2(1-C_1)C_1}{\pi} + \frac{1}{2\pi} \int_{-1}^1 w(\xi) \left[-1 + \frac{1}{2}w(\xi) \right] d\xi \\ &= \frac{2(1-C_1)C_1}{\pi} - \frac{2(1-C_1)}{\pi} + \frac{1}{4\pi} \int_{-1}^1 [w(\xi)]^2 d\xi = -\frac{2(1-C_1)^2}{\pi} + \frac{1}{4\pi} \int_{-1}^1 [w(\xi)]^2 d\xi. \end{aligned}$$

Substituting $w(\xi)$ from Eq. (E18) and C_1 from Eq. (E15), we get after some simplifications that

$$C_2 = \frac{21 - 2\pi^2}{18\pi}. \quad (\text{E 21})$$

Appendix F Neumann Green's functions

In this Appendix, we summarize the available results on various Neumann Green's for both interior and exterior settings when the singularity is either on the boundary and in the bulk. Table F 1 collects their definitions and formulas for three shapes: the unit disk, ellipses, and rectangles (some derivations are provided below). Even though the exterior (bulk) Neumann Green's function $G_{\text{eb}}(\mathbf{x}, \boldsymbol{\xi})$ is not discussed in the main text, we provide its definition for completeness. For a fixed point $\boldsymbol{\xi} \in \Omega_0 = \mathbb{R}^2 \setminus C$ in the exterior of a compact set C , $G_{\text{eb}}(\mathbf{x}, \boldsymbol{\xi})$ satisfies

$$\Delta_{\mathbf{x}} G_{\text{eb}} = -\delta(\mathbf{x} - \boldsymbol{\xi}) \quad \text{in } \Omega_0, \quad \partial_n G_{\text{eb}} = 0 \quad \text{on } \partial\Omega_0, \quad (\text{F 1 a})$$

$$G_{\text{eb}}(\mathbf{x}, \boldsymbol{\xi}) \sim -\frac{1}{2\pi} \ln |\mathbf{x}| + o(1) \quad \text{as } |\mathbf{x}| \rightarrow \infty, \quad (\text{F 1 b})$$

whereas the regular part $R_{\text{eb}}(\boldsymbol{\xi})$ characterizes its singular behavior near $\boldsymbol{\xi}$:

$$R_{\text{eb}}(\boldsymbol{\xi}) = \lim_{\mathbf{x} \rightarrow \boldsymbol{\xi}} (G_{\text{eb}}(\mathbf{x}, \boldsymbol{\xi}) + \frac{1}{2\pi} \ln |\mathbf{x} - \boldsymbol{\xi}|). \quad (\text{F 2})$$

Note that the $o(1)$ condition in the asymptotic behavior (F 1 b) determines this function uniquely. For instance, for the exterior of the unit disk, we can readily derive by summing an eigenfunction expansion that

$$G_{\text{eb}}(\mathbf{x}, \boldsymbol{\xi}) = -\frac{1}{2\pi} \left(\ln |\mathbf{x} - \boldsymbol{\xi}| + \ln |\mathbf{x} - \boldsymbol{\xi}|/|\boldsymbol{\xi}|^2 - \ln |\mathbf{x}| \right), \quad (\text{F 3})$$

from which $R_{\text{eb}}(\boldsymbol{\xi}) = -\ln(1 - 1/|\boldsymbol{\xi}|^2)/(2\pi)$.

F.1 Surface Neumann Green's function for the exterior of the unit disk

In this Appendix, we provide a rigorous derivation of Eq. (6.13) for the surface Neumann Green's function $G_e(\mathbf{x}, \boldsymbol{\xi})$ for the exterior of the unit disk.

To establish the result in Eq. (6.13), we let $r = |\mathbf{x}|$ and we decompose G_e as $G_e(\mathbf{x}, \boldsymbol{\xi}) = -(2\pi)^{-1} \ln |\mathbf{x}| + H_e(\mathbf{x}, \boldsymbol{\xi})$,

to obtain that $H_e(\mathbf{x}, \boldsymbol{\xi})$ satisfies

$$\Delta_{\mathbf{x}} H_e = 0 \quad \text{in} \quad |\mathbf{x}| > 1; \quad \partial_r H_e = \frac{1}{2\pi} \quad \text{on} \quad |\mathbf{x}| = 1, \quad \mathbf{x} \neq \boldsymbol{\xi}, \quad (\text{F 4 } a)$$

$$H_e \sim -\frac{1}{\pi} \ln |\mathbf{x} - \boldsymbol{\xi}| \quad \text{as} \quad \mathbf{x} \rightarrow \boldsymbol{\xi}; \quad H_e \rightarrow 0 \quad \text{as} \quad |\mathbf{x}| \rightarrow \infty, \quad (\text{F 4 } b)$$

where $\Delta_{\mathbf{x}}$ is the Laplacian in the \mathbf{x} -variable. Consider now the interior surface Neumann Green's function inside the disk $|\mathbf{y}| \leq 1$ satisfying Eq. (2.9), which we decompose as $G(\mathbf{y}; \boldsymbol{\xi}) = |\mathbf{y}|^2/(4\pi) + H_i(\mathbf{y}, \boldsymbol{\xi})$, where $H_i(\mathbf{y}, \boldsymbol{\xi})$ satisfies

$$\Delta_{\mathbf{y}} H_i = 0 \quad \text{in} \quad |\mathbf{y}| < 1; \quad \partial_{\rho} H_i = \frac{-1}{2\pi} \quad \text{on} \quad |\mathbf{y}| = 1, \quad \mathbf{y} \neq \boldsymbol{\xi}, \quad (\text{F 5 } a)$$

$$H_i \sim -\frac{1}{\pi} \ln |\mathbf{y} - \boldsymbol{\xi}| \quad \text{as} \quad \mathbf{y} \rightarrow \boldsymbol{\xi}; \quad H_i \quad \text{bounded as} \quad \mathbf{y} \rightarrow \mathbf{0}. \quad (\text{F 5 } b)$$

Here $\rho = |\mathbf{y}|$ and $\Delta_{\mathbf{y}}$ denotes the Laplacian in the \mathbf{y} variable. From Eq. (2.28) it follows that

$$H_i(\mathbf{y}, \boldsymbol{\xi}) = -\frac{1}{\pi} \ln |\mathbf{y} - \boldsymbol{\xi}| + C, \quad (\text{F 6})$$

where C is a constant. By using conformal invariance under Kelvin's transformation $\mathbf{y} = \mathbf{x}/|\mathbf{x}|^2$ in the unit disk, and noting that $\partial_r = -\partial_{\rho}$ on $r = \rho = 1$, it follows that H_e is given by

$$H_e(\mathbf{x}, \boldsymbol{\xi}) = H_i\left(\frac{\mathbf{x}}{|\mathbf{x}|^2}, \boldsymbol{\xi}\right) = -\frac{1}{\pi} \ln \left| \frac{\mathbf{x}}{|\mathbf{x}|^2} - \boldsymbol{\xi} \right|, \quad (\text{F 7})$$

where we observe that $H_e \rightarrow 0$ as $|\mathbf{x}| \rightarrow \infty$. Finally, if $|\boldsymbol{\xi}| = 1$, we can readily calculate that

$$\left| \frac{\mathbf{x}}{|\mathbf{x}|^2} - \boldsymbol{\xi} \right| = \frac{|\mathbf{x} - \boldsymbol{\xi}|}{|\mathbf{x}|}. \quad (\text{F 8})$$

Upon substituting Eq. (F 8) into Eq. (F 7) and using $G_e = -(2\pi)^{-1} \ln |\mathbf{x}| + H_e$, we obtain the result in Eq. (6.13).

F.2 Neumann Green's functions for an ellipse

For an ellipse with semiaxes a and b ($a > b$), $\Omega_0 = \{\mathbf{x} = (x_1, x_2) \in \mathbb{R}^2 : (x_1/a)^2 + (x_2/b)^2 < 1\}$, a rapidly converging representation for the “bulk” Neumann Green's function was derived in [49]. In the elliptic coordinates introduced in Eq. (A 1), Eq. (5.21a) from [49] reads

$$G_b(\mathbf{x}, \boldsymbol{\xi}) = \frac{|\mathbf{x}|^2 + |\boldsymbol{\xi}|^2}{4\pi ab} - \frac{3(a^2 + b^2)}{16\pi ab} + \frac{\alpha_b - \alpha_>}{2\pi} + S(\mathbf{x}, \boldsymbol{\xi}), \quad (\text{F 9})$$

where $\mathbf{x} = (\alpha, \theta)$, $\boldsymbol{\xi} = (\alpha_0, \theta_0)$, $\alpha_> = \max\{\alpha, \alpha_0\}$, $\beta = (a - b)/(a + b)$, $\alpha_b = \operatorname{atanh}(b/a) = \frac{1}{2} \ln(1/\beta)$ describes the boundary $\partial\Omega_0$,

$$S(\mathbf{x}, \boldsymbol{\xi}) = -\frac{1}{2\pi} \sum_{n=0}^{\infty} \sum_{j=1}^8 \ln |1 - \beta^{2n} z_j|, \quad (\text{F 10})$$

and

$$\begin{aligned} z_1 &= e^{-|\alpha - \alpha_0| + i(\theta - \theta_0)}, & z_2 &= e^{-4\alpha_b + |\alpha - \alpha_0| + i(\theta - \theta_0)}, & z_3 &= e^{-2\alpha_b - \alpha - \alpha_0 + i(\theta - \theta_0)}, & z_4 &= e^{-2\alpha_b + \alpha + \alpha_0 + i(\theta - \theta_0)}, \\ z_5 &= e^{-4\alpha_b + \alpha + \alpha_0 + i(\theta + \theta_0)}, & z_6 &= e^{-\alpha - \alpha_0 + i(\theta + \theta_0)}, & z_7 &= e^{-2\alpha_b + |\alpha - \alpha_0| + i(\theta + \theta_0)}, & z_8 &= e^{-2\alpha_b - |\alpha - \alpha_0| + i(\theta + \theta_0)}. \end{aligned}$$

Setting $\boldsymbol{\xi}$ to the boundary $\partial\Omega_0$, we get some simplifications. In particular, we have $\alpha \leq \alpha_0 = \alpha_b$ that implies

$$z_1 = z_4 = e^{-\alpha_b + \alpha + i(\theta - \theta_0)}, \quad z_3 = z_2 = e^{-3\alpha_b - \alpha + i(\theta - \theta_0)},$$

$$z_5 = z_8 = e^{-3\alpha_b + \alpha + i(\theta + \theta_0)}, \quad z_7 = z_6 = e^{-\alpha_b - \alpha + i(\theta + \theta_0)}.$$

As a consequence, we obtain a rapidly converging representation for the surface Neumann Green's function:

$$G(\mathbf{x}, \boldsymbol{\xi}) = \frac{|\mathbf{x}|^2 + |\boldsymbol{\xi}|^2}{4\pi ab} - \frac{3(a^2 + b^2)}{16\pi ab} - \frac{1}{\pi} \sum_{n=1}^{\infty} \sum_{j=1}^4 \ln |1 - \beta^{2n} z_{2j-1}|. \quad (\text{F 11})$$

The regular part of this function can be deduced as $\mathbf{x} \rightarrow \boldsymbol{\xi}$. Setting $\theta = \theta_0$ and $\alpha = \alpha_0 - \epsilon$, we find as $\epsilon \rightarrow 0$:

$$G(\mathbf{x}, \boldsymbol{\xi}) \approx \frac{|\mathbf{x}|^2 + |\boldsymbol{\xi}|^2}{4\pi ab} - \frac{3(a^2 + b^2)}{16\pi ab} - \frac{1}{\pi} \ln(1 - e^{-\epsilon}) - \frac{1}{\pi} \sum_{n=1}^{\infty} \ln(1 - \beta^{2n}) - \frac{1}{\pi} \sum_{n=0}^{\infty} \sum_{j=2}^4 \ln |1 - \beta^{2n} z_{2j-1}|,$$

where

$$z_3 = e^{-4\alpha_b} = \beta^2, \quad z_5 = z_7 = e^{-2\alpha_b + 2i\theta_0} = \beta e^{2i\theta_0}.$$

On the other hand, we have for $\theta = \theta_0$ that

$$\begin{aligned} |\mathbf{x} - \boldsymbol{\xi}|^2 &= a_E^2 [(\cosh \alpha \cos \theta - \cosh \alpha_0 \cos \theta_0)^2 + (\sinh \alpha \sin \theta - \sinh \alpha_0 \sin \theta_0)^2] \\ &\approx a_E^2 \epsilon^2 (\sinh^2 \alpha_0 + \sin^2 \theta_0) \quad \text{as } \epsilon \rightarrow 0, \end{aligned}$$

so that

$$|\mathbf{x} - \boldsymbol{\xi}| \approx \epsilon a_E \sqrt{\sinh^2 \alpha_0 + \sin^2 \theta_0} \quad \text{as } \epsilon \rightarrow 0. \quad (\text{F 12})$$

We can thus express ϵ in terms of $|\mathbf{x} - \boldsymbol{\xi}|$ to obtain the following infinite series representation for the regular part in terms of the aspect ratio $\beta = (a - b)/(a + b)$:

$$R(\boldsymbol{\xi}) = \frac{|\boldsymbol{\xi}|^2}{2\pi ab} - \frac{3(a^2 + b^2)}{16\pi ab} + \frac{1}{\pi} \ln \left(a_E \sqrt{\sinh^2 \alpha_0 + \sin^2 \theta_0} \right) - \frac{2}{\pi} \sum_{n=1}^{\infty} \left(\ln(1 - \beta^{2n}) + \ln |1 - \beta^{2n-1} e^{2i\theta_0}| \right). \quad (\text{F 13})$$

F.3 Neumann Green's functions for the exterior of an ellipse

Finally, we consider the exterior of an ellipse with semiaxes $a > b$: $\Omega_0 = \{(x_1, x_2) \in \mathbb{R}^2 : (x_1/a)^2 + (x_2/b)^2 > 1\}$. We first derive the “bulk” Neumann Green's function $G_{\text{eb}}(\mathbf{x}, \boldsymbol{\xi})$ for this domain and then let the singularity point $\boldsymbol{\xi}$ tend to the boundary to get $G_e(\mathbf{x}, \boldsymbol{\xi})$ and its regular part $R_e(\boldsymbol{\xi})$.

Bulk Neumann Green's function

In elliptic coordinates introduced in Eq. (A 1), we search the bulk Neumann Green's function as the unique solution of Eqs. (F 1) in the form

$$G_{\text{eb}}(\mathbf{x}, \boldsymbol{\xi}) = \sum_{k=-\infty}^{\infty} A_k(\alpha) e^{ik(\theta - \theta_0)}, \quad (\text{F 14})$$

with unknown functions $A_k(\alpha)$. Substitution of this form into the equation for the Green's function yields

$$-\Delta_{\mathbf{x}} G(\mathbf{x}, \boldsymbol{\xi}) = -\frac{1}{h_{\alpha}^2} (\partial_{\alpha}^2 + \partial_{\theta}^2) \sum_{k=-\infty}^{\infty} A_k(\alpha) e^{ik(\theta - \theta_0)} = \frac{1}{h_{\alpha}^2} \delta(\alpha - \alpha_0) \delta(\theta - \theta_0),$$

where $h_{\alpha} = a_E \sqrt{\cosh^2 \alpha - \cos^2 \theta}$ is the scale factor, and $a_E = \sqrt{a^2 - b^2}$. Multiplying by $e^{ik' \theta}$ and integrating over θ from $-\pi$ to π , we obtain a set of equations for $A_k(\alpha)$:

$$(-\partial_{\alpha}^2 + k^2) A_k(\alpha) = \frac{1}{2\pi} \delta(\alpha - \alpha_0). \quad (\text{F 15})$$

Note that $A_k(\alpha)$ should satisfy $A'_k(\alpha_b) = 0$, where α_b is the location of the elliptic boundary (i.e., $\tanh \alpha_b = b/a$). As a consequence, we can search for solutions separately on $\alpha_b < \alpha < \alpha_0$ and $\alpha > \alpha_0$:

$$A_k(\alpha) = \begin{cases} a_k \cosh(k(\alpha - \alpha_b)), & \alpha_b < \alpha < \alpha_0, \\ b_k e^{-k\alpha}, & \alpha > \alpha_0, \end{cases} \quad (\text{F 16})$$

where we assumed that $k > 0$. The unknown coefficients a_k and b_k are obtained by requiring the continuity of $A_k(\alpha)$ together with the jump condition for the derivative at $\alpha = \alpha_0$. This yields that

$$b_k e^{-k\alpha_0} = a_k \cosh(k(\alpha_0 - \alpha_b)), \quad -kb_k e^{-k\alpha_0} - ka_k \sinh(k(\alpha_0 - \alpha_b)) = -1/(2\pi), \quad (\text{F 17})$$

from which we determine

$$a_k = \frac{1}{2\pi k} e^{-k(\alpha_0 - \alpha_b)}, \quad b_k = \frac{1}{2\pi k} e^{k\alpha_b} \cosh(k(\alpha_0 - \alpha_b)). \quad (\text{F 18})$$

We conclude that

$$A_k = \frac{1}{2\pi k} e^{-k(\alpha_> - \alpha_b)} \cosh(k(\alpha_< - \alpha_b)), \quad (\text{F 19})$$

where $\alpha_< = \min\{\alpha, \alpha_0\}$ and $\alpha_> = \max\{\alpha, \alpha_0\}$. We can further simplify this expression to

$$A_k = \frac{1}{4\pi k} \left[e^{-k|\alpha - \alpha_0|} + e^{-k(\alpha + \alpha_0 - 2\alpha_b)} \right]. \quad (\text{F 20})$$

We recall that this solution holds for $k > 0$. By symmetry, it also holds for $k < 0$, if k is replaced by $|k|$.

For $k = 0$, a general solution of the Laplace equation on the interval $\alpha_b < \alpha < \alpha_0$ is $A_0 = a_0 + c_0 \alpha$, where we must set $c_0 = 0$ to ensure that the Neumann condition at α_b is satisfied. In turn, we have $A_0 = d_0 + b_0 \alpha$ for $\alpha > \alpha_0$. We set $a_0 = d_0 + b_0 \alpha_0$ to ensure the continuity of A_0 at α_0 . The coefficient b_0 is determined by the jump of the derivative, which yields $b_0 = -1/(2\pi)$. We conclude that, in terms of a constant d_0 to be fixed, A_0 has the form

$$A_0 = d_0 - \frac{1}{2\pi} \alpha_>.$$

Combining these results, we get

$$\begin{aligned} G(\mathbf{x}, \boldsymbol{\xi}) &= d_0 - \frac{\alpha_>}{2\pi} + \frac{1}{4\pi} \sum_{k \neq 0} \frac{e^{ik(\theta - \theta_0)}}{|k|} (e^{-|k||\alpha - \alpha_0|} + e^{-|k|(\alpha + \alpha_0 - 2\alpha_b)}), \\ &= d_0 - \frac{\alpha_>}{2\pi} - \frac{1}{4\pi} \left[\ln(1 - e^{-|\alpha - \alpha_0| + i(\theta - \theta_0)}) + \ln(1 - e^{-|\alpha - \alpha_0| - i(\theta - \theta_0)}) \right. \\ &\quad \left. + \ln(1 - e^{-(\alpha + \alpha_0 - 2\alpha_b) + i(\theta - \theta_0)}) + \ln(1 - e^{-(\alpha + \alpha_0 - 2\alpha_b) - i(\theta - \theta_0)}) \right]. \end{aligned}$$

Since $|\mathbf{x}|^2 = a_E^2 (\cosh^2 \alpha - \sin^2 \theta) \approx a_E^2 \cosh^2 \alpha$ when $|\mathbf{x}| \gg a_E$, we have $\alpha_> = \alpha \approx \ln(2|\mathbf{x}|/a_E)$ as $|\mathbf{x}| \rightarrow \infty$, where we used that $\cosh^{-1}(z) = \ln(z + \sqrt{z^2 - 1})$. Since the Neumann Green's function behaves at infinity according to Eq. (F 1b), the constant term d_0 must compensate the constant contribution from $\alpha_>$. This condition yields $d_0 = \ln(2/a_E)/(2\pi)$, and so we conclude that that

$$\begin{aligned} G_{\text{eb}}(\mathbf{x}, \boldsymbol{\xi}) &= \frac{\ln(2/a_E) - \alpha_>}{2\pi} - \frac{1}{4\pi} \left[\ln(1 - 2 \cos(\theta - \theta_0) e^{-|\alpha - \alpha_0|} + e^{-2|\alpha - \alpha_0|}) \right. \\ &\quad \left. + \ln(1 - 2 \cos(\theta - \theta_0) e^{-(\alpha + \alpha_0 - 2\alpha_b)} + e^{-2(\alpha + \alpha_0 - 2\alpha_b)}) \right]. \end{aligned} \quad (\text{F 21})$$

To evaluate the regular part, we set $\theta = \theta_0$ and $\alpha = \alpha_0 + \epsilon$, so that

$$G_{\text{eb}}(\mathbf{x}, \boldsymbol{\xi}) \approx \frac{1}{2\pi} \left[\ln(2/a_E) - \alpha_0 - \ln(1 - e^{-\epsilon}) - \ln(1 - e^{-2(\alpha_0 - \alpha_b)}) \right].$$

Using again Eq. (F 12) to express ϵ in terms of $|\mathbf{x} - \boldsymbol{\xi}|$, we conclude that

$$R_{\text{eb}}(\boldsymbol{\xi}) = \frac{1}{2\pi} \left[\frac{1}{2} \ln(\sinh^2 \alpha_0 + \sin^2 \theta_0) + \ln(2) - \alpha_0 - \ln(1 - e^{-2(\alpha_0 - \alpha_b)}) \right]. \quad (\text{F 22})$$

Surface Neumann Green's function

Setting $\boldsymbol{\xi} \in \partial\Omega$ in Eq. (F 21), we get a simplification for the surface Neumann Green's function:

$$G_e(\mathbf{x}, \boldsymbol{\xi}) = \frac{\ln(2/a_E) - \alpha}{2\pi} - \frac{1}{2\pi} \ln(1 - 2 \cos(\theta - \theta_0) e^{-(\alpha - \alpha_b)} + e^{-2(\alpha - \alpha_b)}). \quad (\text{F 23})$$

In turn, setting $\theta = \theta_0$ and $\alpha = \alpha_b + \epsilon$, and using Eq. (F 12), we find that

$$R_e(\boldsymbol{\xi}) = \frac{1}{2\pi} [\ln(2a_E) - \alpha_0 + \ln(\sinh^2 \alpha_0 + \sin^2 \theta_0)]. \quad (\text{F 24})$$

References

- [1] O. Bénichou and R. Voituriez. Narrow escape time problem: Time needed for a particle to exit a confining domain through a small window. *Phys. Rev. Lett.*, 100:168105, 2008.
- [2] A. M. Berezhkovskii, L. Dagdug, V. A. Lizunov, J. Zimmerberg, and S. M. Bezrukov. Communication. Clusters of absorbing disks on a reflecting wall: Competition for diffusing particles. *J. Chem. Phys.*, 136:211102, 2012.
- [3] S. Bergman and M. Schiffer. *Kernel functions and elliptic differential equations in mathematical physics*. Academic Press, New York, 1953.
- [4] P. C. Bressloff. Target competition for resources under multiple search-and-capture events with stochastic resetting. *Proc. R. Soc. A*, 476:20200475, 2020.
- [5] P. C. Bressloff. Narrow capture problem: An encounter-based approach to partially reactive targets. *Phys. Rev. E*, 105(3):034141, 2022.
- [6] P. C. Bressloff. Encounter-based reaction-subdiffusion model I: Surface adsorption and the local time propagator. *J. Phys. A: Math. Theor.*, 56:435004, 2023.
- [7] P. C. Bressloff. Encounter-based reaction-subdiffusion model II: Partially absorbing traps and the occupation time propagator. *J. Phys. A: Math. Theor.*, 56:435005, 2023.
- [8] L. Bundrock, A. Girouard, D. S. Grebenkov, M. Levitin, and I. Polterovich. The exterior Steklov problem for Euclidean domains. *in preparation*, 2025.
- [9] A. Cengiz and S. D. Lawley. Narrow escape with imperfect reactions. *Phys. Rev. E*, 110:054127, 2024.
- [10] A. Chaigneau and D. S. Grebenkov. A numerical study of the generalized Steklov problem in planar domains. *J. Phys. A: Math. Theor.*, 57:445201, 2024.
- [11] X. Chen and A. Friedman. Asymptotic analysis for the narrow escape problem. *SIAM J. Math. Anal.*, 43:2542–2563, 2011.
- [12] J. Cherry, A. E. Lindsay, A. Navarro Hernandez, and B. Quaife. Trapping of planar Brownian motion: Full first passage time distributions by kinetic Monte Carlo, asymptotic, and boundary integral methods. *SIAM Multi. Model. Simul.*, 20:1284–1314, 2022.
- [13] C. Chevalier, O. Bénichou, B. Meyer, and R. Voituriez. First-passage quantities of Brownian motion in a bounded domain with multiple targets: A unified approach. *J. Phys. A: Math. Theor.*, 44:025002, 2011.
- [14] A. F. Cheviakov and M. J. Ward. Optimizing the principal eigenvalue of the Laplacian in a sphere with interior traps. *Math. Computer Model.*, 53:1394–1409, 2011.
- [15] A. F. Cheviakov, M. J. Ward, and R. Straube. An asymptotic analysis of the mean first passage time for narrow escape problems. Part II. The sphere. *SIAM Multi. Model. Simul.*, 8:836–870, 2010.
- [16] T. J. Christiansen and K. Datchev. Low energy scattering asymptotics for planar obstacles. *Pure Appl. Anal.*, 5:767–794, 2023.
- [17] B. Colbois, A. Girouard, C. Gordon, and D. Sher. Some recent developments on the Steklov eigenvalue problem. *Rev. Mat. Complut.*, 37:1–161, 2024.
- [18] F. C. Collins and G. E. Kimball. Diffusion-controlled reaction rates. *J. Coll. Sci.*, 4:425–437, 1949.
- [19] D. Coombs, R. Straube, and M. J. Ward. Diffusion on a sphere with localized traps: Mean first passage time, eigenvalue asymptotics, and Fekete points. *SIAM J. Appl. Math.*, 70:302–332, 2009.
- [20] L. Dagdug, J. Peña, and I. Pompa-García. *Diffusion Under Confinement. A Journey Through Counterintuition*. Springer Cham, 2024.

[21] M. Delgado, M. J. Ward, and D. Coombs. Conditional mean first passage times to small traps in a 3-D domain with a sticky boundary: Applications to T cell searching behavior in lymph nodes. *SIAM Multi. Model. Simul.*, 13:1224–1258, 2015.

[22] J. Ding and A. Zhu. Eigenvalues of rank-one updated matrices with some applications. *Appl. Math. Lett.*, 20:1223–1226, 2007.

[23] R. Erban and S. J. Chapman. Reactive boundary conditions for stochastic simulations of reaction-diffusion processes. *Phys. Biol.*, 4:16–28, 2007.

[24] M. Felici, M. Filoche, and B. Sapoval. Diffusional screening in the human pulmonary acinus. *J. Appl. Physiol.*, 94(5):2010–2016, 2003.

[25] D. W. Fox and J. R. Kuttler. Sloshing frequencies. *Z. Angew. Math. Phys.*, 34:668–696, 1983.

[26] M. Galanti, D. Fanelli, and F. Piazza. Conformation-controlled binding kinetics of antibodies. *Scient. Rep.*, 6:18976, 2016.

[27] A. Girouard and I. Polterovich. Spectral geometry of the Steklov problem. *J. Spectr. Th.*, 7:321–359, 2017.

[28] A. Godec and R. Metzler. First passage time distribution in heterogeneity controlled kinetics: Going beyond the mean first passage time. *Sci. Rep.*, 6:20349, 2016.

[29] D. S. Grebenkov. Universal formula for the mean first passage time in planar domains. *Phys. Rev. Lett.*, 117:260201, 2016.

[30] D. S. Grebenkov. Spectral theory of imperfect diffusion-controlled reactions on heterogeneous catalytic surfaces. *J. Chem. Phys.*, 151:104108, 2019.

[31] D. S. Grebenkov. Diffusion toward non-overlapping partially reactive spherical traps: Fresh insights onto classic problems. *J. Chem. Phys.*, 152:244108, 2020.

[32] D. S. Grebenkov. Joint distribution of multiple boundary local times and related first-passage time problems with multiple targets. *J. Stat. Mech.*, 2020:103205, 2020.

[33] D. S. Grebenkov. Paradigm shift in diffusion-mediated surface phenomena. *Phys. Rev. Lett.*, 125:078102, 2020.

[34] D. S. Grebenkov. Diffusion-controlled reactions: An overview. *Molecules*, 28:7570, 2023.

[35] D. S. Grebenkov. Diffusion-controlled reactions with non-Markovian binding/unbinding kinetics. *J. Chem. Phys.*, 158:214111, 2023.

[36] D. S. Grebenkov. Encounter-based approach to the escape problem. *Phys. Rev. E*, 107:044105, 2023.

[37] D. S. Grebenkov. Mixed Steklov-Neumann problem: Asymptotic analysis and applications to diffusion-controlled reactions. *accepted to SIAM Multi. Model. Simul.; preprint on ArXiv: 2409.00213v1*, 2025.

[38] D. S. Grebenkov and A. Chaigneau. The Steklov problem for exterior domains: Asymptotic behavior and applications. *J. Math. Phys.*, 66:061502, 2025.

[39] D. S. Grebenkov, R. Metzler, and G. Oshanin. Strong defocusing of molecular reaction times results from an interplay of geometry and reaction control. *Commun. Chem.*, 1:96, 2018.

[40] D. S. Grebenkov, R. Metzler, and G. Oshanin. Full distribution of first exit times in the narrow escape problem. *New J. Phys.*, 21:122001, 2019.

[41] D. S. Grebenkov and G. Oshanin. Diffusive escape through a narrow opening: New insights into a classic problem. *Phys. Chem. Chem. Phys.*, 119:2723–2739, 2017.

[42] D. S. Grebenkov and S. Traytak. Semi-analytical computation of Laplacian Green functions in three-dimensional domains with disconnected spherical boundaries. *J. Comput. Phys.*, 379:91–117, 2019.

[43] T. Guérin, M. Dolgushev, O. Bénichou, and R. Voituriez. Imperfect narrow escape problem. *Phys. Rev. E*, 107:034134, 2023.

[44] C. Guerrier and D. Holcman. The first 100 nm inside the pre-synaptic terminal where calcium diffusion triggers vesicular release. *Front. Synaptic. Neurosci.*, 10:23, 2018.

[45] A. Hassell and V. Ivrii. Spectral asymptotics for the semiclassical Dirichlet to Neumann operator. *J. Spectr. Th.*, 7:881–905, 2017.

[46] P. Henrici, B. A. Troesch, and L. Wuytack. Sloshing frequencies for a half-space with circular or strip-like aperture. *Z. Angew. Math. Phys.*, 21:285–318, 1970.

[47] D. Holcman and Z. Schuss. Control of flux by narrow passages and hidden targets in cellular biology. *Phys. Progr. Report*, 76:074601, 2013.

[48] D. Holcman and Z. Schuss. The narrow escape problem. *SIAM Rev.*, 56:213–257, 2014.

[49] S. A. Iyaniwura, T. Wong, C. B. Macdonald, and M. J. Ward. Optimization of the mean first passage time in near-disk and elliptical domains in 2-D with small absorbing traps. *SIAM Rev.*, 63:525–555, 2021.

[50] Behrndt J. and A. F. M. ter Elst. Dirichlet-to-Neumann maps on bounded Lipschitz domains. *J. Diff. Eq.*, 259:5903–5926, 2015.

[51] T. Kolokolnikov, M. Titcombe, and M. J. Ward. Optimizing the fundamental Neumann eigenvalue for the Laplacian in a domain with small traps. *Europ. J. Appl. Math.*, 16:161–200, 2005.

- [52] T. Kolokolnikov, M. J. Ward, and J. Wei. Spot self-replication and dynamics for the Schnakenberg model in a two-dimensional domain. *J. Nonlin. Sci.*, 19:1–56, 2009.
- [53] V. Kozlov and N. Kuznetsov. The ice-fishing problem: The fundamental sloshing frequency versus geometry of holes. *Math. Methods Appl. Sci.*, 27:289–312, 2004.
- [54] V. Kurella, J. Tzou, D. Coombs, and M. J. Ward. Asymptotic analysis of first passage time problems inspired by ecology. *Bull. Math. Bio.*, 77:83–125, 2015.
- [55] S. D. Lawley and J. P. Keener. A new derivation of Robin boundary conditions through homogenization of a stochastically switching boundary. *SIAM J. Appl. Dyn. Syst.*, 14:1845–1867, 2015.
- [56] M. Levitin, D. Mangoubi, and I. Polterovich. *Topics in Spectral Geometry: (Graduate Studies in Mathematics, vol. 237)*. American Mathematical Society, 2023.
- [57] M. Levitin, L. Parnovski, I. Polterovich, and D. Sher. Sloshing, Steklov and corners: Asymptotics of sloshing eigenvalues. *J. Anal. Math.*, 146:65–125, 2022.
- [58] K. Lindenberg, G. Oshanin, and Metzler R. (Eds.). *Chemical Kinetics: Beyond the Textbook*. New Jersey: World Scientific, 2019.
- [59] A. E. Lindsay, A. Bernoff, and M. J. Ward. First passage statistics for the capture of a Brownian particle by a structured spherical target with multiple surface traps. *SIAM Multi. Model. Simul.*, 15:74–109, 2017.
- [60] J. Masoliver. *Random Processes: First-Passage and Escape*. World Scientific Publishing, 2018.
- [61] R. C. McCann, R. D. Hazlett, and D. K. Babu. Highly accurate approximations of Green’s and Neumann functions on rectangular domains. *Proc. R. Soc. Lond. A*, 457:767–772, 2001.
- [62] R. Metzler, G. Oshanin, and S. (Eds.) Redner. *First-passage Phenomena and Their Applications*. Singapore: World Scientific, 2014.
- [63] E. Neher and T. Sakaba. Multiple roles of calcium ions in the regulation of neurotransmitter release. *Neuron*, 59:861, 2008.
- [64] F. Piazza. The physics of boundary conditions in reaction-diffusion problems. *J. Chem. Phys.*, 157:234110, 2022.
- [65] S. Pillay, M. J. Ward, A. Peirce, and T. Kolokolnikov. An asymptotic analysis of the mean first passage time for narrow escape problems: Part I: Two-dimensional domains. *SIAM Multi. Model. Simul.*, 8:803–835, 2010.
- [66] A. A. Polosin. On the asymptotic behavior of eigenvalues and eigenfunctions of an integral convolution operator with a logarithmic kernel on a finite interval. *J. Diff. Eq.*, 58:1242–1257, 2022.
- [67] S. Redner. *A Guide to First-Passage Time Processes*. Cambridge University Press, Cambridge, U.K., 2001.
- [68] M. Reva, D. DiGregorio, and D. S. Grebenkov. A first-passage approach to diffusion-influenced reversible binding and its insights into nanoscale signaling at the presynapse. *Sci. Rep.*, 11:5377, 2021.
- [69] E. Saff. Logarithmic potential theory with applications to approximation theory. *Surv. Approx. Th.*, 5:165–200, 2010.
- [70] F. Sala and A. Hernández-Cruz. Calcium diffusion modeling in a spherical neuron. Relevance of buffering properties. *Biophys. J.*, 57:313–324, 1990.
- [71] H. Sano and M. Tachiya. Partially diffusion-controlled recombination. *J. Chem. Phys.*, 71:1276–1282, 1979.
- [72] B. Sapoval. General formulation of Laplacian transfer across irregular surfaces. *Phys. Rev. Lett.*, 73:3314–3316, 1994.
- [73] Z. Schuss. *Brownian Dynamics at Boundaries and Interfaces in Physics, Chemistry and Biology*. Springer, New York, 2013.
- [74] Z. Schuss, A. Singer, and D. Holcman. The narrow escape problem for diffusion in cellular microdomains. *Proc. Nat. Acad. Sci. USA*, 104:16098–16103, 2007.
- [75] A. Singer, Z. Schuss, D. Holcman, and R. S. Eisenberg. Narrow escape, Part I. *J. Stat. Phys.*, 122:437–463, 2006.
- [76] S. D. Traytak. Competition effects in steady-state diffusion-limited reactions: Renormalization group approach. *J. Chem. Phys.*, 105:10860, 1996.
- [77] S. D. Traytak and M. Tachiya. Diffusion-controlled reactions in an electric field: Effects of an external boundary and competition between sinks. *J. Chem. Phys.*, 107:9907–9920, 1997.
- [78] M. J. Ward, W. D. Henshaw, and J. B. Keller. Summing logarithmic expansions for singularly perturbed eigenvalue problems. *SIAM J. Appl. Math.*, 53(3):799–828, 1993.
- [79] M. J. Ward and J. B. Keller. Strong localized perturbations of eigenvalue problems. *SIAM J. Appl. Math.*, 53(3):770–798, 1993.